
An analysis of

Depth and gross rock volume uncertainty

BAS MEYER VIOL

SUPERVISOR EBN: GUIDO HOETZ
SUPERVISOR UNIVERSITY: HANNEKE PAULSEN



Copyright © 2015 EBN

PUBLISHED BY EBN

License page

First printing, March 2015



Contents

1	Introduction	5
2	Well depth errors in the Dutch subsurface	9
2.1	Magnitude depth error	9
2.2	Direction depth error	10
3	Depth uncertainty: Stochastic approach	13
3.1	Time-depth conversion	13
3.2	Input uncertainties	20
3.2.1	TWT uncertainty	20
3.2.2	Velocity uncertainty	23
3.3	Gaussian Monte Carlo time-depth conversion	24
4	Depth uncertainty: Deterministic approach	27
4.1	Workflow	27
4.2	Case study	28
4.3	Comparison to Stochastic depth uncertainty method	28
5	GRV uncertainty: Stochastic approach	31
5.1	Workflow	31
5.2	Case Study 1: Updip potential in Chalk reservoir	37
5.2.1	Sensitivity analysis	39
5.3	Case study 2: Volpriehausen dome with varying spill point	45

6	GRV uncertainty: Deterministic approach	49
6.1	Workflow	49
6.2	Case study	50
7	Discussion size GRV uncertainty	53
8	Recommendations	55
9	Conclusions	57
A	Velsto user guide	59
B	Kriging & variograms	69
	Articles	75



1. Introduction

Geoscientists have to deal with a large number of uncertainties when drilling for oil or gas. In the exploration phase one of the main objectives is to estimate the size and position of a reservoir based on seismic data. This estimation is not trivial. The reservoir depth is often mispredicted by 10's-100's of meters [1], while the size of the reservoir is often one of the main uncertainties in estimating reserves [2]. This is the result of the significant uncertainties involved in the process of determining the reservoir depth and size.

An accurate reservoir depth prediction is important for three main reasons [1]. An incorrect depth prognosis can significantly affect the size of the trap which contains hydrocarbons, also referred to as the gross rock volume (GRV). The GRV depends on the depth of the top of the reservoir, the thickness of the reservoir, and the contact between the hydrocarbons and water level (water contact). If the water contact is known (e.g. from other wells), a wrong depth prognosis of the top of the reservoir will have a large impact on the GRV (Figure 1.1a). If the water contact is unknown, a wrong depth prognosis of the top of the reservoir can still have impact on the size and shape of the reservoir and thus on the GRV. A good depth prognosis is not only important for the size of the GRV. To design a well safely a good estimate of the pressure in the reservoir is needed. The pressure in the reservoir is different from the pressure in the layers on top of the reservoir. The well is designed for this. A wrong prognosis of the reservoir depth will result in a wrong prognosis of the pressure, leading to safety issues (Figure 1.1b). A third problem with depth uncertainty is the effectiveness with which a well can be designed. If a wrong depth map is used this can result in missing the target (Figure 1.1c).

To derisk these issues the depth uncertainty of the reservoir should be estimated. Therefore it is very useful to make a depth uncertainty map of the top of the reservoir. With this map the different possible depth scenarios can be taken into account when designing a well. Furthermore the depth uncertainty map can be used to estimate the GRV uncertainty.

Now that the importance of evaluating the depth uncertainty is underlined, we need to understand what the underlying cause of the uncertainty is. Typically the depth map of a reservoir is based on seismic mapping. Seismic data is obtained in the time domain. After being processed, a two-way traveltime (TWT) image of the subsurface is obtained. Bright seismic reflections represent geologically distinct layers. These layers are interpreted in the TWT-domain. In the Southern North Sea typically a multi-layer velocity model, which estimates the velocities (of the seismic waves) of the different layers, is used to convert the time image to a depth image

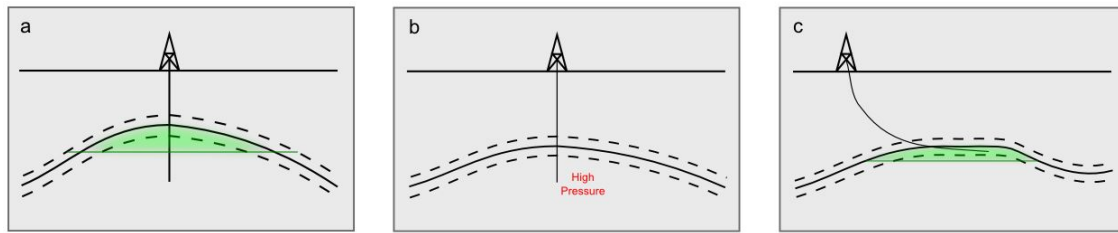


Figure 1.1: Uncertainty in the prognosed depth of the reservoir results in a) uncertainty in the GRV, b) uncertainty in the pressure/characteristics of the reservoir, c) uncertainty in the design of the well. [1]

[3]. Errors made in processing, interpretation, and velocity estimation all result in an error of the depth. In this report the cause and size of the depth uncertainty is investigated, and the impact of this depth uncertainty on the GRV uncertainty is analyzed.

The report starts with a view on the magnitude of the problem. **Chapter 2** looks at depth errors of exploration wells which have been drilled in the Dutch subsurface. This chapter stresses the importance of doing research on this topic.

Eventually we want to make a depth uncertainty map. Different approaches exist to do this, of which two are explained in this report (Figure 1.2). The first approach, explained in **Chapter 3**, estimates the uncertainties in the process of making a depth map (e.g. interpretation, processing, and velocity model). Thereafter a stochastic time-depth (TD) conversion is used to convert these uncertainties to a depth uncertainty. The conversion is performed with the open source software program Velsto [4]. This method does require a good view on the magnitude and cause of the uncertainties. Sometimes it is difficult to estimate this. Therefore a second approach to estimate the depth uncertainty is proposed. This approach uses the difference at the wells between the TD-converted depth of the reservoir and the measured well reservoir depth (this difference is also called the residual), as an indicator of the depth uncertainty. For this method to work, there need to be a lot of wells in the area, to get good statistics. The workflow is explained in **Chapter 4**.

The depth uncertainty map can be used to estimate the impact of this uncertainty on the GRV uncertainty. Again two methods are proposed to do this (Figure 1.2). A well established stochastic method uses the depth uncertainty map to simulate many different equally probable reservoir realisations [5]. A sequential Gaussian simulation (SGS) algorithm is used to make these different realisations. From these realisations a GRV expectation curve can be made, including high and low case scenarios. A full analysis of this *SGS-method* is made in **Chapter 5**. The SGS-method is used to predict the GRV uncertainty in two different structures, one with a constant spill point, and one with a variable spill point. Furthermore a sensitivity analysis is performed on the relevant input parameters of this method.

While the SGS-method provides a reasonably accurate GRV uncertainty, it is also a laborious method. For a quick view on the magnitude of the uncertainty a second 'deterministic' method, referred to as the *plus-minus method*, is proposed [1]. This method scales the depth uncertainty map, and adds or subtracts it from the depth map to define a high and low case scenario. While it gives a fast view on the size of the uncertainty, it is not as accurate as the SGS-method. How this method works and how the scaling is done is explained in **Chapter 6**. While these depth uncertainty- and GRV uncertainty estimation methods give a good understanding of the magnitude and cause of the problem, it is good to keep in mind they do not provide a solution to the problem that there is uncertainty. It is the interpretation and understanding of the uncertainties that is most important.

In determining the potential amount of hydrocarbons in the reservoir the GRV is not the only

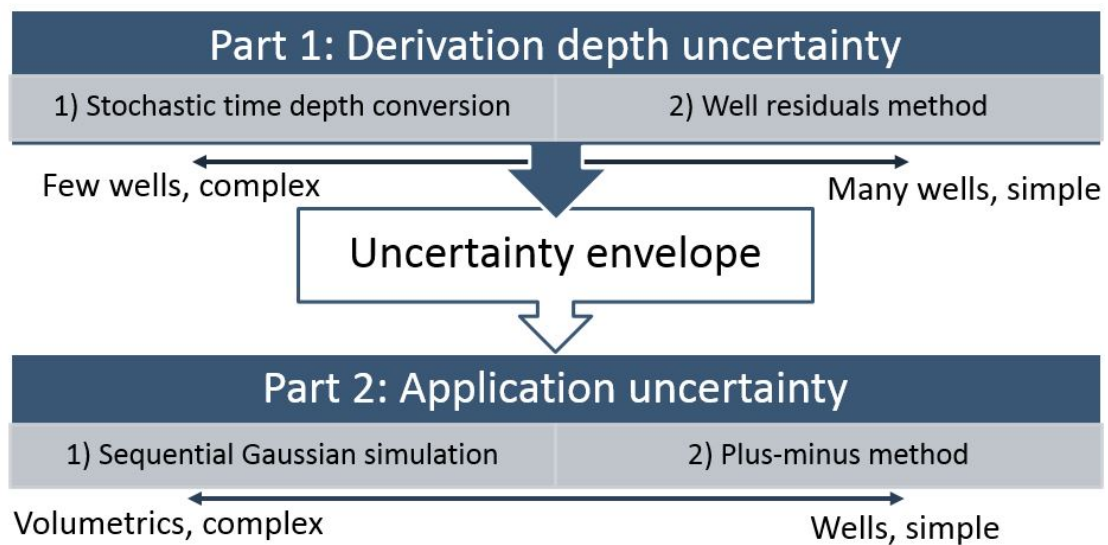


Figure 1.2: 2 different methods to estimate the depth uncertainty: 1) Stochastic time depth conversion, 2) Well residuals method. These methods give a depth uncertainty envelope. With this uncertainty envelope the GRV can be calculated with 2 different approaches: 1) Sequential Gaussian simulation, 2) Plus-minus method.

parameter. The porosity, nett/gross and water saturation are also part of the equation. Therefore **Chapter 7** discusses how to rank the uncertainty in GRV compared to these other parameters. **Chapter 8** gives final recommendations on the approach of uncertainty determination. Finally **Chapter 9** states the conclusions of this project.



2. Well depth errors in the Dutch subsurface

A logical start of an analysis on depth uncertainties is to review depth errors made in the past. In the Dutch subsurface thousands of wells have been drilled in the past 60 years [6]. Due to improving technology and knowledge, the uncertainty in depth of the targets of these wells has decreased over time. To get a good overview of the errors made with current technology the depth error analysis is performed on 101 exploration wells drilled in the Dutch subsurface between 2005-2014. Both the magnitude and direction (predicted too shallow or too deep) of this depth error are relevant. In Section 2.1 we will look at the magnitude of the depth error. This section also shows the relation of the depth error with depth. The direction and distribution (e.g. Gaussian or triangular) of these errors are investigated in Section 2.2.

2.1 Magnitude depth error

The magnitude of the depth error tells us how far the depth at which the reservoir was drilled was off prediction. The average magnitude of the depth error of exploration wells between 2005 and 2014 in the Dutch subsurface is 38.1 meters. The average depth of the reservoir targets is 2915 meters. The reservoir depth error was on average 1.3% of the predicted depth. While this gives an indication of the order of magnitude, it is more useful to plot the depth errors of the individual wells. Figure 2.1 plots the depth error of all individual wells against the depth. A color division is made between different stratigraphic targets. The two most common reservoir targets in the Dutch subsurface are the Rotliegend (50 out of the 101 exploration wells) and the Triassic Bunter (33 out of the 101 exploration wells). The other 18 wells were drilled in Zechstein (6), Devonian (4), Jurassic (3), and Chalk (5) layers. What we see from the pie chart of Figure 2.1 is that almost a third of the wells (29%) is predicted more than 40 meters of target. 10% percent is completely off target by more than 100 meters. To give an indication of the scale of the error, the reservoir thickness is often between 10-100 meters. These figures show that there is definitely room for improvement of the depth prediction of a reservoir, and that taking uncertainties of this prediction into account is important.

Depth dependency

Figure 2.1 shows that deeper wells have a higher chance to be drilled far off target. Of the wells that have an error of more than 100 meters, 7 out of 10 have a target depth of more than 3000 meters. To get a better view on the relation between the size of the depth error and the depth,

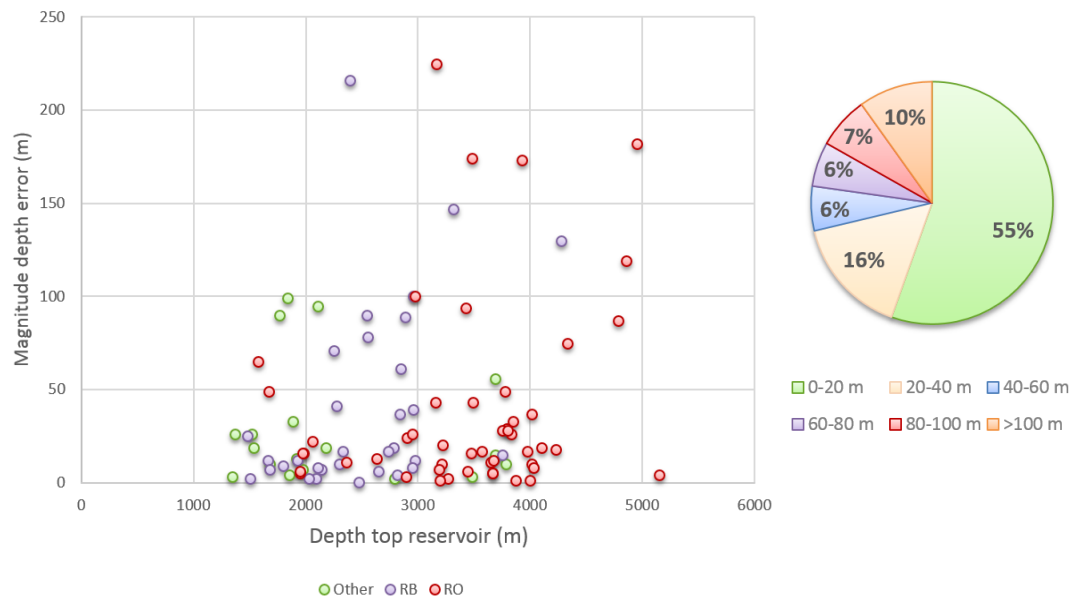


Figure 2.1: On the left the size of the depth error of 101 exploration wells drilled between 2005-2014 plotted against the depth. The colours indicate the reservoir layer of the main target (Rb=Triassic Bunter, RO= Rotliegend). On the right a pie chart which shows the percentage of wells drilled within each error range. The colors represent the different error bins.

the wells are divided into 1000 meter bins and the error is plotted in Figure 2.2. The depth error for wells drilled between 1000-2000 meters is 24.1 meters on average, while the depth error for wells drilled deeper than 4000 meters is 62.6 meters. The depth error increases with depth for two main reasons. The first reason is that velocity errors in the velocity model (f.e. the velocity is estimated too high) propagate through a thicker package, resulting in a larger depth error. If the velocity is estimated wrong the depth error linearly increases with the distance over which this velocity is estimated wrong. The second reason is the generally more complex subsurface above a deeper target. The deeper layers have often been through more stages of rifting and compression, resulting in more difficult structures. This increases the chances of a mistake being made in one of the layers velocities. A realistic depth uncertainty map includes this depth uncertainty increase with depth.

2.2 Direction depth error

It is not only the magnitude of the depth error that interests us. The direction of the depth errors can give a lot of information. Figure 2.3 plots a histogram where the depth error is plotted including the direction. Immediately it becomes clear that the reservoir target is often predicted to shallow, on average 15.7 meters. With an average size of the depth error of 38.1 meters, this bias is both significant and relevant. Therefore a research project at EBN has started on this topic [7]. Because the reason for this depth bias is not exactly known it can not be included in a depth uncertainty map. Therefore in this project we will continue with a symmetrically distributed depth uncertainty map.

Distribution

The uncertainty of a variable is usually presented by a probability density function (PDF). This PDF describes the relative likelihood for this variable to take on a given value. Some examples of PDF's are a Gaussian PDF, a triangular PDF or a block PDF (Figure 2.4). As we want to define the depth uncertainty, we need a PDF to describe it. The most common PDF in nature is

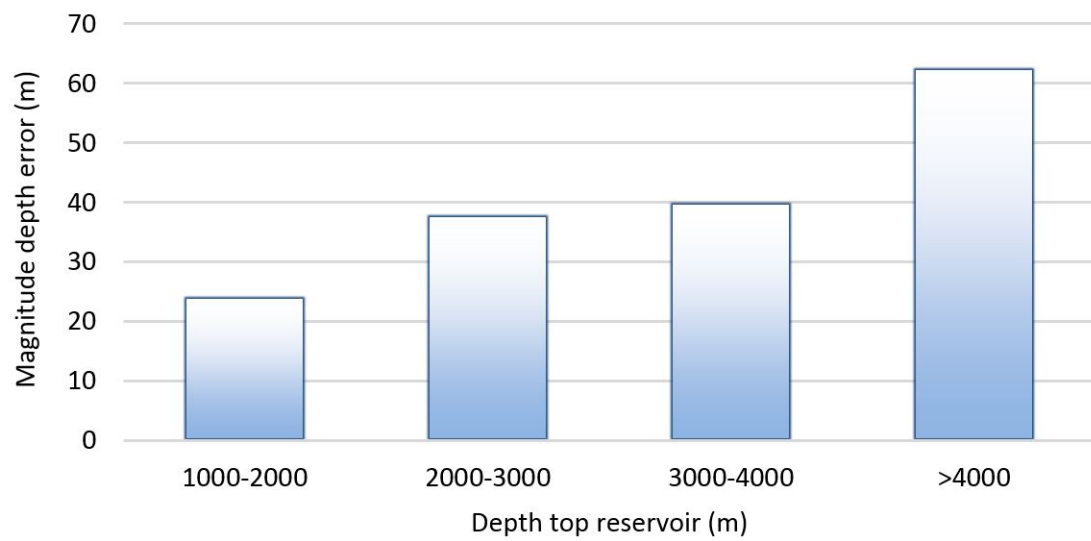


Figure 2.2: Depth error magnitude of 101 exploration wells drilled between 2005-2014 plotted against the depth in 1000 meter bins. The depth error increases with depth.

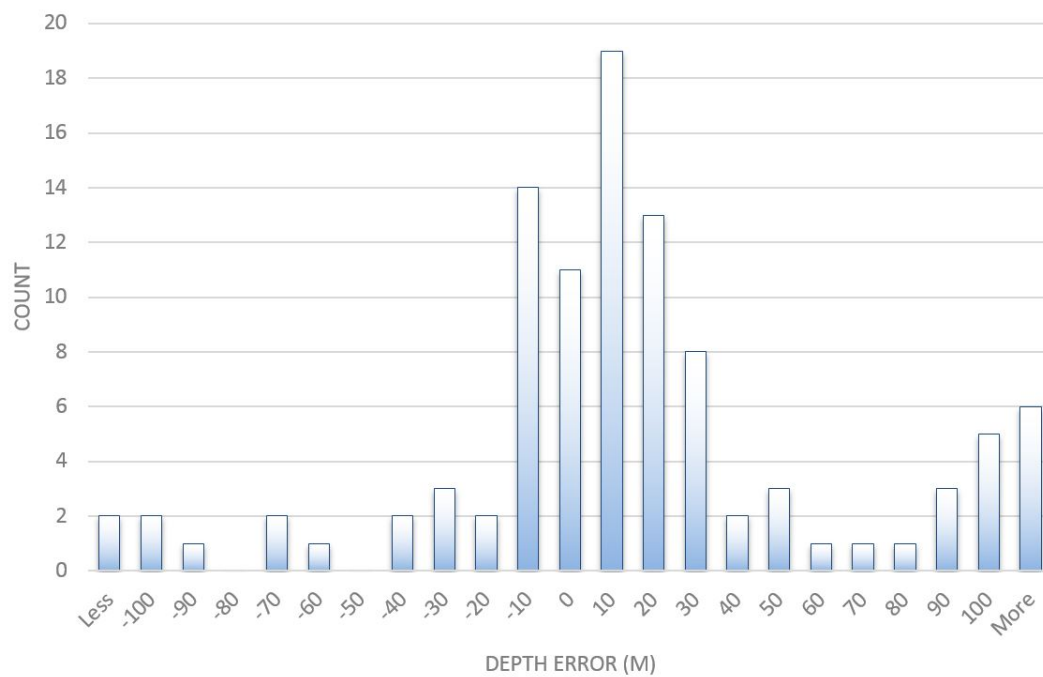


Figure 2.3: Depth error histogram which plots the frequency (count) of depth errors in 10 meter bins.

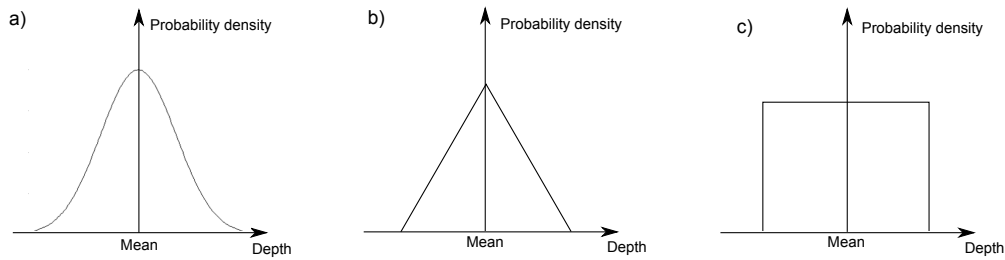
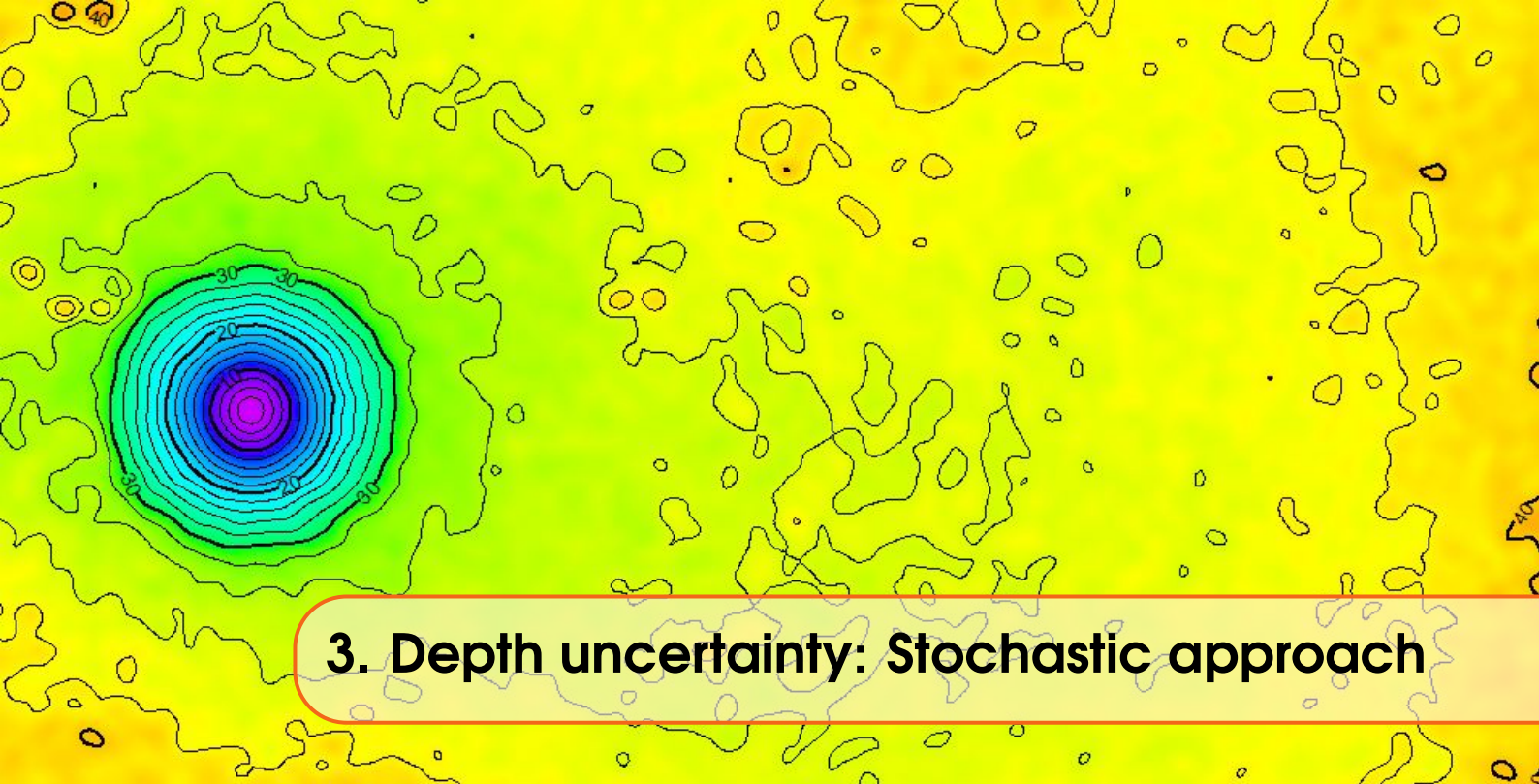


Figure 2.4: Probability density functions. a) Gaussian function, b) Triangular function, c) Block function.

the Gaussian PDF. If we take an infinite amount of measurements from a variable described by a single PDF, the histogram of the outcome shows the same shape as the PDF.

Now of course we do not have an infinite amount of wells drilled, and the depth uncertainties of the reservoir at the wells are certainly not all described by the same PDF. We can however look at the histogram to get an indication of the depth PDF. Figure 2.3 plots a histogram of the depth error with bins of 10 m. The histogram has a Gaussian shape, with a relatively high number of large errors. This makes sense, as large non-Gaussian depth errors are often the results of human mistakes, a lack of data, or a very complex subsurface. Keep in mind that this Gaussian distribution does not tell us that the depth uncertainty in each separate depth model is Gaussian. However we must make an assumption on the depth uncertainty PDF and a Gaussian PDF is the most likely. This assumption is backed in the next chapter where we will look at the origin of the depth error. The origin of the error gives a good view on the PDF.



3. Depth uncertainty: Stochastic approach

In the Dutch subsurface the depth of a reservoir is generally estimated by using a multi-layer velocity model TD-conversion. In this chapter the uncertainty of determining the depth with this approach is estimated. For this purpose we use a stochastic TD-conversion. A stochastic TD-conversion converts uncertainties in the input (velocity model & two-way time (TWT) interpretation) into a depth uncertainty. Figure 3.1 shows the workflow of a stochastic TD-conversion. The first step is to make a reliable depth map. For this we need a reliable interpretation in the TWT domain of the different layers and a reliable velocity model. With a 'deterministic' TD-conversion the Base case (or most likely) depth map is made. The basic principles of this deterministic TD-conversion are explained in Section 3.1. To make a depth uncertainty map the uncertainties in the velocity model and interpreted layers have to be estimated first. The input uncertainties are the only source with which the outcome depth uncertainty is determined, so it is very important to make well-based estimates. In Section 3.2 it is explained how to make good estimations of these input uncertainties. Once the input uncertainties are estimated the final step is the stochastic TD-conversion. A Gaussian Monte-Carlo algorithm is used to convert the TWT & velocity uncertainty to a depth uncertainty. The theory behind this algorithm is explained in Section 3.3. The stochastic TD-conversion is performed with a software program named *Velsto* [4]. Appendix A contains a user guide of this program. A case study of an area with two domal structures in the Dutch offshore is used throughout the chapter to provide a better understanding of the workflow.

3.1 Time-depth conversion

A TD-conversion translates the processed seismic data from the time domain to the depth domain. The geologically distinct layers can be identified from the TWT seismic attribute. Due to an impedance difference in the subsurface, (bright) reflections can be identified on the seismic profiles indexed by seismic TWT. Different layers may have different rock properties including different seismic velocities. After interpreting the different layers a velocity model is made. The challenge of a TD-conversion is to make this velocity model, and use it to convert the time-indexed information (reflections) into depth indexed information (reflectors).

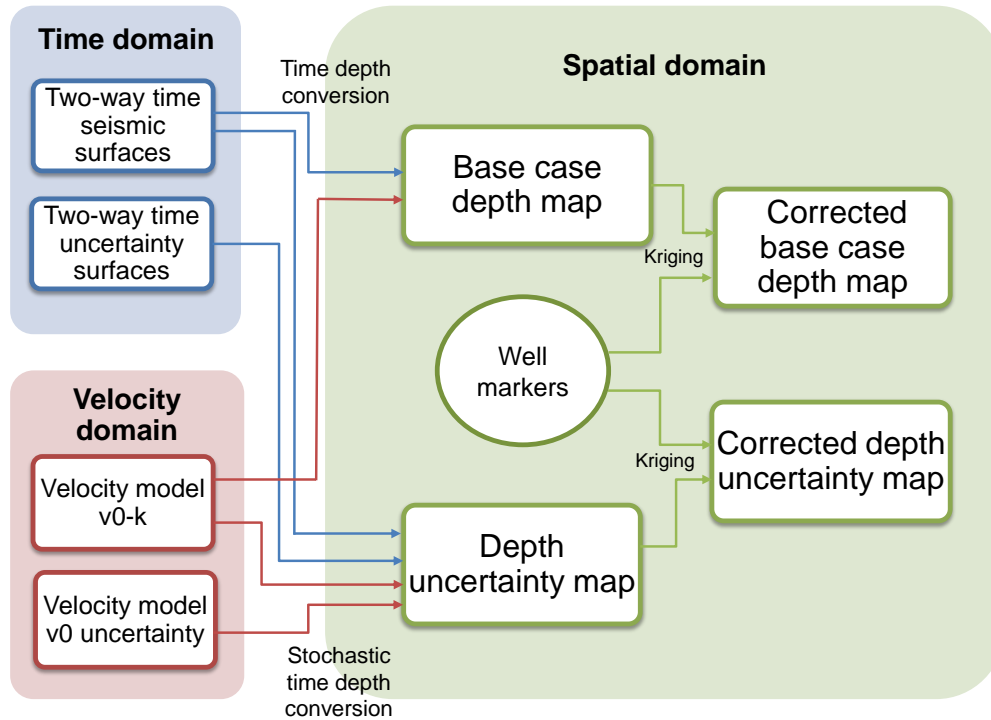


Figure 3.1: Workflow to make a depth & depth uncertainty map.

Velocity model

A reliable velocity model contains three characteristics [8]. It needs to be geologically consistent. Therefore the velocity model must follow an appropriate layering scheme. The model must also take into account the lithologic contrasts, folding and faults. Furthermore in a stratigraphic layer most of the time the velocity is also a function of depth due to compaction [9]. The multi-layer velocity model can incorporate these three characteristics in a convenient way. The different layers represent stratigraphic units. Each layer is described by a velocity function.

There are three possibilities to describe the velocity function of the layers. The first velocity model is the average velocity model. This model ignores the layering and describes the velocity in the whole overburden by a single constant v_{av} , which is the average velocity of the overburden (Figure 3.2a). This simplistic model can be used when there is no clear relation between the stratigraphy and the velocity. The disadvantage of this velocity model is the limited accuracy and hence high uncertainty. If there is a relation between the stratigraphy and the velocity inside the stratigraphy it is more appropriate to use interval velocities v_{int} (Figure 3.2b). These interval velocities are constant within a stratigraphic layer. Most of the time there is also a relation between the velocity in a stratigraphic layer and depth. The third velocity model makes the velocity both depth and stratigraphy dependent (Figure 3.2c). The velocities in such a model are called instantaneous velocities, due to the velocity variations over small depth increments. The most convenient way to describe an instantaneous velocity function is to model it as a linear function of depth: $v_{ins}(z) = v_0 + kz$, with v_0 the velocity at $z = 0$, and k the slope of velocity variation in depth z [10]. As the third option (referred to as the $v_0 - k$ velocity model) is the most accurate and there is enough information available in the Dutch subsurface to use this model, it is used in the case studies of this report.

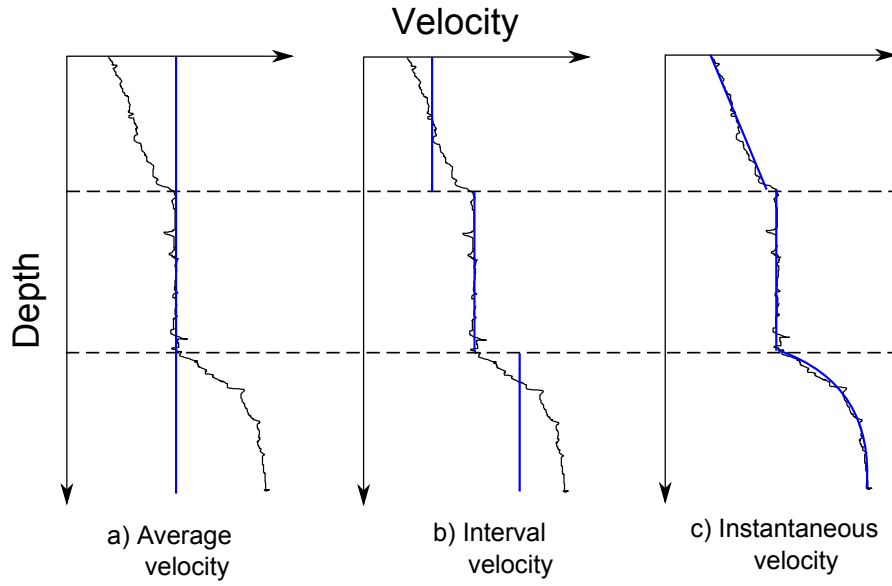


Figure 3.2: Three different type of velocity models to describe the velocity inside the layers.

Velocities

The velocities in the velocity model originate from several sources. In the wells the velocity over small increments is often measured by **sonic logging**. While sonic log velocities are reasonably accurate it is a locally measured property. Therefore it is difficult to describe the velocity function over a large area purely based on sonic logs. The sonic logs do give good indication of the layers with a distinguishable different velocity. With sonic log velocities also the interval velocities of different layers can be determined.

A model which suits the TD-conversion over a large area is the $v_0 - k$ model based on the $v_{\text{int}} - z_{\text{mid}}$ method [11]. In this model the velocity of each layer is described by $v(x, y, z) = v_0(x, y) + k \cdot z$. k is determined according to the $v_{\text{int}} - z_{\text{mid}}$ method applied to collections of $v_{\text{int}} - z_{\text{mid}}$ pairs. For all wells in the region the interval velocity of each layer is measured. This interval velocity is plotted against the mid-depth of that layer. With a linear regression k is obtained (see Figure 3.3). This implies k is assumed constant for each layer. The k -values used in the velocity model in this report come from the VELMOD-2 model [12], in which the above method is applied. v_0 can subsequently be determined so that the velocity model fits at the borehole location by using the following calibration formula [13]:

$$v_0(x, y) = \frac{k \cdot ((z_b - z_t) \cdot \exp(k \cdot \Delta T))}{\exp(k \cdot \Delta T) - 1} \quad (3.1)$$

In this formula $(z_b - z_t)$ is the thickness of the layer, and ΔT is the time it takes the seismic wave to transport through the layer. With this formula v_0 is determined at the well locations. A Kriging interpolation algorithm is used to interpolate the v_0 map for each separate layer [14]. Appendix B explains the principle behind this algorithm.

The velocities in the layers can also be obtained from the processing stage. In the processing stage the **seismic velocities** are modelled in the whole subsurface. A TD-conversion can be based on these velocities. However the modelling velocities in processing can often be quite different from the actual propagation velocities [15]. While making a 3-D velocity model with these seismic velocities is an option this report will focus on the convenient multi-layer TD conversion with a velocity model derived using sonic logs and the $v_{\text{int}} - z_{\text{mid}}$ method.

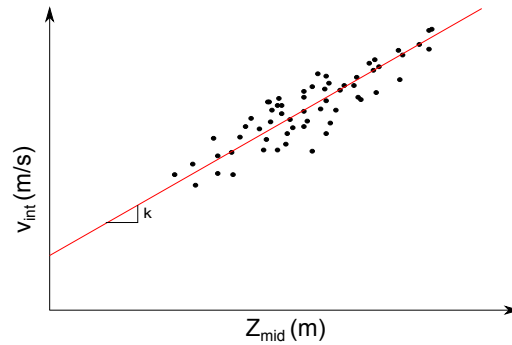


Figure 3.3: Principle of the $v_{int} - z_{mid}$ method. The interval velocities at the wells, where depth markers of the horizons of the layers are available, are plotted against z_{mid} . Linear regression determines a k value which is characteristic for that layer.

Case study

In this report a case study is performed in the F1 and F4 blocks (Figure 3.4). These blocks contain two clearly defined domal structures, with potential reservoirs in the Triassic Volpriehausen and Chalk layer. The structures have been drilled by well F04-01 and F04-03 and were dry. To show the workflow of creating a depth and depth uncertainty map, and estimating the GRV this is not relevant. From a seismic cross-section the structures can clearly be identified (Figure 3.5). In this section the depth map of the top of the Chalk and Volpriehausen reservoir are made.

The relevant seismic TWT-reflectors have been interpreted in this area by EBN. Figure 3.7 and Figure 3.8 show the interpreted TWT reflectors of the top Chalk and top Volpriehausen. To make a velocity model we first look at the sonic logs (converted to velocity) of the wells. Because the sonic log of well F04-03 only comprises a small depth interval, the log from which the relevant layers are distinguished is the F04-01 log. Figure 3.6 shows the sonic log of well F04-01. Three clearly distinguishable velocity intervals can be distinguished, namely the North Sea group, the Chalk group and the Trias group. Jurassic layers are not present in this area, or too thin (<100 m) to include and improve the quality of the velocity model. By looking at the sonic log it might be argued that the Triassic group consists of two velocity intervals, however these intervals could not clearly be interpreted from the seismic in this area. Therefore this distinction is not included in the velocity model.

The k -values from the VELMOD-2 $v_{int} - z_{mid}$ method are used. While k -values can also be obtained from sonic logs, these k -values change very fast locally over the grid. In wells close to each other these k -values can vary significantly. It is therefore preferred to assume a constant k -value derived as an average over a large number of wells by the $v_{int} - z_{mid}$ method. The v_0 maps of the different layers are also obtained from the VELMOD-2 model

Subsequently the velocity model is used to convert the TWT horizons to depth horizons. Figure 3.7 and 3.8 show the depth map of the top Chalk and Volpriehausen layer. If the depth map does not fit at the wells (where the depth of the layers is exactly known), a Kriging algorithm can be used to tie the TD-converted depth to the well depth. The $v_0 - k$ method, with a varying v_0 map, fits the velocity at the wells with Formula 3.1 thus depth-tying is not required anymore.

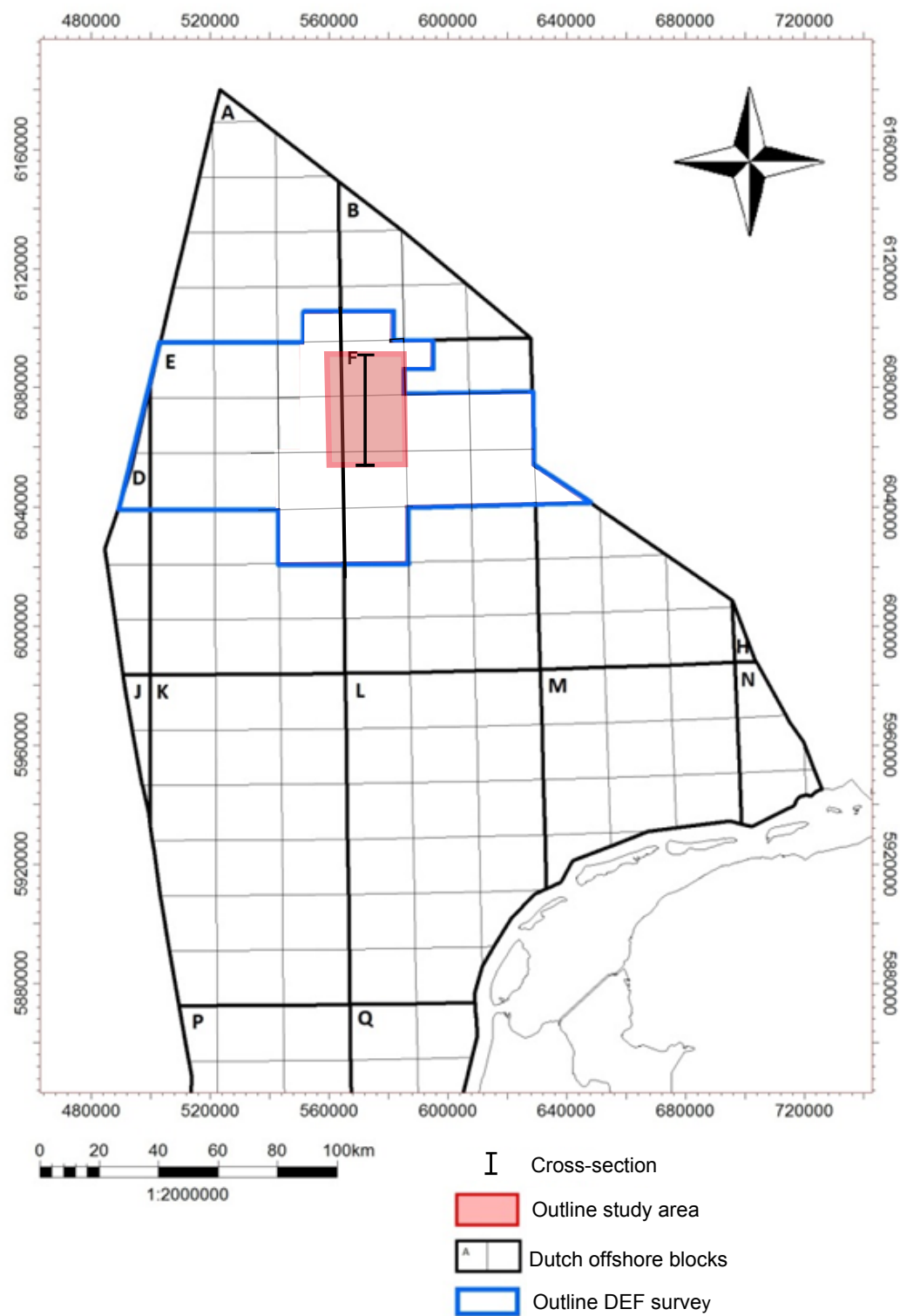


Figure 3.4: A map showing the location of the study area in the Dutch offshore.

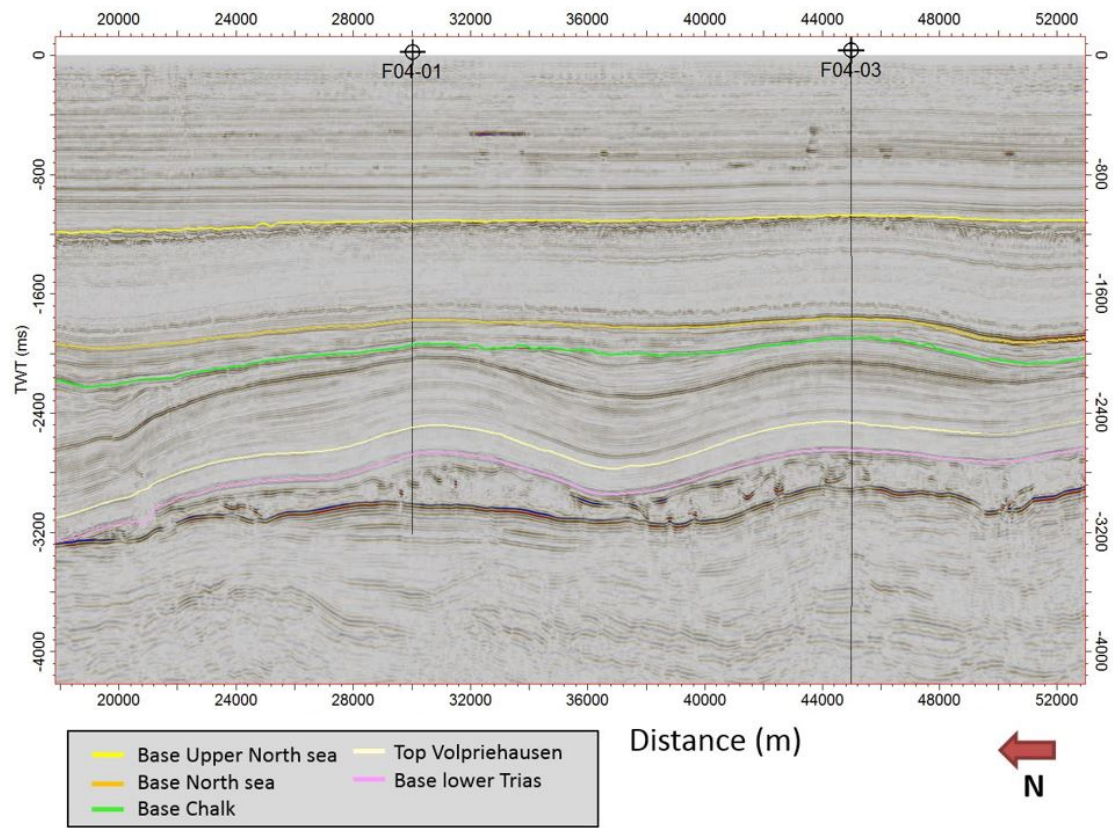


Figure 3.5: North-South cross-section of the study area, with the two domal structures which have been drilled.

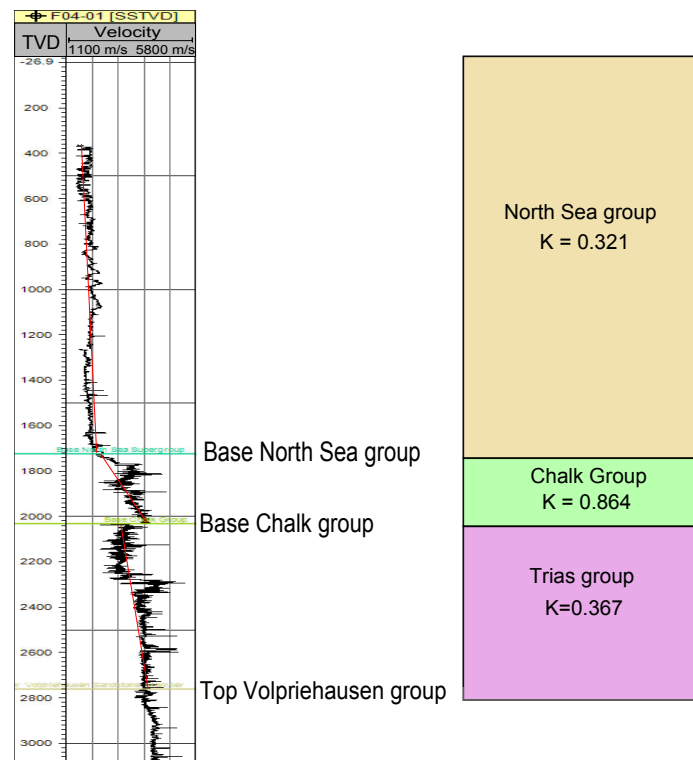


Figure 3.6: Sonic log from well F04-01, along with the velocity model based partly based on this log.

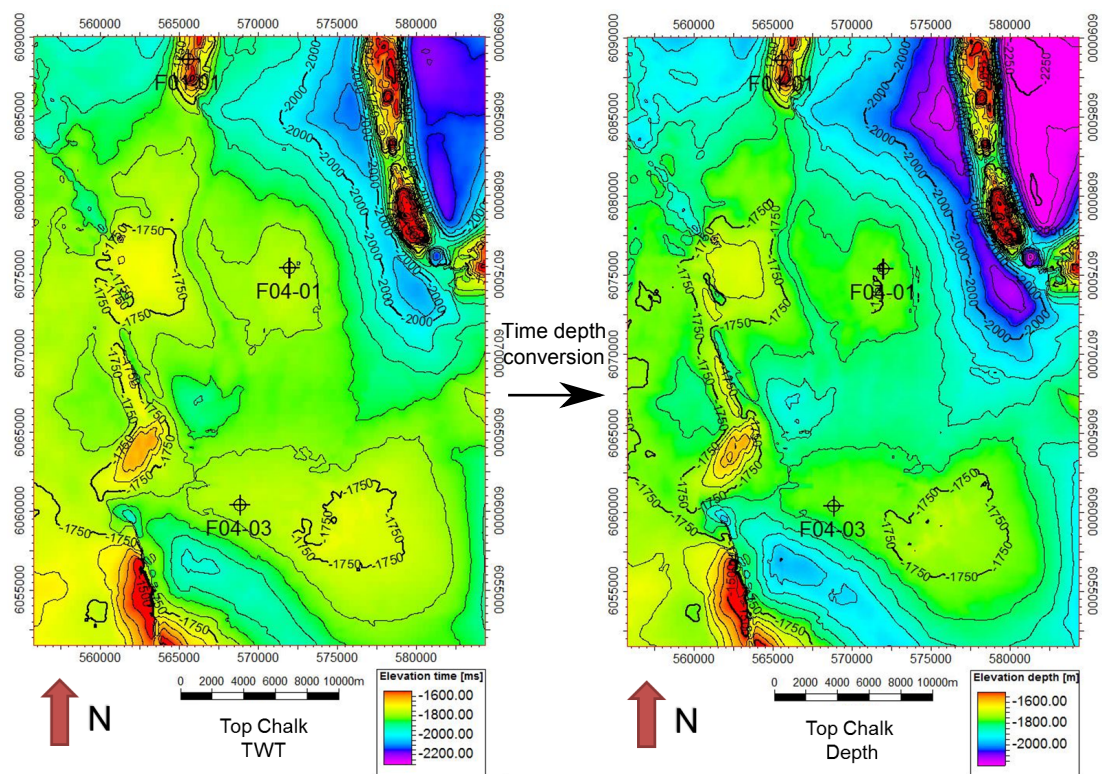


Figure 3.7: The time depth conversion of the top Chalk layer

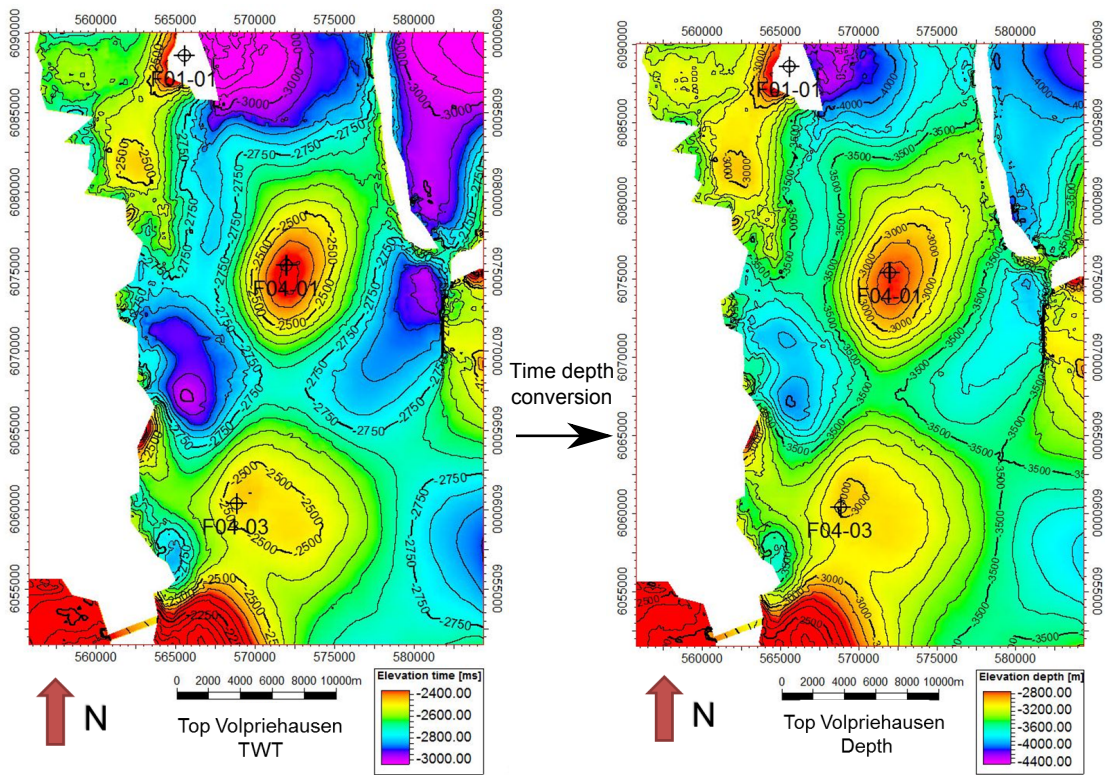


Figure 3.8: The time depth conversion of the top Lower Volpriehausen sandstone layer

3.2 Input uncertainties

The main input uncertainties of the velocity model are divided into a velocity uncertainty and a TWT uncertainty. This section gives a practical guide how to estimate these uncertainties.

3.2.1 TWT uncertainty

To estimate the TWT uncertainty it is important to first know what the cause of this uncertainty is. The seismic workflow involved in constructing a structural TWT model up to TD-conversion can be divided into three main stages, acquisition, processing and interpretation [16]. They all contain uncertainties. These uncertainties can be incorporated in a TWT uncertainty map.

Seismic acquisition

A main distinction can be made between offshore acquisition and onshore acquisition. In offshore acquisition noise is often limited. The seafloor mostly contains gentle surface variations, which makes acquisition offshore a relatively reliable process. Land acquisition can be more difficult. Ground vibrations due to external sources, and topographic variability can cause the data to be noisy. As a noisy image mostly complicates the interpretation, this uncertainty will be incorporated in the interpretation phase.

Seismic processing

The goal of the processing stage is to make an accurate image of the subsurface. This stage involves many steps (e.g. preprocessing, stacking, migration), which makes it difficult to assign an uncertainty. Errors made in processing can lead to a noisy image, and to positioning uncertainties of the reflectors. The uncertainty due to the noisy image is incorporated into the interpretation uncertainty. However structural positioning uncertainties have to be taken into account.

Migration is probably the most crucial processing stage in terms of creating structural uncertainties. The main goal of migration is to place the reflectors to their true positions, and to locate and collapse diffractions. If a multilayer TD-conversion is used to obtain a depth image, the seismic data are migrated in the time domain to create the image on which the picking of the horizons occurs. This migration requires an estimation of the seismic velocities. This estimation can contain a significant uncertainty. Especially if the dip of a structure is large and varying, the structure is sometimes difficult to translate back to the original position [16]. This is because seismic velocities often change more with depth than laterally. In general it is a strongly varying seismic velocity that makes migration a difficult process [17,18]. While migration can lead to lateral position uncertainties, in this report for simplicity these lateral uncertainties are neglected.

For a full analysis and detailed description of the processing errors, an uncertainty evaluation of each processing step is needed [19]. However, this is beyond the scope of this project. The processing uncertainty is often much smaller than the uncertainty from TD-conversion [16]. Therefore a rough estimation of the processing uncertainty suffices for the purpose of stochastic time depth conversion. The estimation that is made is that processing uncertainties increase with increasing dip. The most difficult areas to process are structurally complex areas (e.g. faults, salt domes). In areas with low structural complexity (e.g. gentle dip platforms or highs) processing does not result in a large error. The empirical relation that is used to include the processing uncertainty in the model is (comparable to the structural error of Kombrink et al.[20]):

$$\Delta TWT_{\text{process}} = a \cdot \text{dip} \quad (3.2)$$

With an a of 1 ms/ $^\circ$ the uncertainty can be neglected in gentle structures with low complexity, but is significant in strongly dipping structures. A smoothing sequence is used to ensure the uncertainty is distributed over a larger area (f.e. uncertainty is not only high at the fault itself

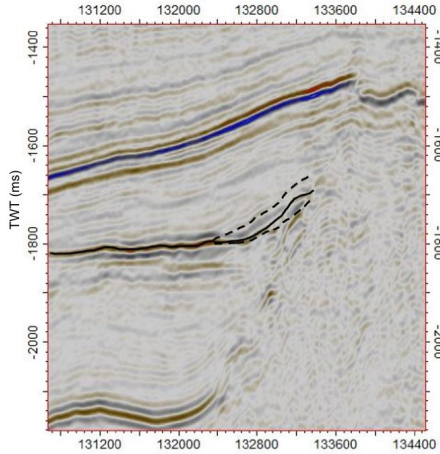


Figure 3.9: The interpretation of the horizon becomes difficult due to the salt diapir. Therefore an optimistic and pessimistic case are interpreted on top of the most likely case.

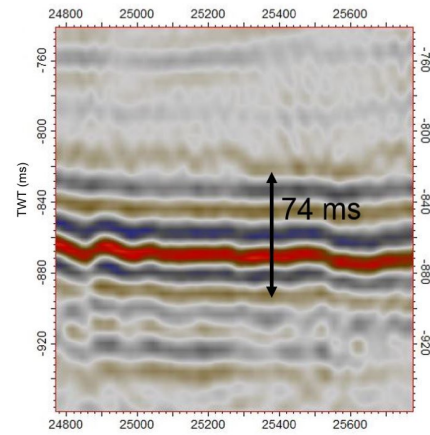


Figure 3.10: Method to estimate the vertical seismic resolution. This figure shows the resolution at 850 ms TWT-depth. The interval of 74 ms contains three wave reflections. The seismic resolution is $74/(3 \cdot 4) \approx 6$ ms.

but also in the area around the fault). For practical purposes the above formula gives a decent approximation.

Interpretation

If the seismic data is noisy it might be difficult to identify which reflection represent the horizon of a layer. The uncertainty associated with low data quality/noisy data is the **picking uncertainty**. The picking uncertainty is especially important for reservoir characterization. If the interpretation of the top of the reservoir is difficult due to low data quality it is advised to interpret a range of top reservoir characterizations. The interpretation range includes an optimistic top reservoir, a most likely top reservoir, and a pessimistic top reservoir [21]. Figure 3.9 shows an example. These interpretations provide an empirical confidence interval for the horizon picking. Especially near salt structures, where the data quality is low, the picking uncertainty is significant. The picking uncertainty is a non-Gaussian non-symmetric uncertainty. Therefore it is difficult to include in a Gaussian Monte-Carlo time depth conversion. If the picking uncertainty is large it is advised to run the TD-conversion for the three interpreted (most likely, optimistic and pessimistic) reservoir tops. If the top of the reservoir can clearly be interpreted in the seismic, a picking uncertainty does not have to be included. If the reservoir interpretation is based on 2-D seismic instead of 3-D seismic an extra interpolation uncertainty can be included in areas where no seismic data is available. This uncertainty increases with distance from the 2-D seismic line.

Apart from an interpretation uncertainty caused by noisy data, the accuracy of the picking is limited by the **resolution** of the data. The seismic resolution is a measure of the minimum thickness of a layer which can be detected in seismic. The wavelength of a wave is $\lambda = v/f$, where v is the velocity of the wave in the layer and f the frequency of the wave. The vertical seismic resolution is defined as $\lambda/4$ [22]. Thus wavelets with high frequencies generally have a better resolution. However low frequency signals penetrate deeper into the subsurface. This means the seismic resolution decreases with depth. To estimate the seismic resolution we look at the seismic data in the F1 and F4 blocks. Figure 3.10 shows the seismic resolution at 850 ms TWT-depth. To estimate the resolution uncertainty, the average TWT of 4 wave reflections is taken. The TWT uncertainty in this example is 6 ms. Several seismic TWT intervals are analysed

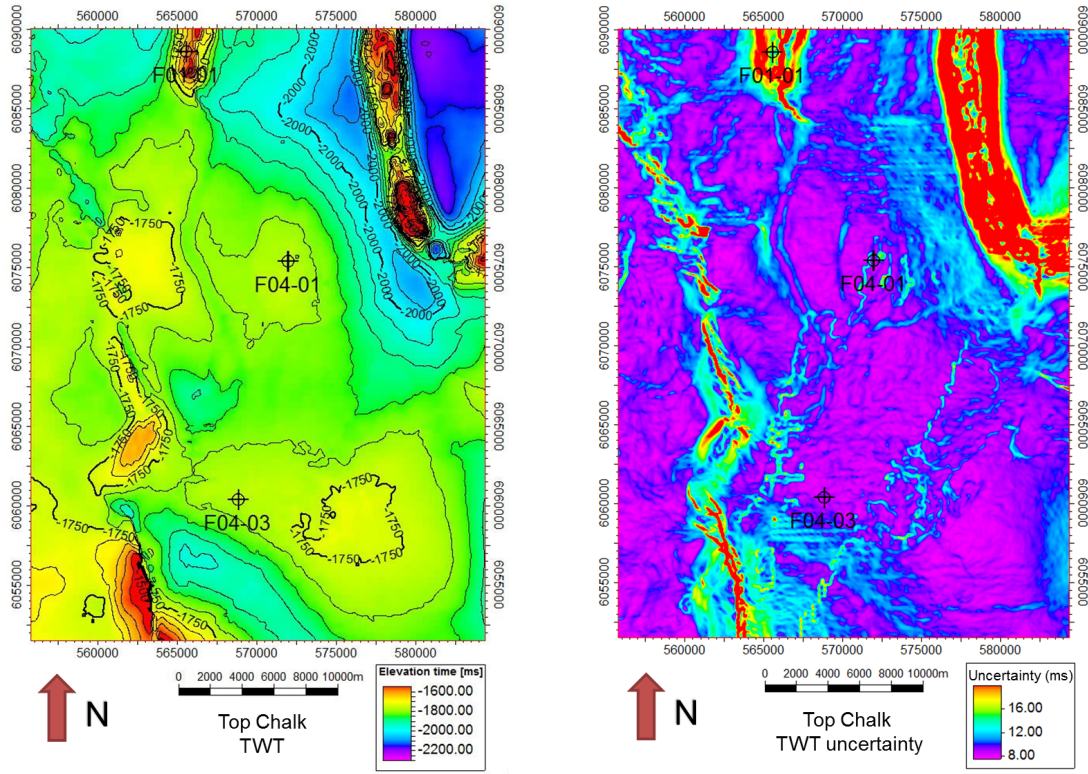


Figure 3.11: On the left the interpreted TWT, and on the right the TWT uncertainty (1 std) of the top Chalk.

at different TWT-depths to estimate the uncertainty. From this we acquire the empirical TWT resolution uncertainty of:

$$\Delta TWT_{\text{res}} = 4\text{ms} + 0.002 \cdot \text{TWT} \quad (3.3)$$

The TWT is expressed in milliseconds. This uncertainty may be dependent upon the velocities of the layers in the area. Therefore it is advised to always measure this uncertainty in the specific area of TD-conversion.

Case study

Determining the uncertainty in TWT is very case specific. It is advised to first identify the relevant processes which cause uncertainty in the TWT. Then a well-based estimate can be made. Figure 3.11 and Figure 3.12 show the estimated TWT uncertainty maps of the top Chalk and top Volpriehausen reservoir layers in the F1 and F4 blocks. The 3-D seismic data has a high resolution. The structure is clearly defined. Therefore the picking uncertainty is neglected. The processing uncertainty is included as $\Delta TWT_{\text{process}} = a \cdot \text{dip}$. The resolution uncertainty is included as $\Delta TWT_{\text{res}} = 4\text{ms} + 0.002 \cdot \text{TWT}$. The total uncertainty is $\Delta TWT = a \cdot \text{dip} + 4\text{ms} + 0.002 \cdot \text{TWT}$. The TWT uncertainty of the top of both reservoirs varies mostly between 8-20 ms, increasing with depth and with dip. For the stochastic TD-conversion we assume the TWT uncertainty has a Gaussian distribution. The TWT uncertainty map represents 1 standard deviation of this distribution.

With high quality 3-D seismic and a well defined trap, the TWT uncertainty is small compared to the velocity uncertainty. If the reservoir is not clearly visible on seismic, or the structure is very complex, the TWT uncertainty certainly becomes significant.

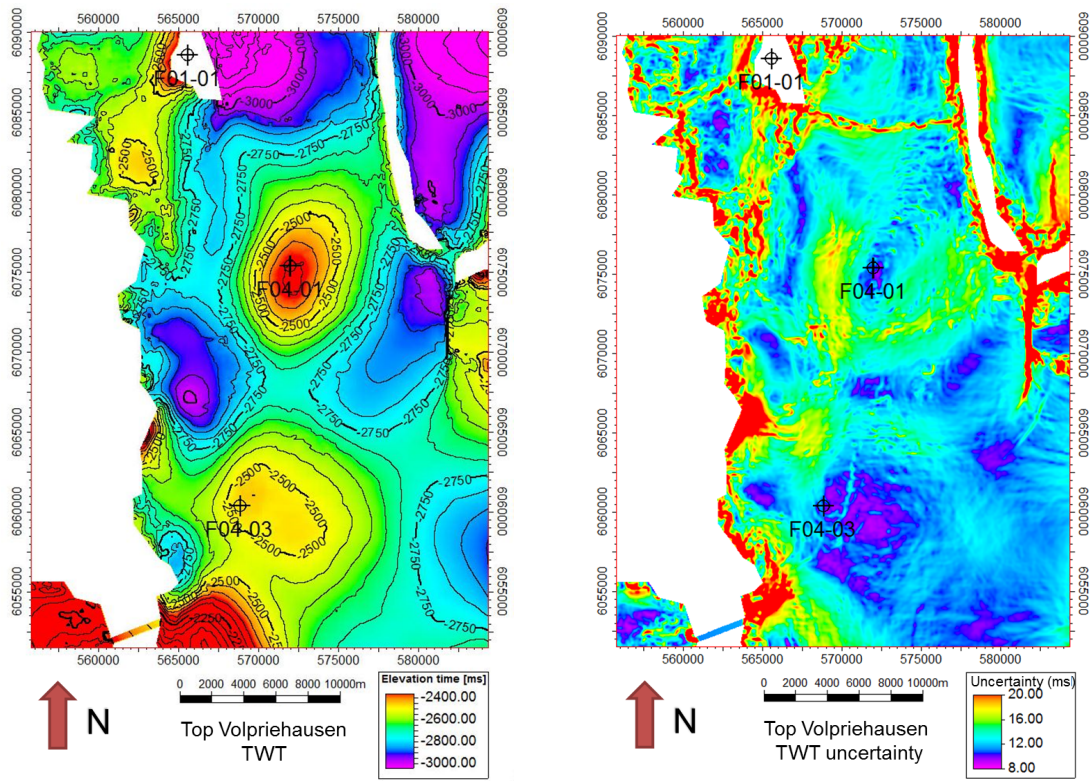


Figure 3.12: On the left the interpreted TWT, and on the right the TWT uncertainty (1 std) of the top Volpriehausen.

3.2.2 Velocity uncertainty

The velocity uncertainty is probably the single most important uncertainty in stochastic TD conversion. It depends on the velocity model, and the input velocities that are used. In this report we use the $v_0 - k$ model, with appropriate layering determined from sonic logs, and $v_0 - k$ velocity parameters derived from the $v_{\text{int}} - z_{\text{mid}}$ method. Therefore the velocity uncertainty comes from an uncertainty analysis of this method.

A realistic velocity uncertainty model contains three characteristics. The uncertainty increases with depth as a result of a higher structural complexity, and a higher velocity of deeper layers in general. Furthermore the uncertainty is dependent upon the stratigraphic layer, as some layers have higher lateral velocity variations than others. Both these characteristics can be included in the model by making the velocity uncertainty layer dependent, in which deeper layers have a higher velocity uncertainty. The velocity uncertainty does not change in the layer itself. It would be unrealistic to say we could differentiate the velocity uncertainty within stratigraphic layers, so it is better to simplify this. A third characteristic is that the velocity uncertainty is lower near the wells. At the wells the velocities are measured. While these measurements still contain uncertainties, the uncertainty is lower here.

A velocity uncertainty model that satisfies these three characteristics is the VELMOD-2 Kriging velocity uncertainty model. In this model the velocity uncertainty is incorporated in v_0 . The v_0 map of each layer was obtained by Kriging (interpolation), with as a main input v_0 at the wells. The advantage of Kriging is that this algorithm also gives an uncertainty map of v_0 for each layer (Kriging standard deviation, see Appendix B for an explanation). The distribution of this uncertainty is Gaussian. The velocity uncertainty increases with distance from the well. The velocity uncertainty is different for different stratigraphic layers, and in general higher for deeper layers. Therefore it satisfies all three properties which should be included in making a velocity

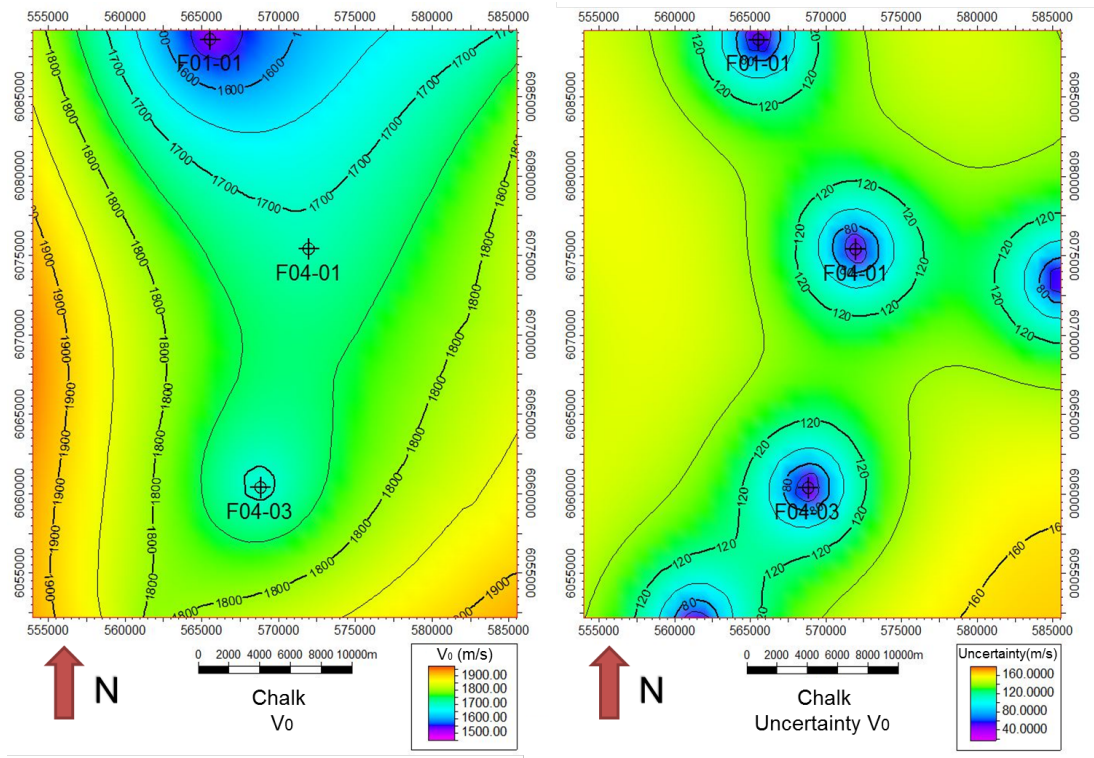


Figure 3.13: Velocity and velocity uncertainty (1 std) in the Chalk layer

uncertainty map.

Case study

An example of a velocity & velocity uncertainty map of the top Chalk is shown in Figure 3.13. The velocity uncertainty of this layer can increase to over 130 m/s, which is approximately 7% of the velocity. To put this in perspective, the TWT uncertainty in most of the area was around 0.5-1 %. This shows the relevance of the velocity uncertainty.

3.3 Gaussian Monte Carlo time-depth conversion

To perform the stochastic TD-conversion a Gaussian Monte Carlo simulation is used. For this simulation it is assumed that both the velocity and the TWT have a Gaussian probability distribution, with uncertainty defined as the standard deviation. For the velocity uncertainty this is a good approximation as the Kriging distribution from which the uncertainty is determined is Gaussian. The TWT probability distribution is made out of several aspects/errors, with different probability distribution functions. The final distribution is complex, but due to the scale of these uncertainties compared to the velocity uncertainty it is reasonable to assume the TWT distribution is Gaussian.

The Gaussian Monte Carlo simulation works as follows. For each grid point in each layer a random TWT is taken from the Gaussian TWT probability density function (PDF) of that layer (Figure 2.1). Then for each grid point in each layer a random velocity is taken from the Gaussian velocity PDF (Figure 2.2). With this velocity the random grid point TWT of each layer is then converted to a depth (Figure 2.3). This process is repeated many times (e.g. 500x), after which the average and standard deviation of the outcome are calculated (Figure 2.4). The outcome is again assumed to be Gaussian. In practice this is a good assumption. The depth uncertainty map

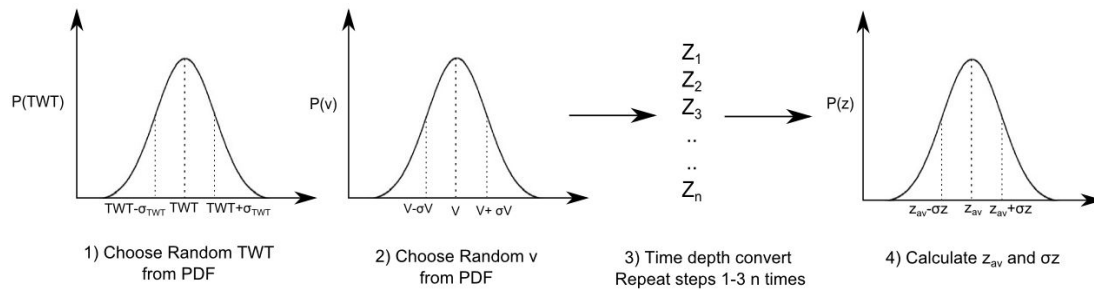


Figure 3.14: Stochastic time depth conversion.

is then defined as the depth standard deviation.

Subsequently a Kriging algorithm can be used to tie the depth uncertainty map to the wells. At the wells the depth uncertainty is 0. The depth uncertainty is corrected around the well up to a range R_{TD} . At a distance $d < R_{TD}$ from the well the depth uncertainty is reduced. At $d > R_{TD}$ the depth uncertainty is not changed. This range is difficult to quantify. Usually it is in the order of 100's meters up to around 2 km [2]. For a complex geology a small range is advised, while for a flat geology a large range may suit better.

Case study

For both the top of the Chalk layer and the top of the Volpriehausen layer a depth uncertainty map is made with a Gaussian Monte-Carlo time depth conversion. Figure 3.15 and Figure 3.16 show the results. The depth uncertainty of the Chalk layer is approximately constant over the whole area at around 40-45 meters. The reasons that it is constant is that the North Sea layer on top is a uniform package with only slight thickness variations. In the North East a salt structure causes the North sea layer to be fractured, uplifted, and deformed. Therefore the depth uncertainty is higher in this area. Around the wells the uncertainty is lower. The Kriging range is 2000 meters. As the structure of the top Chalk is very flat in this area and only contains minor depth variations a large range is chosen.

The Volpriehausen depth uncertainty is higher. This is expected as this layer is deeper and the overburden is more complex. The uncertainty also varies more spatially, as the depth of the layer also varies more. The uncertainty is higher where the layer is deeper. The uncertainty is also higher around the salt structure in the North East. The Kriging range of the well tie is 1.5 km, which is smaller than the range of the top Chalk layer.

To use these depth uncertainty maps it is important to know how to interpret them. The uncertainty map represents the standard deviation of that Gaussian depth distribution. If a well is drilled based on the depth map the chance is 68% that the well is drilled within the standard deviation of the the depth map (for most of the Chalk depth map within 45 meters, and for the Volpriehausen map depending on the location mostly within 60 to 120 meters).

Keep in mind that the standard deviation of the depth at a specific location is not equal to the expected average depth error if an infinite amount of wells would be drilled on this location. The expected average depth error over an infinite amount of measurements of a variable with a Gaussian distribution is given by the expectation value of a one sided Gaussian which is $\sqrt{2/\pi} \cdot \sigma \approx 0.8\sigma$. This means that if we have a depth map, and Gaussian depth uncertainty map of an area, and drill a large number of wells based on this map the average error will be 0.8 times the standard deviation.

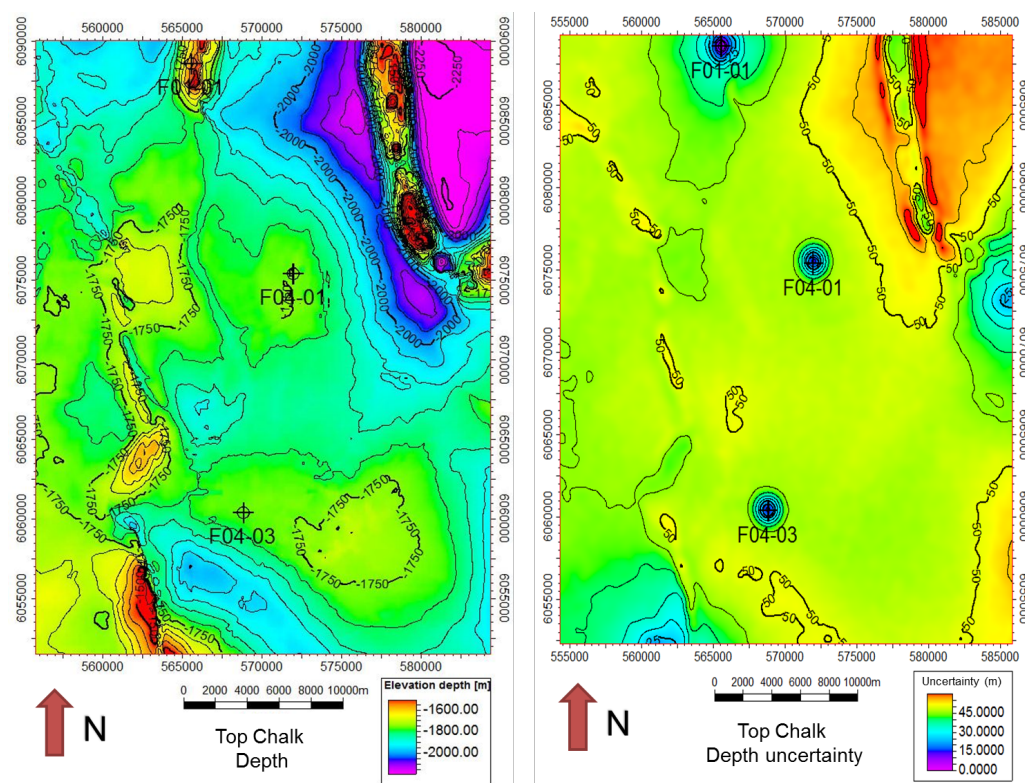


Figure 3.15: Depth (left) and depth uncertainty (right, 1 std) of the top Chalk layer

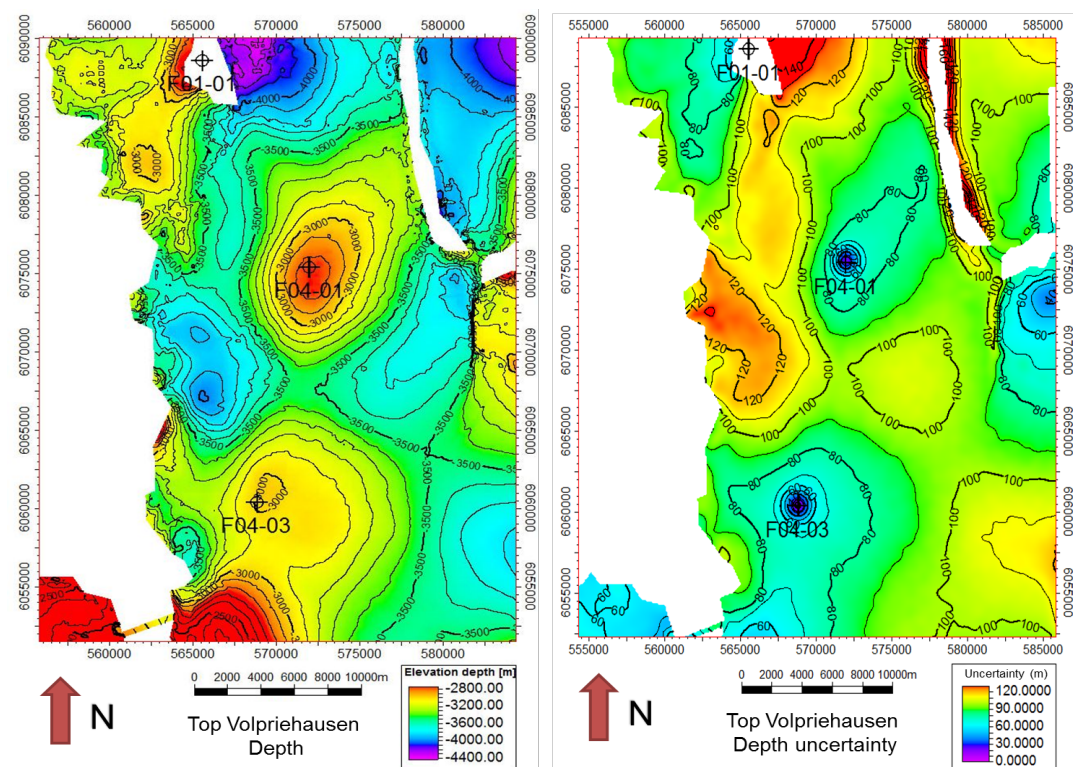
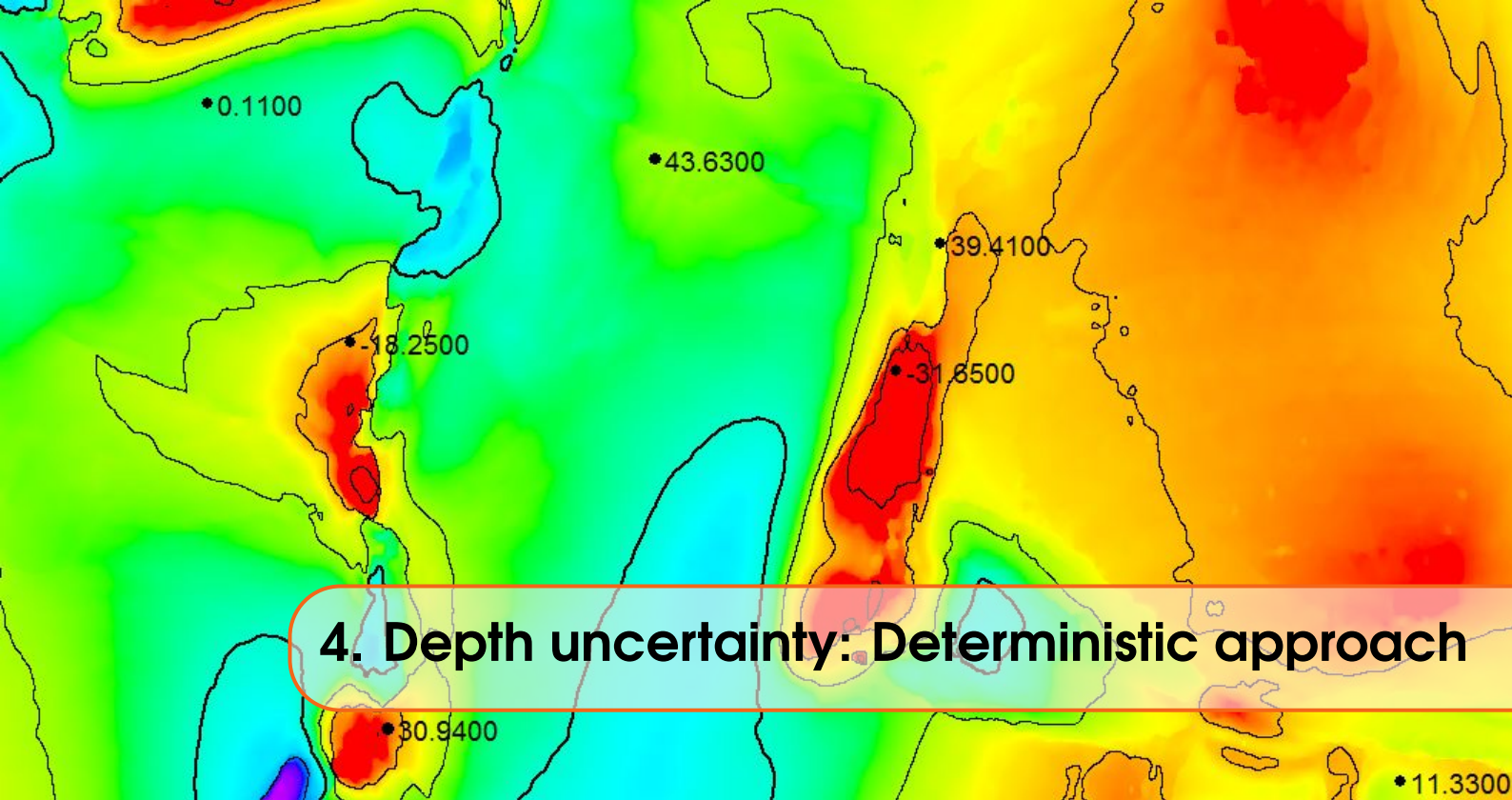


Figure 3.16: Depth (left) and depth uncertainty (right, 1 std) of the top Volpriehausen layer.



4. Depth uncertainty: Deterministic approach

Stochastic time depth conversion requires an estimate of the input uncertainties to create a depth uncertainty map. A second method, which does not require this, is the *well residuals method*. This chapter briefly explains the workflow of this method, and gives an example.

4.1 Workflow

The only input required for this method are the TWT maps of the horizons, a velocity model, and well markers of the horizons. Before starting this workflow check if lot of wells (preferably >20) have been drilled in the area, because this is where we eventually get the depth uncertainty from. If there are not enough wells in the region it is better to use the stochastic TD-conversion.

The first step of this workflow is to make a depth map by a deterministic TD-conversion. It is important for this method that the velocity model that is used is calibrated to the wells (The TD-converted depth agrees with the well marker depth of each horizon, thus the residual is zero). The $v_0 - k$ velocity model (explained in Section 3.1) can be used for example. In this model v_0 of each layer at the well location is calculated with Formula 3.1 such that after TD-conversion the residual is zero. The v_0 map is made by an interpolation algorithm.

Then a new velocity map is made by the same interpolation algorithm, in which the velocity v_0 at one of the well control points (f.e. well A) is left out. The velocity at this well is now the result of an interpolation between the other well point velocities. This velocity model represents a situation with no velocity data at the well A, as if the well has not been drilled yet. A new TD-conversion is conducted with the adjusted velocity model. This time the residual at well A is most likely not zero. This process can be repeated for each well, resulting in a residual at each well. These residuals give a good overview of the depth errors that would be made with the used velocity model, if a well was drilled without having the prior knowledge of the velocity at the well location.

To convert this to a depth uncertainty map we make use of the geostatistics of the residuals. In this analysis several assumptions have to be made. The first assumption is that the depth errors (residuals) have approximately a normal distribution. This way we can approximate the depth uncertainty by the standard deviation of the residuals. A second assumption is that the depth uncertainty is zero at the wells and increases up to a certain maximum at a range R . In general this means that close to the wells, up to a range R , we are more certain of the depth of the reservoir. A variogram analysis can be used to determine the range. If the number of wells in

a region is very high, and many wells are within the range R of each other, a reliable variogram analysis can be performed. However the range is often small (< 2 km), which means the part of the variogram between 0 and R is poorly constrained. Therefore often an assumption has to be made for the range.

While this method is straightforward and contains no uncertain input estimations, it does have a few disadvantages. First of all the method does not take into account structurally complex regions, or depth at which the well is drilled. The depth uncertainty is uniform along the whole map. If there are large depth differences of the mapped horizon, and the structural complexity varies much this is not a reliable assumption. Furthermore it is a requirement that many wells have been drilled in the region, to make the statistics reliable. With a small number of wells this method can not be used.

4.2 Case study

The well residuals method is used to estimate the top chalk depth uncertainty in the DEF blocks. 20 wells are used for this analysis. two notes have to be made: 1) The number of wells in this region is actually low to obtain good statistics. 2) There is a large distance between most of the wells, which means the depth uncertainty within the range ($< R$) of the well can not be defined with this method and has to be estimated. The reason that this region is still chosen for the case study is that the results can be compared to the results of the depth uncertainty made with a stochastic workflow.

Figure 4.1 shows the TWT of the top Chalk. A velocity model with a single layer (North Sea layer) that fits at the wells is made. The $v_{int} - z_{mid}$ method is used to calculate the v_0 at the wells. $k = 0.321$ is obtained from the VELMOD-2 model. A convergent interpolation algorithm is used to make the v_0 of the North Sea layer. The result is shown in Figure 4.2. With a deterministic TD-conversion the depth map is made (Figure 4.3). Thereafter for each well a v_0 map is made, by performing a convergent interpolation with that specific well v_0 control point left out. With this velocity map a TD-conversion is performed to obtain the residual of that specific well. This is done for all 20 wells resulting in the residuals of Figure 4.3. The variogram is not defined within the range as there are no wells within 1-2 km of each other. A range of 2 km is used, similar to the range chosen in the previous chapter for this layer. The average (absolute) residual is 15.44 meters. The standard deviation of the residuals is 19.3 meters. The depth uncertainty map is 0 at the wells and increases up to the standard deviation of 19.3 meters at a distance $> R$. This map is shown in Figure 4.4. It represents the Gaussian standard deviation of the depth map.

4.3 Comparison to Stochastic depth uncertainty method

The depth uncertainty with this method is half of the depth uncertainty obtained from stochastic TD-conversion. This can be explained. The stochastic TD-conversion used a velocity model (VELMOD-2) which is made for the whole Dutch offshore. The Kriging velocity uncertainty which we use in stochastic TD-conversion is therefore also based on this large region. In this large region the velocities vary more, so the Kriging velocity uncertainty (which is constant at $d > R$ from the wells) is also higher. A more local velocity model would most likely have lead to a lower Kriging velocity uncertainty. As it is this velocity uncertainty that mostly determines the depth uncertainty in stochastic TD-conversion, the uncertainty from stochastic TD-conversion is higher than the uncertainty from the well residuals method.

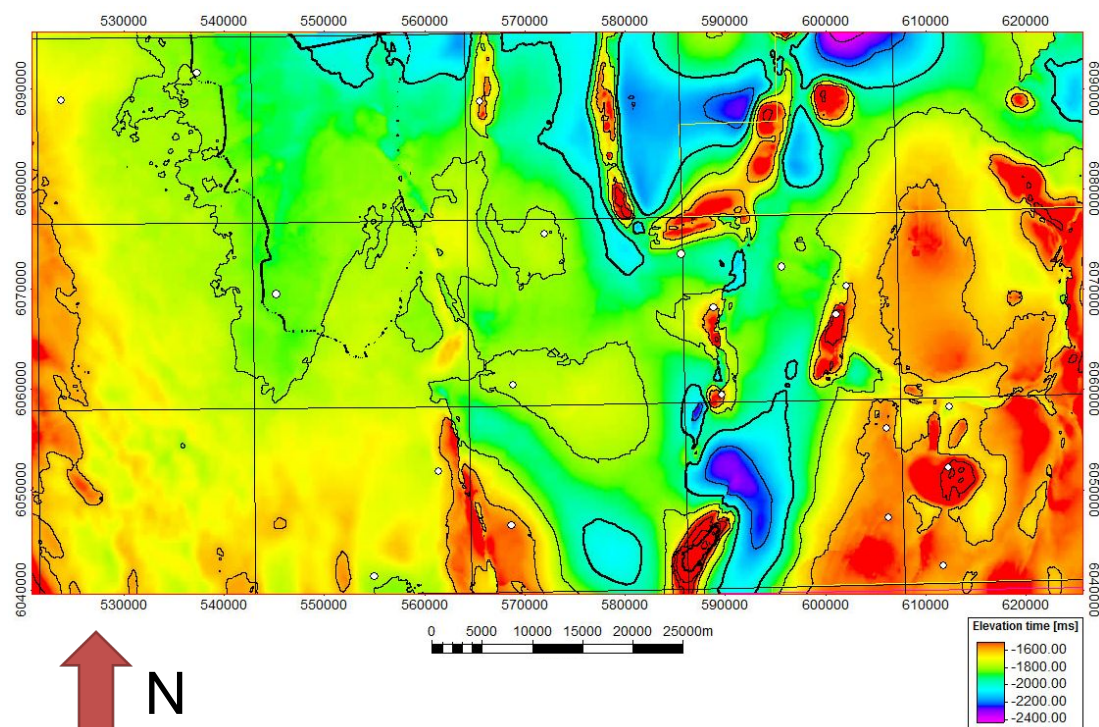


Figure 4.1: The TWT map of the top Chalk. The white dots denote the locations of the wells.

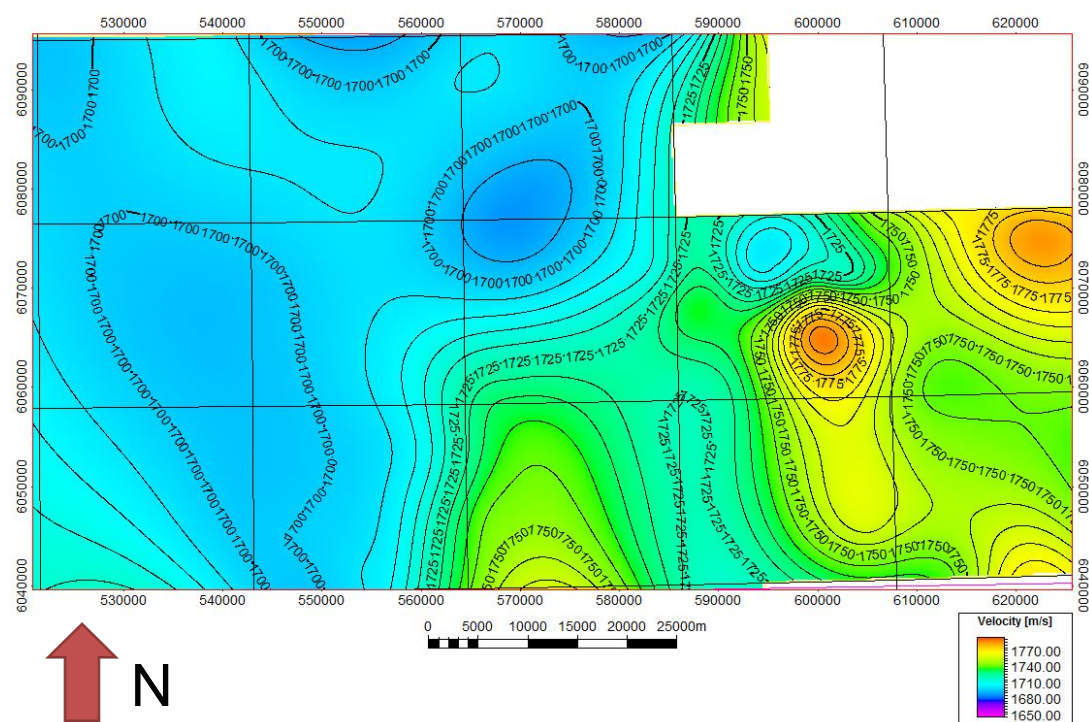


Figure 4.2: v_0 map of the North Sea layer. v_0 at the wells is based on the $v_{int} - z_{mid}$ method, while convergent interpolation is used to make the map.

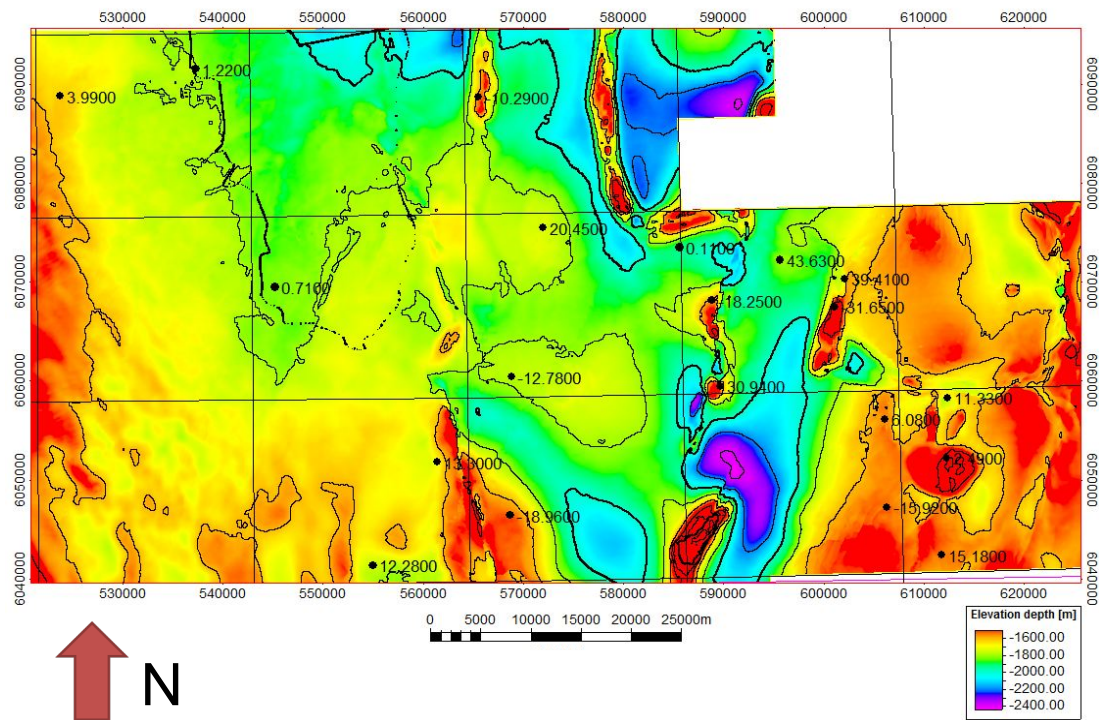


Figure 4.3: Depth map, with the residuals at each well.

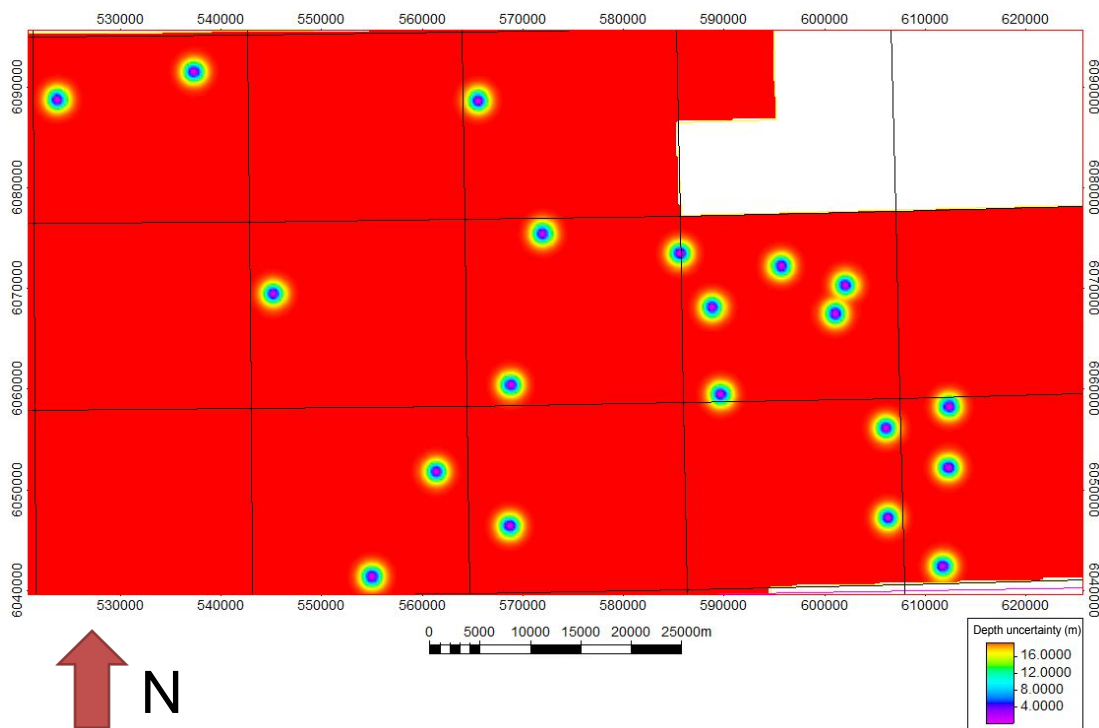


Figure 4.4: The depth uncertainty map based on the well residuals method.



5. GRV uncertainty: Stochastic approach

The uncertainty in the gross rock volume (GRV) can be large and even dominate the uncertainty in the recoverable reserves [24]. Therefore it is important to obtain good estimates of the uncertainty in this GRV. The GRV is determined by mapping the depth of the top of the reservoir (or caprock), and consequently assigning a thickness and a water contact to this reservoir. These three parameters all contain uncertainties, which have a large impact on the volumetrics. This report describes two approaches to model these uncertainties. The first approach is stochastic, and uses a sequential Gaussian simulation (SGS) to generate many different realisations of the reservoir. The second approach is deterministic and directly makes use of the depth uncertainty to model the GRV uncertainty. This chapter focuses on the stochastic approach. In the next chapter the deterministic approach is evaluated.

This chapter is divided into three parts. First the workflow of the stochastic approach is explained in Section 5.1. Thereafter two case studies are presented. The first case study is a domal structure with a constant hydrocarbon contact. The GRV uncertainty only results from the uncertainty in depth of the caprock. Section 5.2 estimates the GRV uncertainty of this structure with the SGS-method. Because the SGS-method relies on several input parameters which are not well defined, a sensitivity analysis is performed. In some cases the water contact or spill point is unknown. Therefore a second case study is performed in Section 5.3 on a structure in which the spill point varies for different constructed reservoir realisations. This case study also contains the option to include a thickness uncertainty.

5.1 Workflow

The prerequisite input for the SGS-method is a deterministic TD-converted top reservoir map z_{BC} , a top reservoir depth uncertainty map Δz , and the depth markers at the wells. The workflow is schematically presented in Figure 5.1, and consist of 4 main steps.

Step 1: Generating a surface realisation

The first step is to construct a possible surface realisation of the top of the reservoir. This is achieved by adding a random but spatially correlated depth error to the base case top reservoir depth map z_{BC} . The generated surface realisation can be defined as $z_{rel,n} = z_{BC} + z_{err,n}$, with $z_{err,n} = \Delta z \cdot z_{ran,n}$ (Figure 5.2). Here Δz is the depth uncertainty map, which was defined in the previous chapter as the Gaussian standard deviation of the depth. $z_{ran,n}$ is a randomly generated

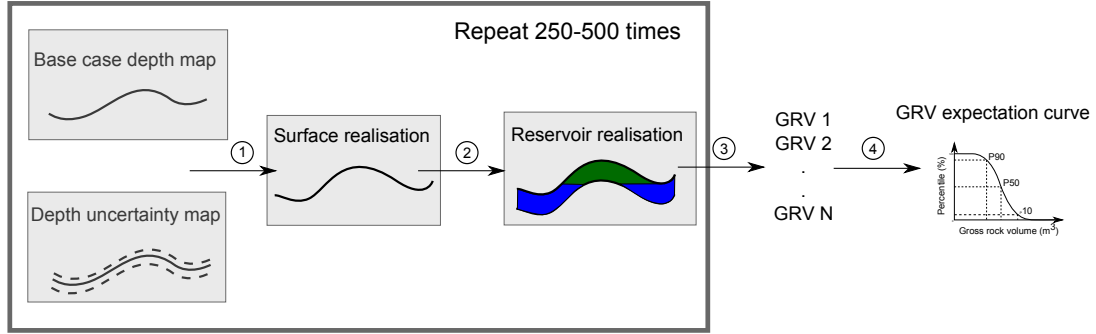


Figure 5.1: Workflow to stochastically calculate the GRV uncertainty in four steps.

map constrained by a sequential Gaussian simulation (SGS) algorithm. What we do by making $z_{err,n}$ is draw a random but correlated value from the Gaussian depth uncertainty map for each grid point, and add this to the base case depth. This way we obtain different surface realisation (Figure 5.3 schematically shows three of these surface realisations).

The difficulty of this method resides in constraining $z_{ran,n}$. SGS creates a random surface with a Gaussian distribution with predefined mean μ and standard deviation σ . The surface is correlated over a predefined range R , and tied to the wells. For a more thorough description of the SGS algorithm I refer to Deutsch & Journel [25]. Here follows a practical description to constrain $z_{ran,n}$.

Well tie: At the well markers the depth uncertainty is 0. To realise this we set $z_{ran,n} = 0$ at the wells. This implies that for Δz the non-well tied depth uncertainty map is used. Choosing for the well tie in $z_{ran,n}$ instead of in Δz ensures the smoothest surface realisation is created, by avoiding a 'bulls eye' error around the well.

Mean (μ): We define the mean depth uncertainty as 0. This implies the most likely depth (of each grid point) of the top of the reservoir is the base case depth. It also implies the chance of having a negative depth error is as large as having a positive depth error. If the mean error would not be 0, the base case depth map is not the most likely depth map. Therefore always keep the mean at 0. If for example the top of the reservoir is difficult to interpret, and the uncertainty in interpretation is not symmetric, solve this by running a deterministic TD-conversion for different interpretations. Figure 5.5a shows a $z_{ran,n}$ map with a mean of 0 and a mean of 0.5. The standard deviation of this map is 0.75. The map with a mean of 0.5 would overestimate the errors, and have a sharp bias.

Standard deviation (σ): The standard deviation of $z_{ran,n}$ determines the size of the errors. Figure 5.5b plots $z_{ran,n}$ with a standard deviation of 0.5 and 1, and a mean of 0. If the standard deviation is defined as 1 and the mean is 0, approximately 68% of each constructed $z_{ran,n}$ map has a value between -1 and 1. As this randomly generated map is multiplied with the Gaussian depth standard deviation map this would mean that 68% of the errors lie within 1 standard deviation of the depth uncertainty map. If the depth uncertainty map is defined as 1 standard deviation of the depth (as is the case in this report), the standard deviation of $z_{ran,n}$ should be 1. If the depth uncertainty map is defined as 2 standard deviations depth than the standard deviation of $z_{ran,n}$ should be 0.5.

Range (R): The range determines over what distance spatial fluctuations occur. Figure 5.5c

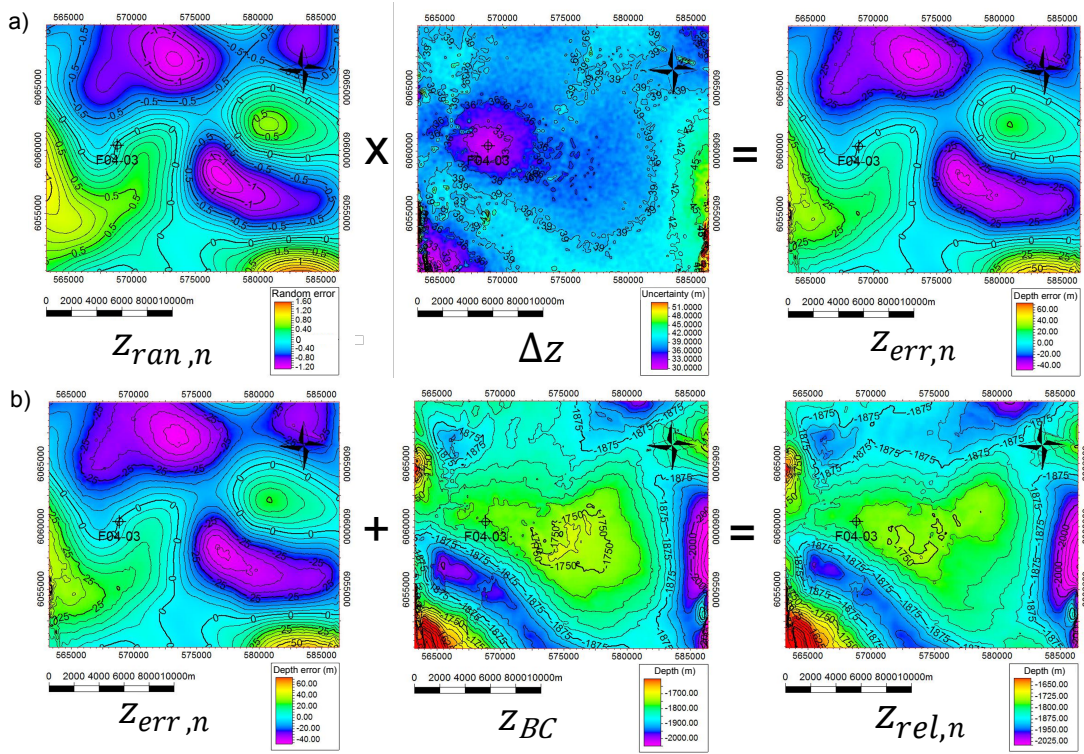


Figure 5.2: a) Process of making a depth error map. b) Process of making a random surface realisation.

shows $Z_{ran,n}$ for a range of 5 km and a range of 20 km (standard deviation of 0.75 and mean of 0). It would be realistic if the range of spatial fluctuations of the error is of the same size as spatial fluctuations of the surface itself. Therefore it is best to perform a variogram analysis to detect the range of top reservoir surface. Normally this range is in the order of 5-20 km [12]. Fluctuations with a very short range (10-100 meters) can be ignored in a GRV uncertainty analysis, because they average out.

Step 2: Generating a reservoir realisation

Once a top reservoir realisation is made, a thickness is assigned to the reservoir. This thickness can be either constant, or position dependent. The only input with which we can estimate the thickness of the reservoir, is the thickness of the reservoir at the wells. If only one well has been drilled in the area the thickness of the reservoir can be chosen equal to the thickness of the reservoir in the well. If there are several wells in the area an interpolation algorithm can be used to estimate the thickness in between the wells. The thickness of a reservoir is often assumed to be more or less constant [26]. If the thickness is measured at the wells, and deviations between wells are small the uncertainty can be ignored in the GRV uncertainty analysis. If large thickness variations are expected a thickness uncertainty can be included in the SGS algorithm by simply varying the thickness of the reservoir for different realisations.

The next step is to include a fluid contact in the reservoir. If the fluid contact is approximately known (f.e. from wells) it can be included in the model as a constant. If the fluid contact is unknown, and the structure is considered to be filled to the spill point, a spill point detection algorithm can be implemented. A spill point detection algorithm tries to find the spill point of each possible reservoir realisation, and implements the depth of the spill point as the fluid contact. To detect the spill point, first the regions where the spill point is possibly located have to be defined. In these regions the dip of each depth realisation is calculated. At the positions where

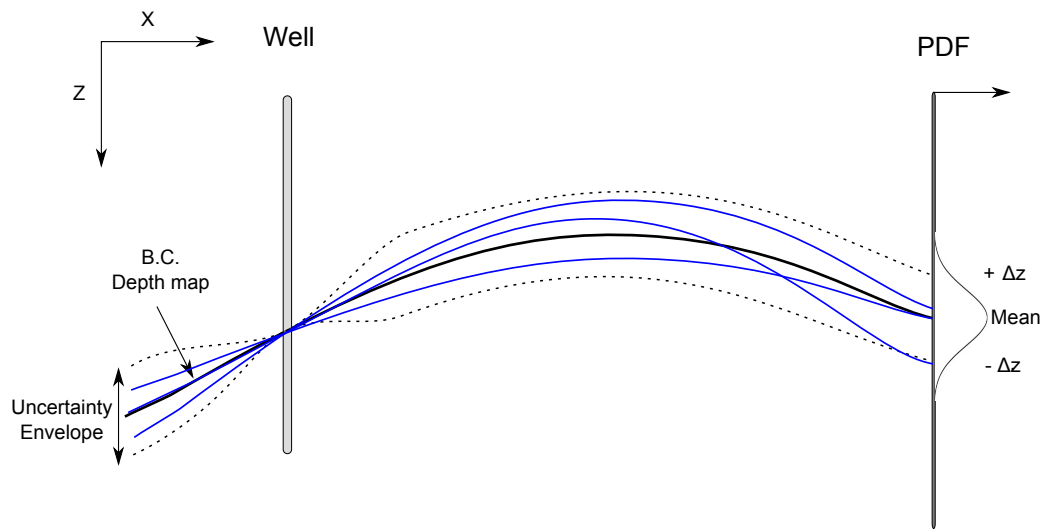


Figure 5.3: Schematic representation of the stochastic SGS method, with three different top reservoir realisations represented by the blue lines.

the dip is zero (saddle point), hydrocarbons will spill from the trap. The most shallow point where the dip is zero is then defined as the spill point. To avoid secondary saddle points each surface realisation is first smoothed. Note that to finally calculate the GRV of each realisation the non-smoothed reservoir realisation is used. If you do not assume the structure to be filled to spill point, a water contact uncertainty can be implemented simply by varying the water contact for each realisation.

Step 3/4: Making a GRV expectation curve

With a top reservoir, thickness, and fluid contact the GRV of each reservoir realisation can be calculated. The GRV's of all reservoir realisations are plotted in an expectation curve (Figure 5.4). This curve plots the percentage of realisations above a certain GRV. The 90th percentile (P90) is considered as a low case GRV, while the 10th percentile (P10) is considered as a high case GRV. These values are somewhat arbitrary, the 85th and 15th percentile could also be chosen as low and high case GRV.

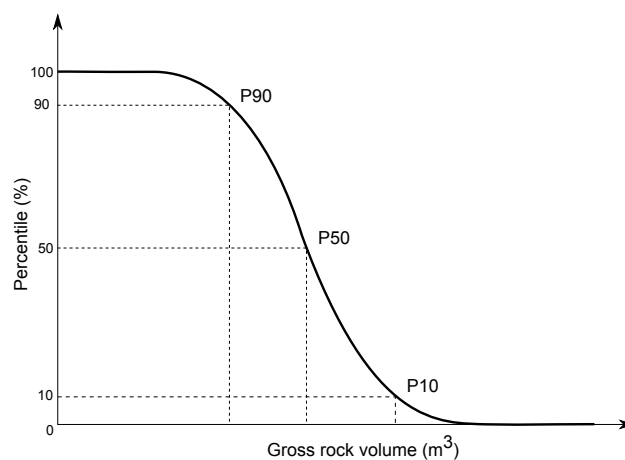


Figure 5.4: Schematic representation of a GRV expectation curve. High and low case can be defined as respectively the P10 and P90 of this curve.

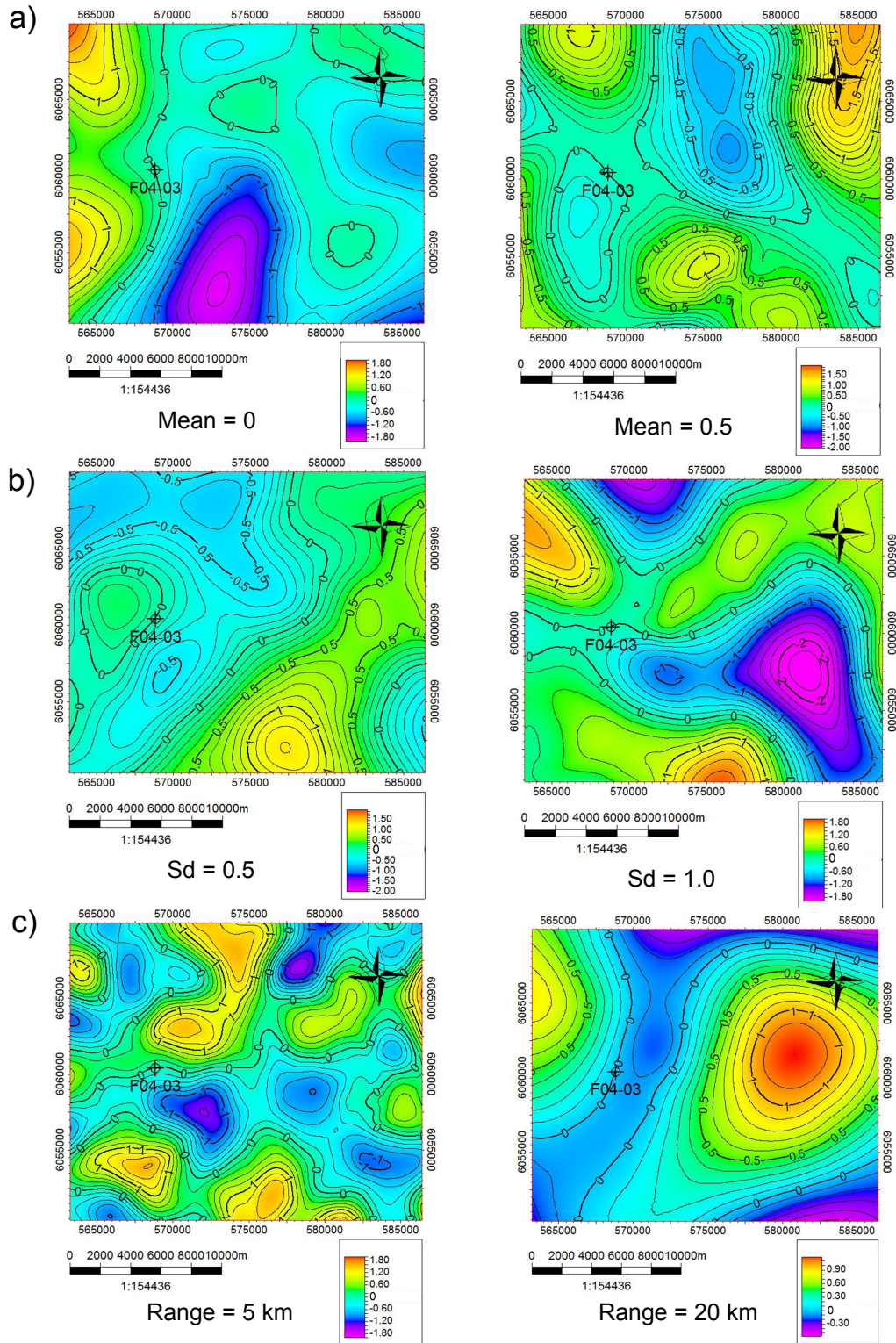


Figure 5.5: Variables in making $z_{ran,n}$ with SGS. a) The mean, b) The standard deviation, c) The range.

Advantages: The method gives a realistic volumetric estimate, assuming all surface realisations are equally likely. It is also possible to implement a variable spill point detection if no wells with fluid contact information are available.

Disadvantages: The method creates many surface realisations, and is therefore fairly laborious. Furthermore the method requires extra input parameters such as the variogram range, which is often poorly constrained and has a large influence on the outcome of the simulation.

5.2 Case Study 1: Updip potential in Chalk reservoir

The first structure on which the stochastic GRV uncertainty analysis is performed is a domal Chalk trap in the F4-block. The structure has been drilled on the flank by well F04-03 without encountering hydrocarbons. However the structure still contains updip potential. In this case study a stochastic TD-conversion is performed on the structure. The resultant depth and depth uncertainty map are used for a GRV uncertainty analysis.

Stochastic time depth conversion

The TD-conversion uses a 2-layer model, consisting of the Neogene Upper North Sea Group (NU), and the Paleogene Middle and Lower North Sea Group (NM+NL). The TWT of the base Upper North Sea group and base Middle+Lower North sea group (Top Chalk) were interpreted based the 3-D DEF seismic survey. Figure 5.6a shows the TWT of the top of the Chalk reservoir. The North sea layer on top of the Chalk functions as a sealing layer for this analysis. The TWT uncertainty map is made by using the process described in Section 3.2.1. The velocity, and velocity model that is used is the $v_0 - k$ VELMOD-2 model from TNO. The velocity uncertainty is included in v_0 .

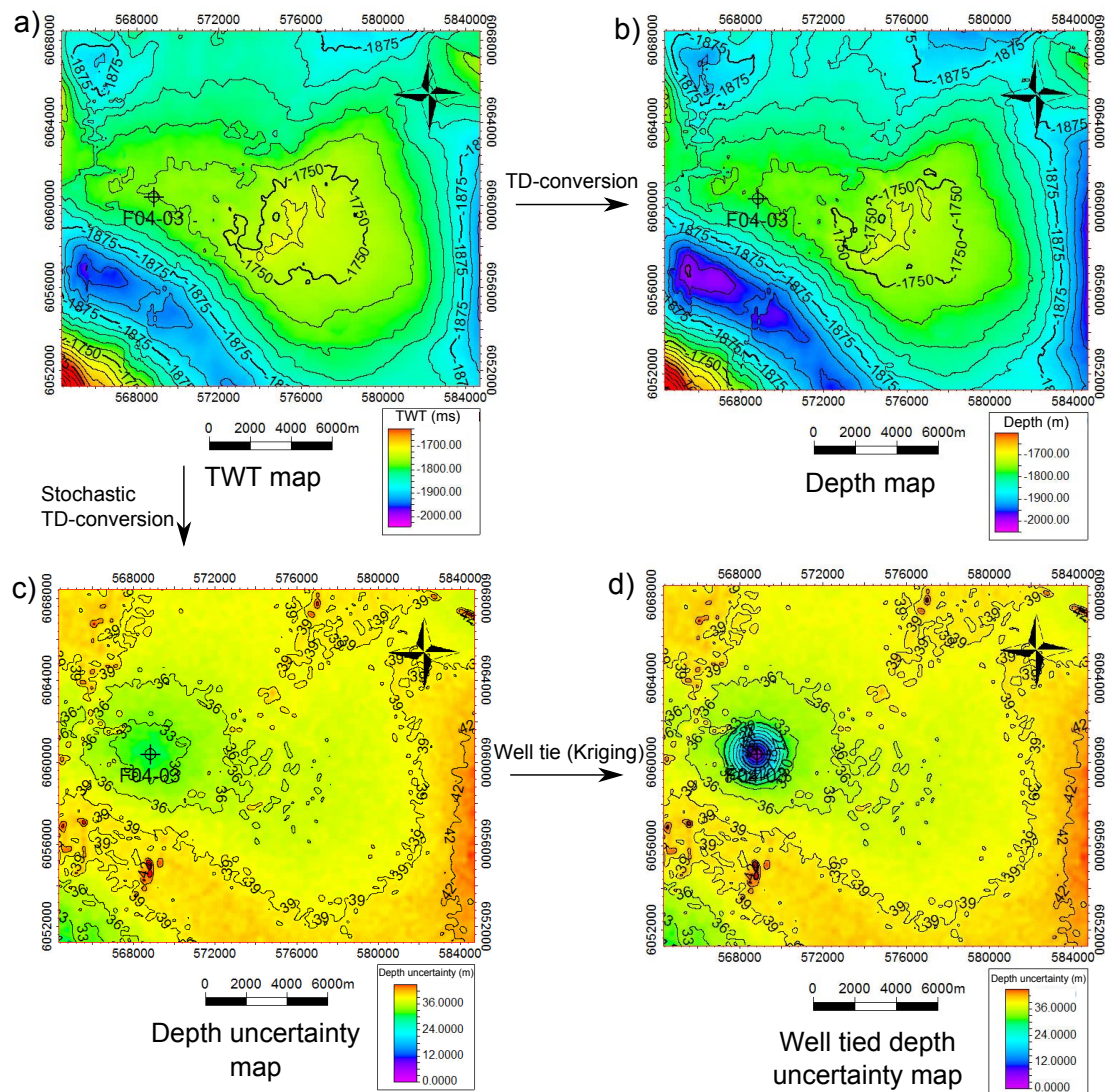


Figure 5.6: Top Chalk a) TWT map, b) Depth map, c) Depth uncertainty map, d) Well tied depth uncertainty map

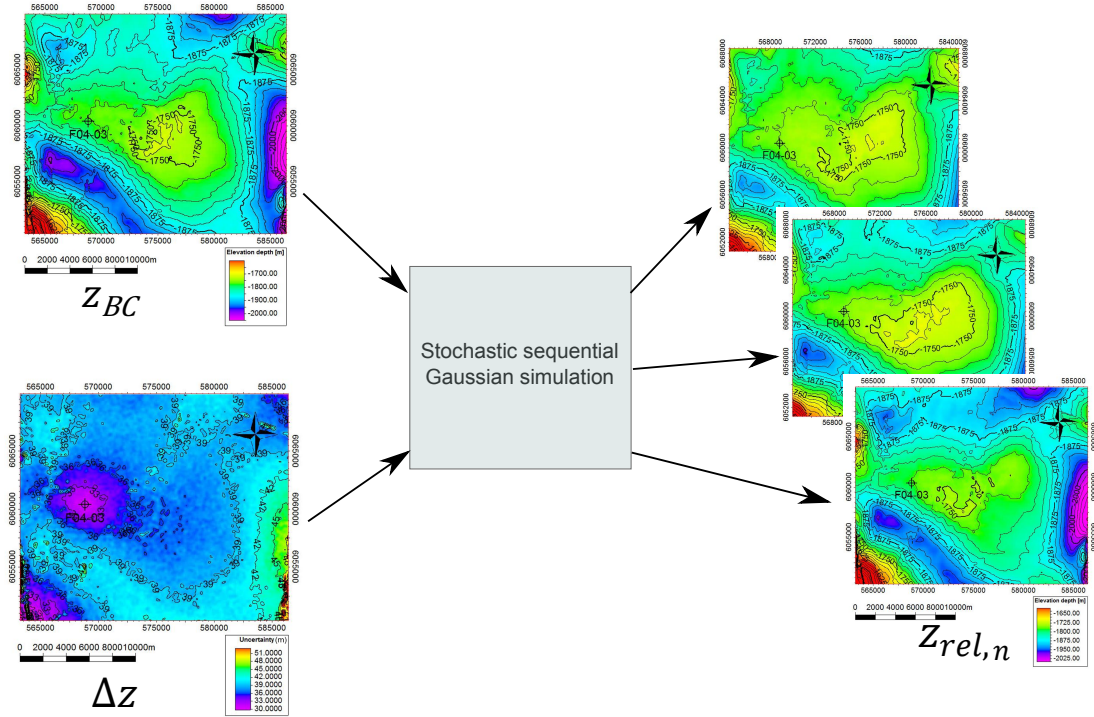


Figure 5.7: Three different surface realisations made with SGS.

The base case depth map resulting from a base case TD-conversion is shown in Figure 5.6b. The depth map shows that the structure contains an updip potential of around 50 m. The updip potential base case GRV of this structure is $1.89 \cdot 10^9 \text{ m}^3$, assuming the whole updip Chalk layer is a reservoir. With a stochastic TD-conversion the depth uncertainty map of Figure 5.6c is made. The non-well tied depth uncertainty varies mostly between 30 and 40 meters. The uncertainty map can be well-tied with a Kriging algorithm resulting in Figure 5.6d. The non-well tied depth uncertainty map will be used for the SGS, as the well tie is included in the SGS algorithm.

Sequential Gaussian simulation

With SGS the reservoir is simulated 500 times. Figure 5.7 shows three of these top reservoir realisations. The variogram range of the SGS map is 10 km. This is approximately equal to the variogram range of the depth of the structure itself. The fluid contact is constant in this simulation at the reservoir depth of the well (1789 meters). For each realisation it is assumed the whole updip Chalk layer is a reservoir. The GRV of each of these realisations was calculated and the results are plotted in an expectation curve (Figure 5.8). This gives a P90 GRV of $0.72 \cdot 10^9 \text{ m}^3$ and a P10 GRV of $5.30 \cdot 10^9 \text{ m}^3$. The P50 GRV is $2.61 \cdot 10^9 \text{ m}^3$ which is an overestimation of the base case GRV.

This immediately brings us to one of the side-effects of this method. Suppose we have a base case structure which is at some point flat at the hydrocarbon contact. This situation is depicted in Figure 5.9 a. Now with SGS a random depth error is added many times to create different surface realisations. In a lot of these realisations the error will cause the reservoir to be lifted above the hydrocarbon contact (Figure 5.9b). The method thus creates GRV, which causes a slight overestimation of the volumes. While in structures with large depth differences compared to the depth uncertainty this effect is relatively small, in flat structures (like this case study) with a relatively large depth uncertainty the effect can be larger. Therefore always be cautious and remember the difference between the base case GRV and the SGS P50 GRV. The base case GRV

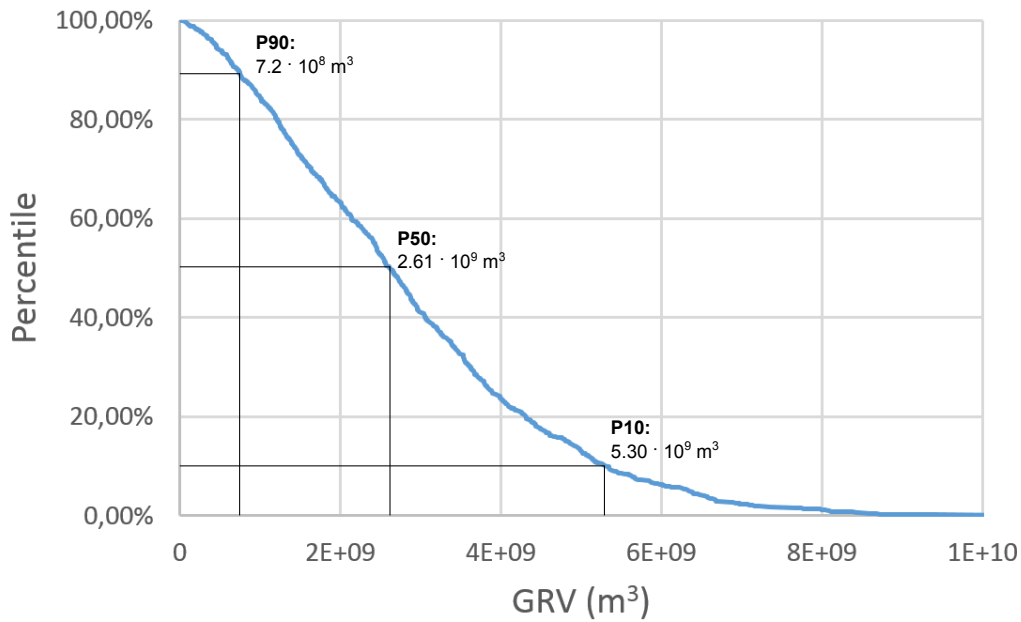


Figure 5.8: The GRV expectation curve for F04-03.

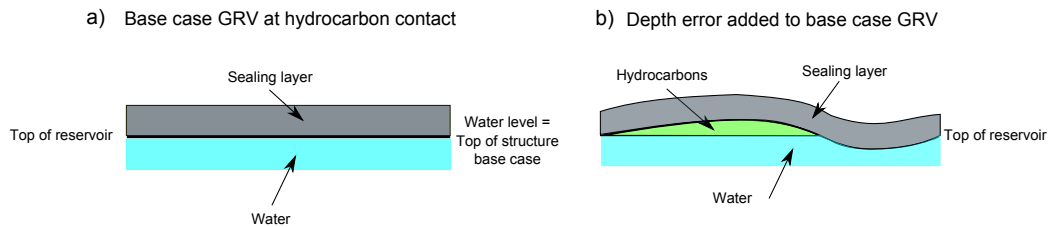


Figure 5.9: The side-effect of SGS. a) The base case GRV containing no hydrocarbons. b) A random surface realisations, which contains hydrocarbons.

is the most likely GRV, while the P50 volume is the volume with a 50% change that the actual volume is higher than the P50 volume.

5.2.1 Sensitivity analysis

In the SGS workflow we have made several assumptions. One of these assumptions is that the variogram range of the depth error is equal to the range of the surface itself. While this assumption seems correct, depth variations of the base case depth map can also take place on a different scale. Therefore the sensitivity of this range is tested. We have furthermore assumed in the process that our depth uncertainty map is correct. It is interesting to test what happens if the depth uncertainty is higher or lower than expected. A third variable, which is best to test first is the number of different reservoir realisations that have to be made to get a reliable GRV expectation curve. With this analysis we start.

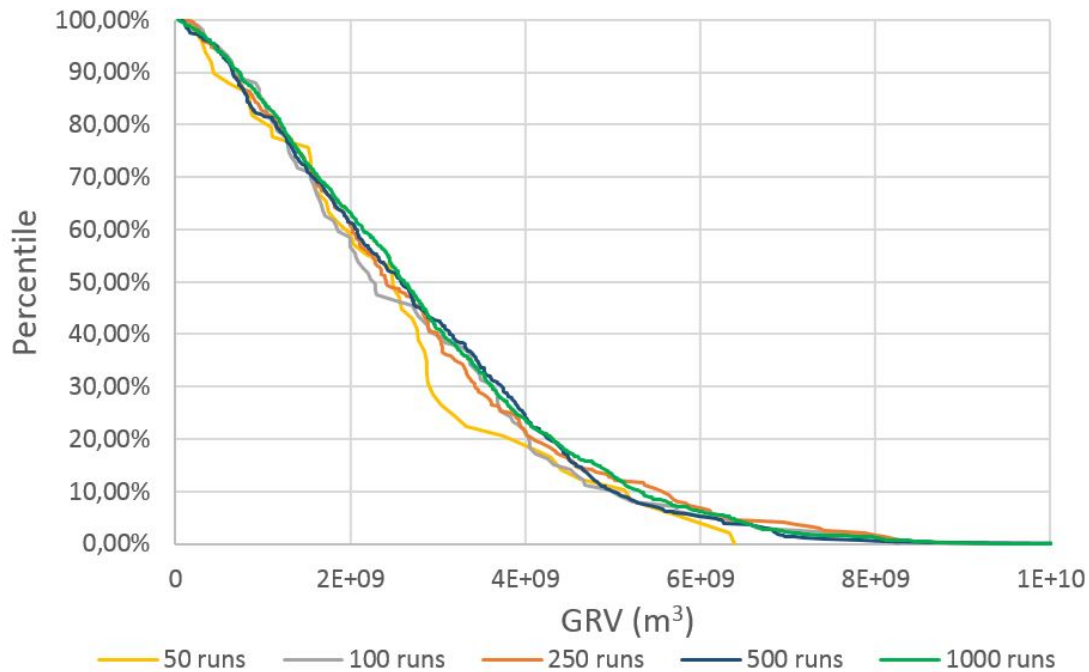


Figure 5.10: The GRV expectation curve plotted for different number of runs.

Number of runs

The number of runs determines the number of different reservoir realisations which are made. A higher number of runs gives in a higher accuracy of the results, but also requires more computation time. Therefore it is important to find a balance between having a good accuracy and a low computation time. Figure 5.10 shows the GRV expectation curve for varying number of runs. The expectation curve shows that 50 runs is clearly not enough. The experiment with 100 runs already gives a decent result, however it is still difficult to determine the best number of runs from this graph.

A better way to find the number of runs that would give a decent result, is to rerun the whole experiment several times with constant parameters, and look at variations of the P10, P50 and P90 of the expectation curve. The experiment is rerun 5 times, respectively with 50, 100, 250 and 500 runs after which the standard deviation (std) of the P10, P50 and P90 are calculated. This shows the variance if the experiment would be rerun. The result is shown in Table 5.11. A clear improvement of the experiment (lower std) is achieved by increasing the number of runs from 50 to 100, and from 100 to 250. The improvement of the std when increasing the number of runs from 250 to 500 is only small, while the increase in computation time is large. Therefore in the rest of the report the experiment is performed with 250 runs, unless stated different. It is furthermore remarkable from this table that the P90 std is much higher than the P50 and P10 std. The P90 GRV of this case study is very low. Therefore the percentage std is high.

# Runs	50	100	250	500
Std P90	24%	16%	13%	11%
Std P50	9%	6%	4%	3%
Std P10	7%	6%	3%	4%

Figure 5.11: The standard deviation of the P10, P50 and P90 for different number of runs.

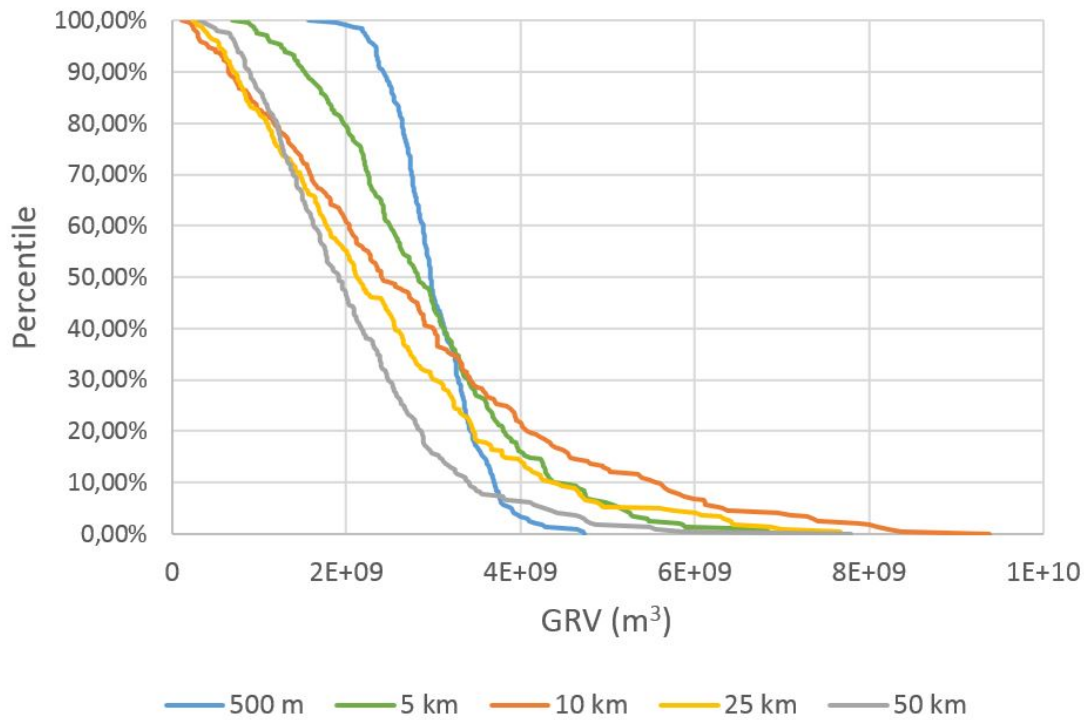


Figure 5.12: The expectation curve for different ranges of the SGS algorithm.

Range

A very important variable which is difficult to constrain is the variogram range of the SGS algorithm. Figure 5.12 shows the GRV expectation curve for different variogram ranges. This graph shows the extent to which the variogram range influences the GRV expectation curve. To get a better view on the effect of the range on the expected high (P10), low (P90) and mid (P50) case GRV, these cases are plotted against the range in Figure 5.13.

The domal trap structure is 5-10 km in diameter. For a small variogram range (500 m - 1 km) compared to the trap size, the uncertainty is low. Depth variations from the base case occur on small distances, which means they average out for the GRV expectation (Figure 5.15 a). The highest uncertainties are found in the mid-range (5-30 km's). The depth variations from base case take place over the same distance as the structure itself, causing large uncertainty (Figure 5.15 b). For very large ranges the depth errors from the base case change slowly. As at the well the depth uncertainty is 0, this means that the structure close to a well also has a lower uncertainty (Figure 5.15 c).

Apart from the high and low case Figure 5.12 also shows that the P50 changes with the variogram range. A smaller range gives a higher P50. In a relatively flat structure, where the range is much smaller than the horizontal size of the structure, in many of the modeled realisations some parts of the structure will be uplifted by the depth error above the water contact, as shown in Figure 5.9. Therefore the P50 is relatively high for low ranges. This effects is only significant if the depth uncertainty is of the same order of magnitude as the structure itself. Figure 5.14 shows that if we decrease the depth uncertainty by a factor 2 that this effect is much smaller.

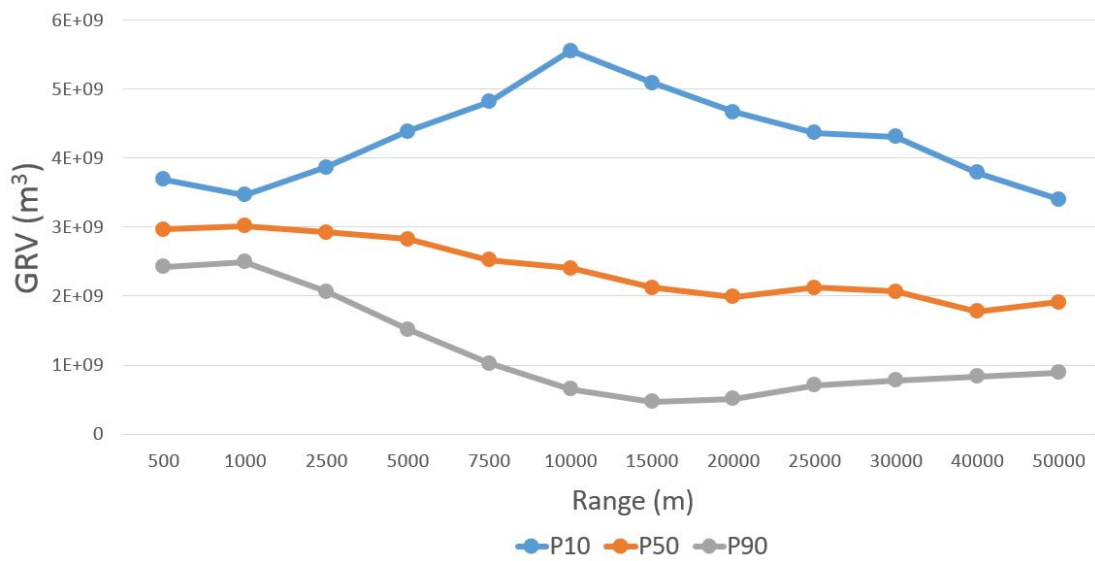


Figure 5.13: The P10, P50 and P90 for different ranges.

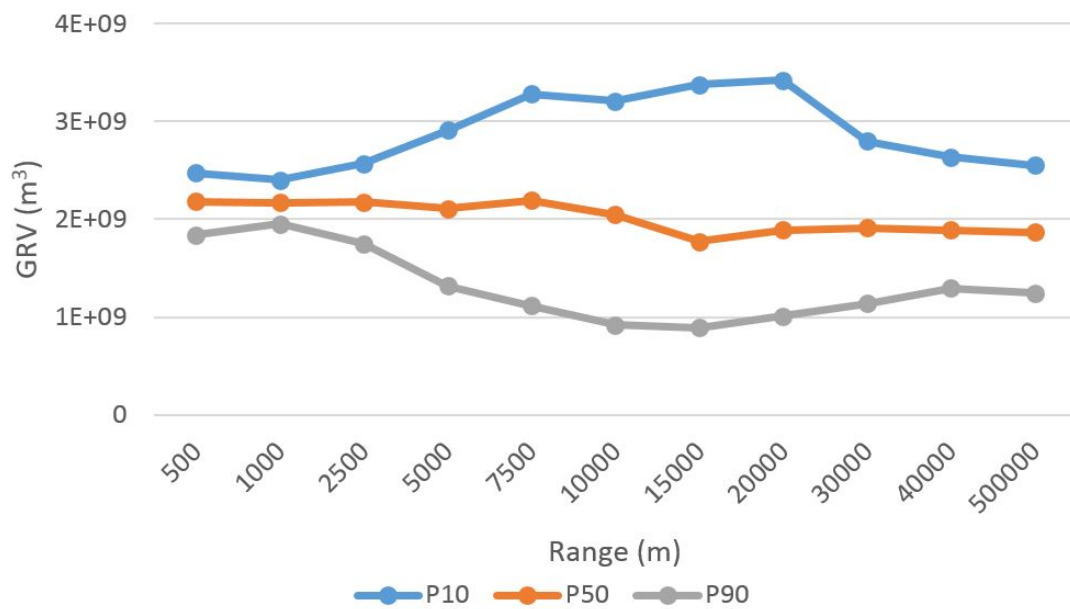


Figure 5.14: The P10, P50 and P90 for different ranges. The depth uncertainty map is divided by 2. This graph shows that the P50 GRV of does not change with range if the depth uncertainty is relatively small compared to the structure.

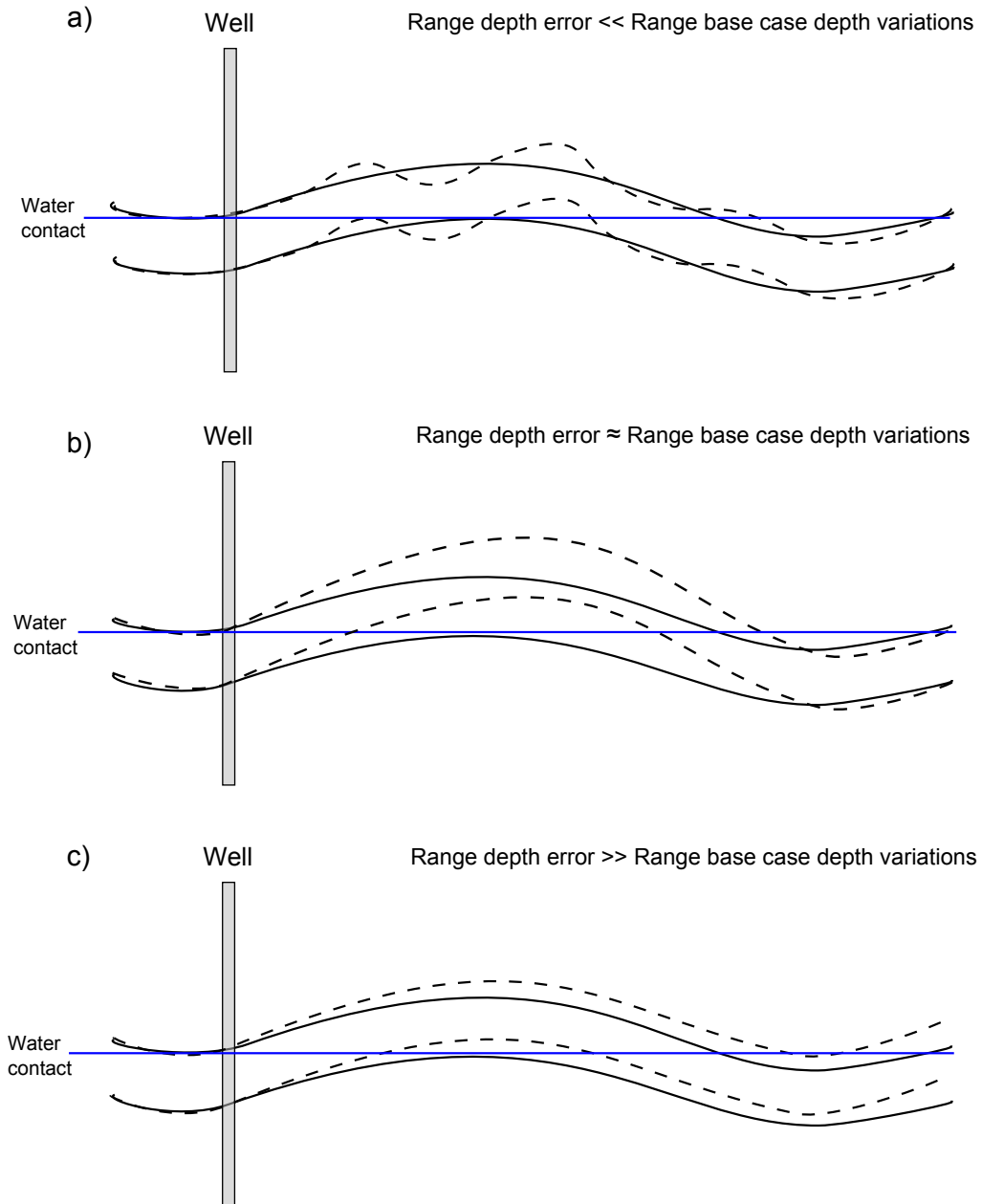


Figure 5.15: Schematic representation of reservoir realisations made with a different variogram range of the depth error. The solid black line represents the base case reservoir, while the dashed line represents a possible surface realisation. The blue line represents the water contact a) A small depth error range compared to the size of the structure itself results in a small GRV uncertainty. b) A depth error range in the order of the structure itself results in a high GRV uncertainty. c) Larger ranges again result in a lower GRV uncertainty.

Standard deviation/depth uncertainty map

In the SGS algorithm the standard deviation of $z_{ran,n}$ is set to 1. This way the depth uncertainty map represents the 1 STD depth uncertainty. This depth uncertainty map is based on several assumptions. Therefore it is good to investigate the sensitivity of the GRV uncertainty on the depth uncertainty map. We do this by scaling the depth uncertainty map by a constant c before running the experiment, such that $\Delta z_{scaled} = c \cdot \Delta z$. Figure 5.17 plots the GRV expectation curve for different c . A lower depth uncertainty conveniently results in a lower GRV uncertainty. With a higher depth uncertainty the P50 is overestimated.

Figure 5.16 plots the GRV P10, P50 and P90 against c . We see that P10 linearly increases with the depth uncertainty. The P90 also shows a linear trend up to a certain minimum (with a c of around 1 in this example). The P50 increases for a $c > 1.4$ due to the effect shown in Figure 5.9. This effect also results in a slight increase of the P90. The P10 linearly increases with c . We can conclude from this that you have to be cautious with using the SGS-method with a high depth uncertainty.

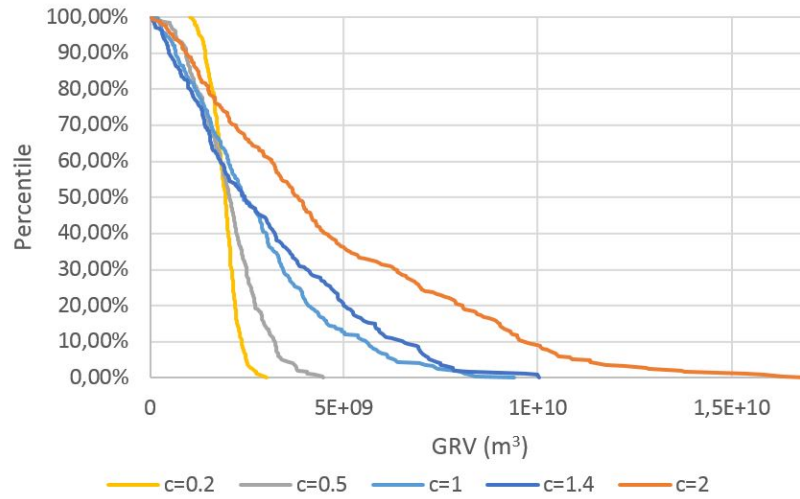


Figure 5.16: GRV expectation curve plotted for different c , where c represents the factor with which the depth uncertainty map is scaled ($\Delta z_{scaled} = c \cdot \Delta z$).

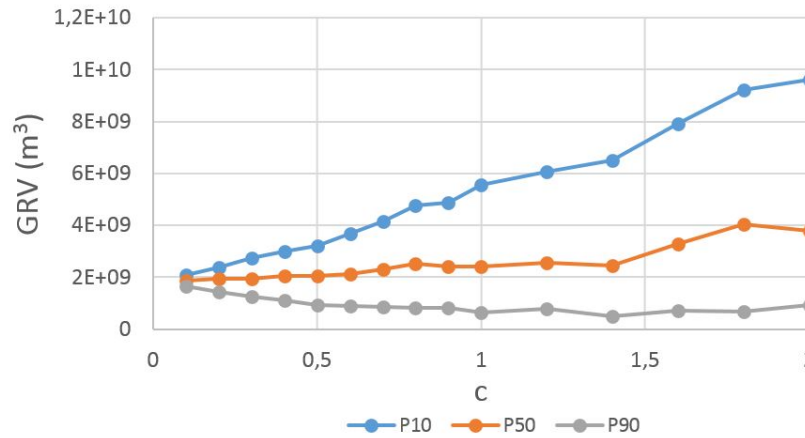


Figure 5.17: P10, P50 and P90 plotted for different c , where c represents the factor with which the depth uncertainty map is scaled ($\Delta z_{scaled} = c \cdot \Delta z$).

5.3 Case study 2: Volpriehausen dome with varying spill point

The second case study assesses the GRV uncertainty of a structure with an unknown water contact. In this case study a variable spill point algorithm is implemented to detect the water contact of each reservoir realisation.

Stochastic TD-conversion

The structure is a large domal Lower Volpriehausen sandstone reservoir structure in the F1 block deposited during the Lower Triassic. The structure has a diameter of approximately 15 km in North-South direction by 10 km in East-West direction. The thickness of the reservoir is approximated (from wells) between 45-55 m. Figure 5.18a shows an interpreted TWT map of the top Lower Volpriehausen sandstone structure. The interpretation of the TWT of the Volpriehausen and overlying layers is based on the 2013 3-D seismic DEF survey. The structure was drilled in 1971 by well F04-01 and was reported dry. However for the purpose of this case study, which functions as a showcase for the methodology we will assume it is filled to the spill point. Furthermore it is assumed that the layer on top of the Volpriehausen and the faults in the Eastern part of the structure are sealing.

The velocity model that is used for TD-conversion is the VELMOD-2 model. A three layer model containing the North Sea layer, Chalk layer and Trias layer is used for TD-conversion resulting in the depth map of Figure 5.18b. Stochastic time depth conversion was used to determine the uncertainty in the depth of the layers. Figure 5.18c and d show the non-well tied and well tied depth uncertainty map from stochastic time depth conversion. The non-well tied depth uncertainty map is used in the GRV uncertainty analysis. The base case GRV is $5.88 \cdot 10^9 \text{ m}^3$.

Sequential Gaussian simulation with variable spill point

The spill point of this structure depends on the TD-conversion. To calculate the GRV uncertainty 500 reservoir realisations are made with the SGS-method, each with a different spill point. To determine the GRV, first the spill point of each structure must be detected. While this can be done manually, it is much more efficient if an automatic spill point detection is made.

To make a spill point detection algorithm we first assign the regions in which the spill point could possibly be located. The TWT map of the top of the reservoir is used for this. Figure 5.18a shows the three possible locations of the spill point. For each region the depth of the saddle points is detected by looking for the dip minima/saddle points. The shallowest saddle point is the spill point.

To test the accuracy of this method 30 spill points have been identified both manually and with this algorithm. The average depth error of the spill point with this detection mechanism is 5 meters, but as the error sometimes gives a deeper spill point and sometimes gives a shallower spill point the effect of this error on the GRV uncertainty is much smaller. On a large structure with a potential hydrocarbon column of several 100's of meters the spill point algorithm gives a similar result as a manual detection.

After the algorithm was tested 500 runs were performed and the location of the spill point was detected in each run. Figure 5.19 shows the position of the spill point for 500 runs. The most likely location the spill point is in the South of the structure (68.8 %). The chance that the spill point is located in the West is 31.2% .

The GRV expectation curve of the 500 runs is plotted in Figure 5.20. The P90 and P10 volume are respectively $4.81 \cdot 10^9 \text{ m}^3$, and $6.51 \cdot 10^9 \text{ m}^3$. The uncertainty is much smaller than in the previous Chalk structure. That is because the size of this structure is much larger compared to its uncertainty. The P50 GRV is $5.88 \cdot 10^9 \text{ m}^3$ and is comparable to the base case GRV.

As stated in the introduction of this chapter, apart from a reservoir depth uncertainty (and

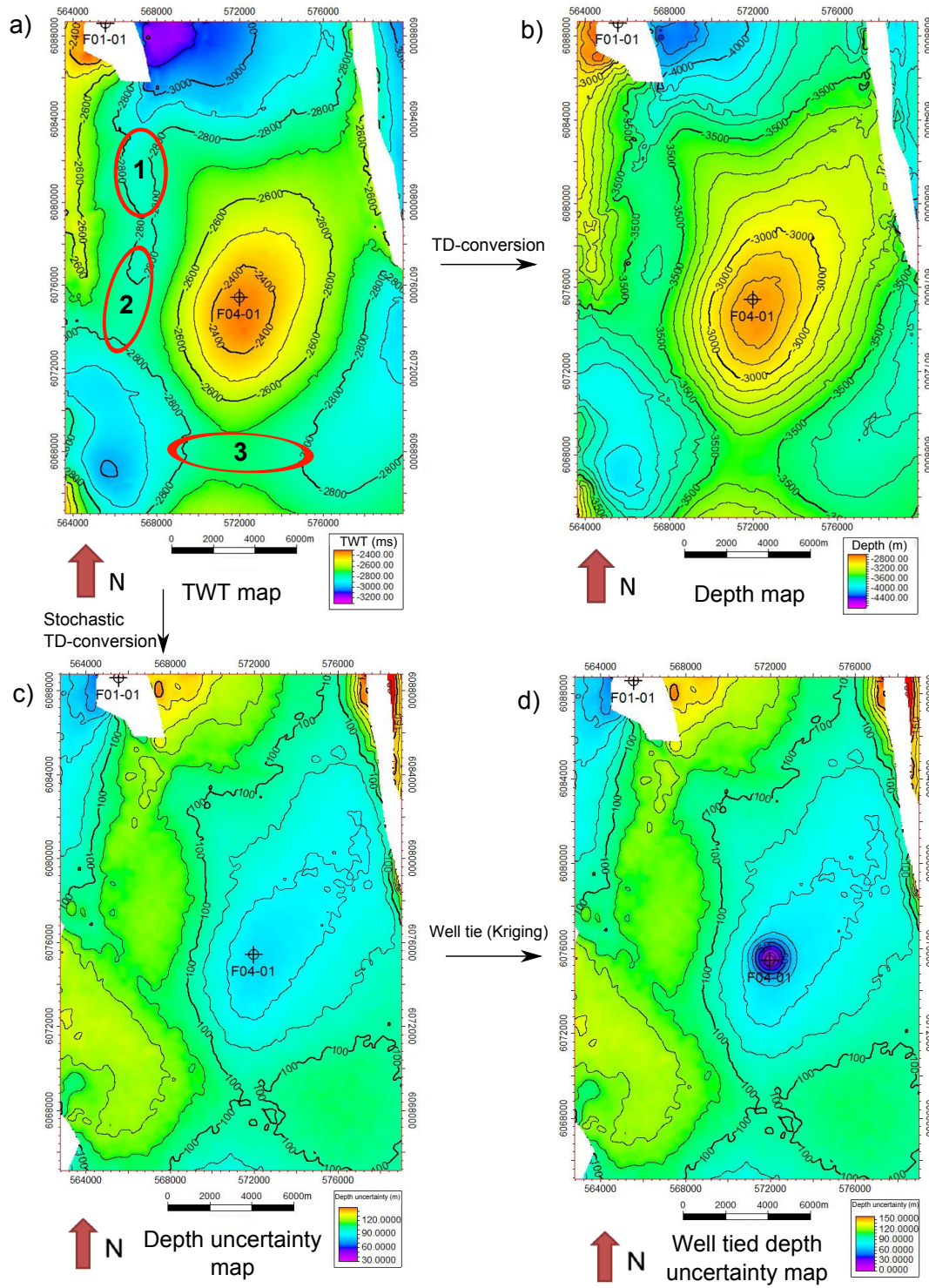


Figure 5.18: Top Volpriehausen a) TWT map with the possible locations of the spill point, b) Depth map, c) Depth uncertainty map, d) Well tied depth uncertainty map

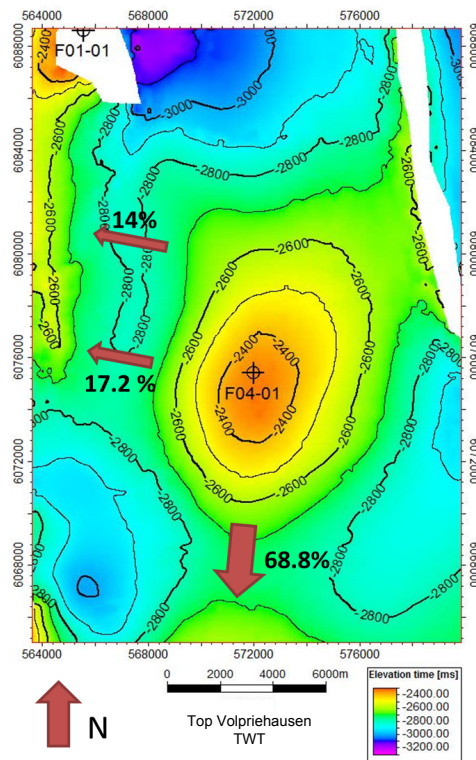


Figure 5.19: Location of the spill point of the 500 SGS reservoir realisations.

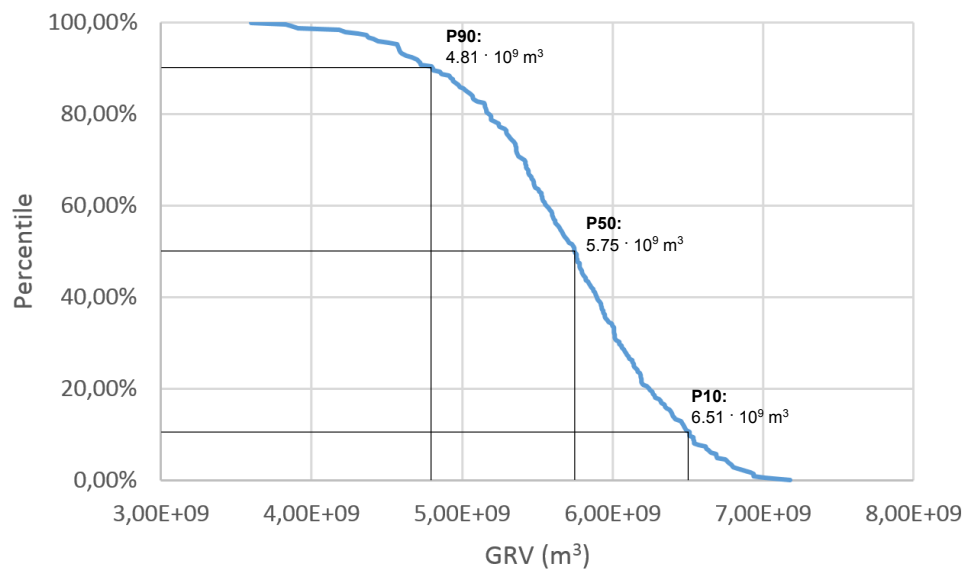


Figure 5.20: GRV expectation curve of structure of F04-01.

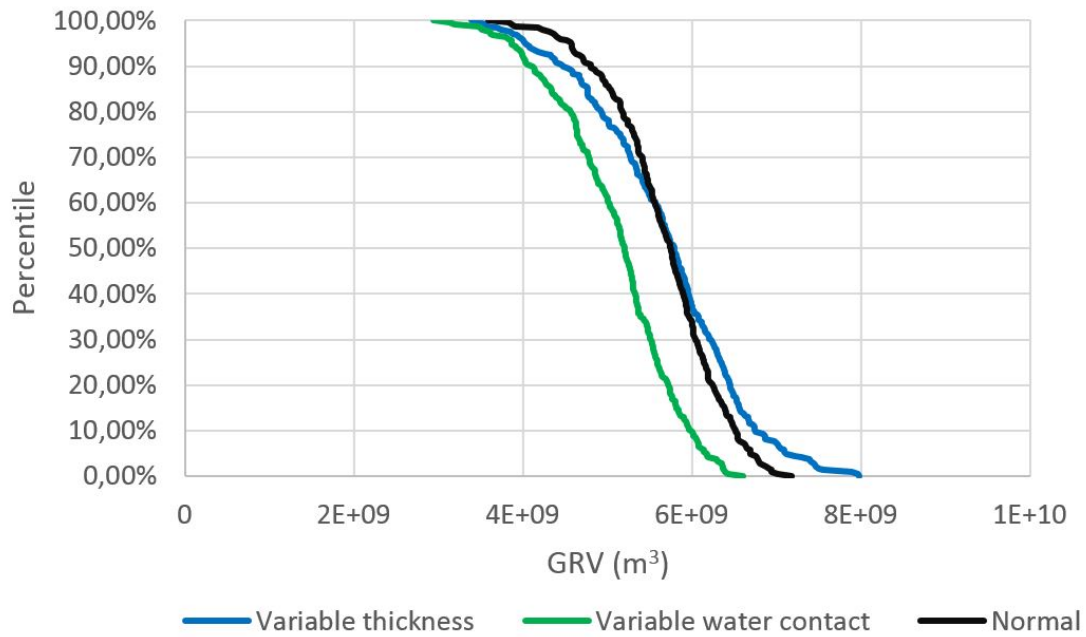


Figure 5.21: GRV expectation curve of structure of F04-01 which shows the effect of including water contact uncertainty (maximum 100 meters) or GRV uncertainty (maximum 10 meters).

shape of the GRV) there can also be uncertainty in the water contact or the thickness of the reservoir. we will look at the effect of both. Up till now it is assumed the water contact of each realisation is at the depth of the spill point. We could also assume that the water contact is within 100 meters of the depth of the spill point. In this example a block PDF describes the distribution. This implies that the chance that the water contact is f.e. 30 meters above the spill point is equal to the chance that the water contact is 90 meters above the spill point. The water contact however is always above the spill point and within 100 meters of the spill point. The GRV expectation curve is shown in Figure 5.21. As expected the total GRV is lower in this example than if we assume the structure is filled to spill point.

To add an uncertainty in the thickness again a block PDF is used, such that each reservoir realisation has a different thickness. The range of the thickness uncertainty we take between -10 and 10 meters. The result is shown in Figure 5.21. This time we see that the uncertainty (P90 and P10) increases compared to the situation with no thickness uncertainty, while the P50 stays approximately constant.



6. GRV uncertainty: Deterministic approach

While the SGS-method gives a well-based estimate of the GRV uncertainty, it does have several disadvantages. Several extra input parameters are required, and the process takes a fair amount of time. Therefore for a quick view on the GRV uncertainty it might be better to use a more straightforward method, which does not require the extra input. The *plus-minus method* offers just this. In Section 6.1 the workflow of this method is described. Thereafter in Section 6.2 this method is used on the Chalk structure in the F4 block, described in the previous chapter.

6.1 Workflow

The only required input for the plus-minus method, is the base case depth map and the well tied depth uncertainty map. Furthermore for this method it is required that the fluid contact is known, or assumed to be a known constant. The high case depth (corresponds to P10 volume) is defined as $z_{HC} = z_{BC} + \Delta z \cdot c$, while the low case depth (corresponds to P90 volume) is defined as $z_{LC} = z_{BC} - \Delta z \cdot c$ (see Figure 6.1). Again Δz is the depth uncertainty map, and c is a constant. If $c = 0$ the base case GRV is obtained. The difficulty lies in establishing a c -value that defines the high and the low case. While the c -value can be calibrated with the SGS method this would require extra effort with no use if you would have to do this. Therefore we will try to give you a realistic estimate of the size of c . Remember that this method can only be used for a first order estimate of the GRV uncertainty.

Advantages: The method is very simple to implement once the depth uncertainty map is available. Aside from the depth uncertainty map no extra input is needed to calculate the GRV uncertainty.

Disadvantages: An estimate must be made of the c -value that defines the upper and lower case GRV. A good estimate requires calibration with the stochastic SGS method. Another disadvantage is that this method can only be used when the water contact is known or assumed constant.

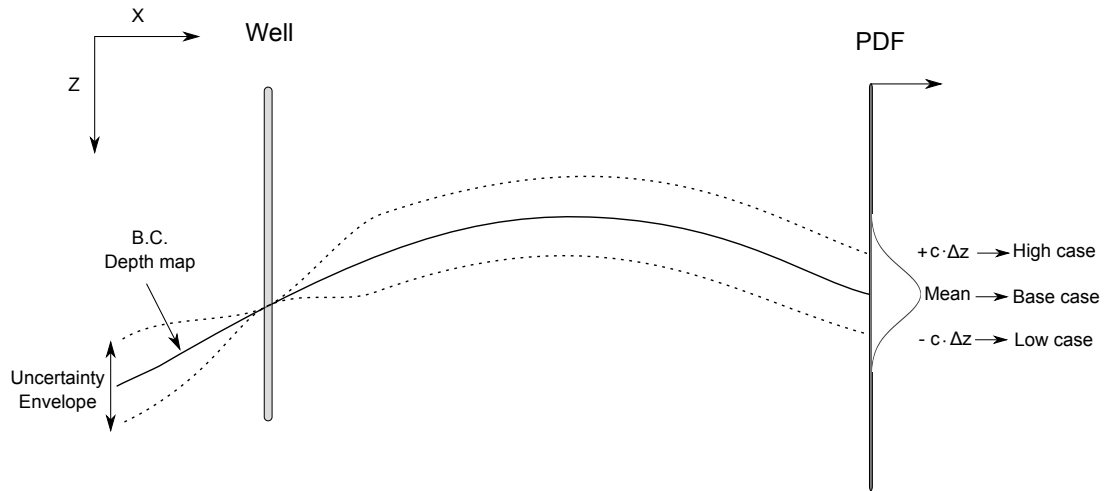


Figure 6.1: Schematic representation of the plus-minus method.

6.2 Case study

To compare the results of the SGS-method and the plus-minus method we use the Chalk structure of the F4 block again. While the SGS-method had the well tie included in the SGS algorithm, this time the depth uncertainty map itself has to be well tied. The best way to compare the SGS-method results with the plus-minus method results is to plot the GRV against the c -value of the plus-minus method. The result is shown in Figure 6.3. If $c = -0.53$, the P90 case of the SGS-method is obtained (Figure 6.2a). A c of 0.89 gives the P10 case (Figure 6.2c), while a c of 0 gives the base case. Now of course if you need to calibrate this method with the SGS-method for each specific case, this method makes itself dispensable. Therefore this method should not be used to make a realistic GRV uncertainty estimate. Because of its swiftness it *can* be used to get a first order estimate of this uncertainty. By looking at the GRV uncertainty resultant from the plus-minus method with a c -value between 0.5 and 1.0, the size of the uncertainty can be observed. Thereafter it can be decided if it is worthwhile to perform a stochastic GRV uncertainty analysis with the SGS-method to get a more accurate estimate.

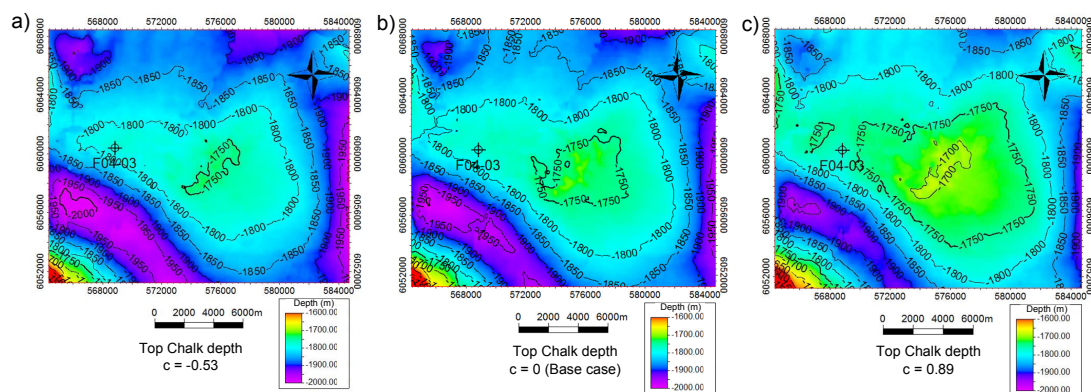


Figure 6.2: The top Chalk depth map of the a) Low case, b) Base case, and c) High case.

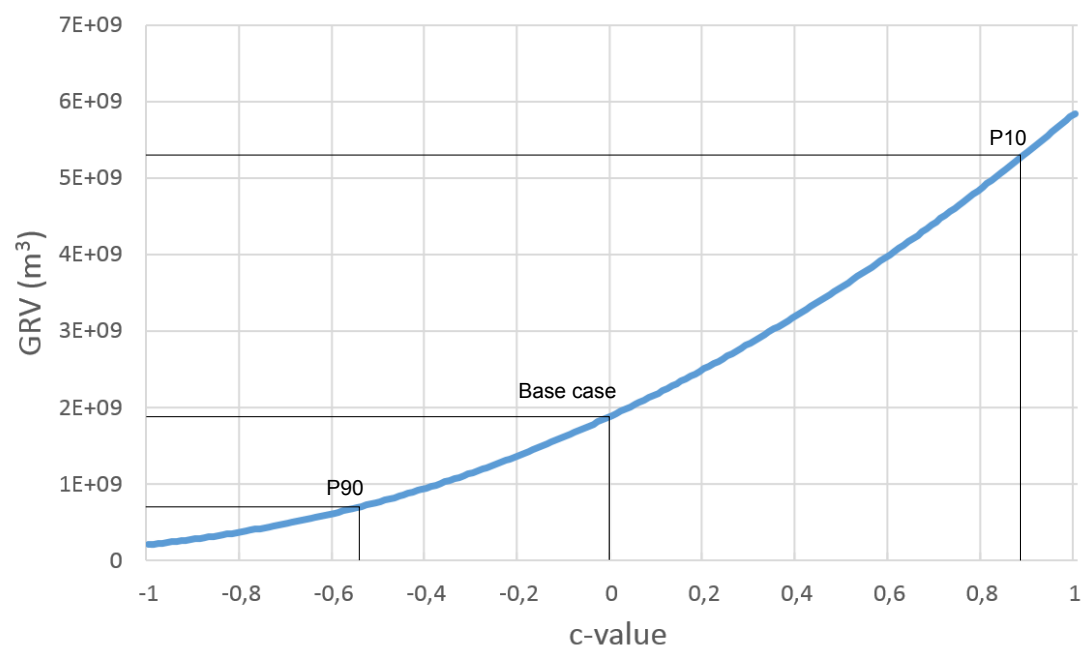
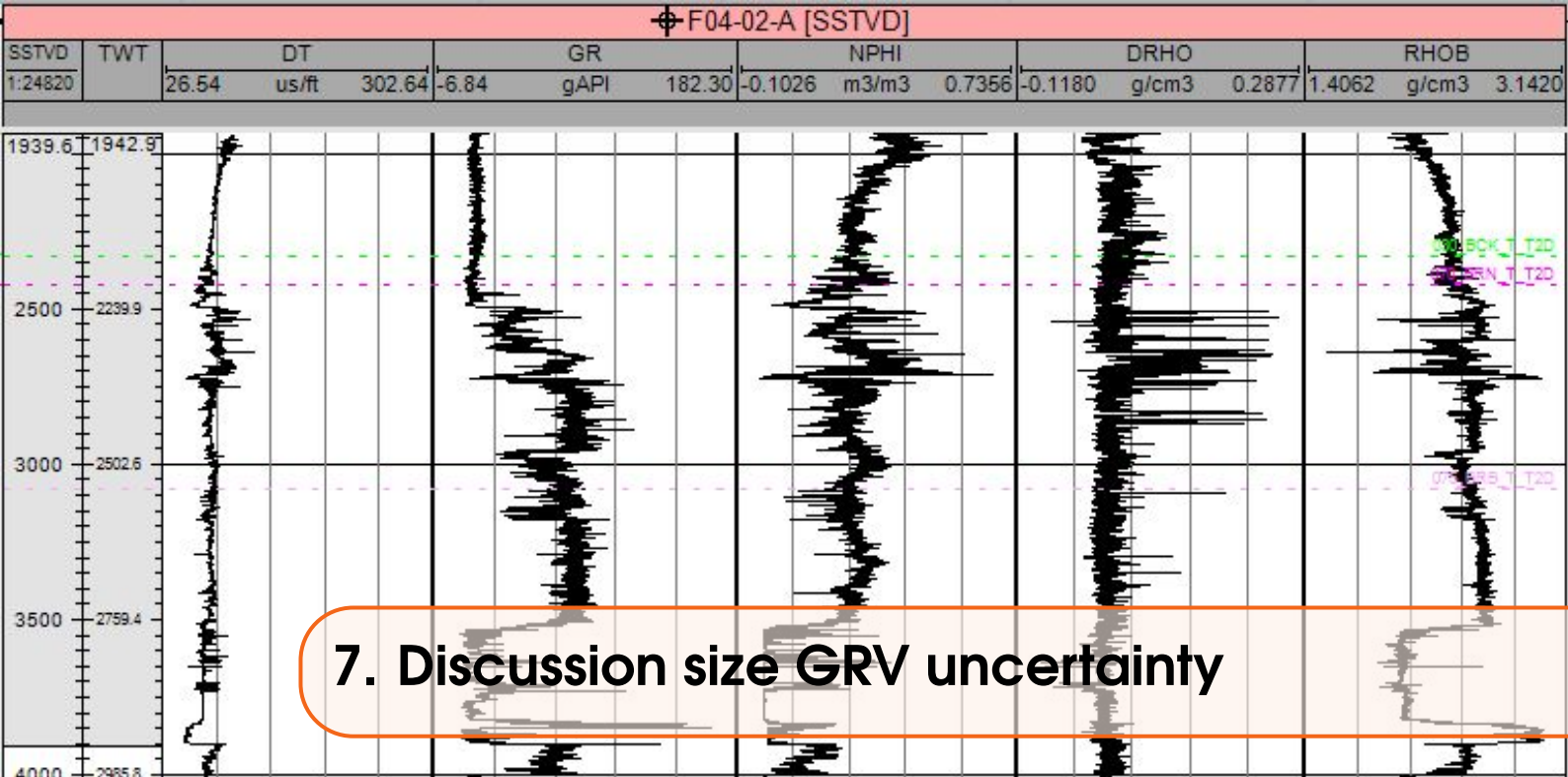


Figure 6.3: GRV plotted against the c -value.



While the GRV is an important part of the total volume of hydrocarbons initially in place (hiip), there are several other parameters involved in this calculation. The hiip is defined as:

$$HIIP = GRV \cdot N/G \cdot \Phi \cdot (1 - S_w), \quad (7.1)$$

with N/G the net/gross ratio of the formation, ϕ the porosity, and S_w the water saturation. These parameters all contain uncertainty. The size of these uncertainties is case dependent. This chapter shortly describes how to rank the uncertainty in GRV compared to the other variables.

We know how a high and low case is made for the GRV. A similar analysis should be performed on the porosity, N/G and water saturation to determine a high and low case scenario. The N/G ratio is the proportion of the GRV formed by the reservoir rock. The N/G varies between 0 and 1. Often stochastic modeling algorithms are used for facies modeling [28]. Input comes from well data (if available) and geological interpretation. These algorithms create multiple realisations of facies architecture by changing random seed numbers. The input parameters (f.e. fraction of shale) should also be varied to quantify the uncertainty for lack of knowledge of the facies. From this facies modeling a high and low case scenario can be obtained.

The porosity uncertainty comes from two sources. The porosity is measured at the well. The logging tool measurement and processing contains uncertainty however. Furthermore the porosity changes inside the reservoir. Both these uncertainties have to be accounted for. Several techniques for determining the porosity distribution in the interwell areas exist. These techniques include interpolation between well positions, kriging based on geological facies-based modeling and the use of seismic attributes of porosity to constrain the distribution in the interwell areas [29,30]. The uncertainty depends on the technique. Again from these techniques a high and low case porosity can be obtained. If no well is drilled in the reservoir yet, an estimate can often be made from reservoirs in the same lithostratigraphic layer at approximately the same depth in the area.

The water saturation is almost impossible to estimate without well data. The water saturation is calculated from open-hole resistivity measurements. Archie's equation is used to calculate the water saturation. However there is a considerable amount of uncertainty in the parameters of this equation [31]. These uncertainties should be estimated to get high and low case scenario's of the water saturation.

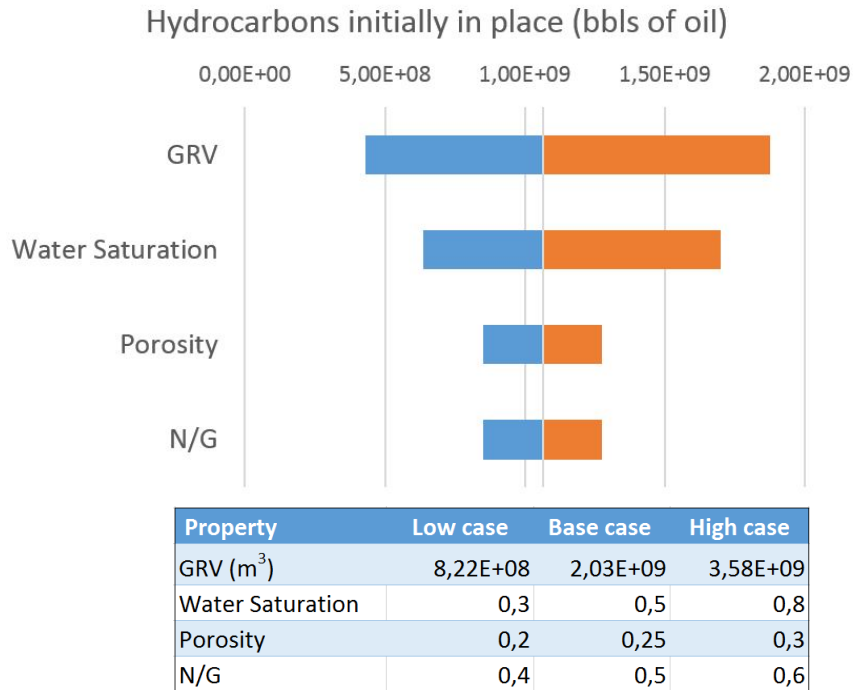


Figure 7.1: An example of a tornado plot showing the relevance of the uncertainty in GRV, porosity, N/G and water saturation

If an uncertainty analysis is performed on all these parameters the relative importance of the uncertainties can be plotted in a tornado plot. A tornado plot plots the influence of the uncertainty in each parameter on the hiip. For each parameter the high and low case scenario is taken, while keeping the other parameters values at the base case. Figure 7.1 shows an example of a tornado plot. The table contains the high case, low case, and base case values of the parameters. This plot functions to show how to grade the relevance of uncertainty of each parameter. In this example the GRV contains the highest uncertainty. To determine the total uncertainty in hiip often a simple Monte Carlo simulation is run. The PDF's of each parameter should be assigned first. Then a random value for each of the parameters is chosen from the PDF to make one possible hiip realisation. This process is then repeated 1000-2000 times. From the results a P10 and P90 hiip can be determined.



8. Recommendations

Recommendations on the depth uncertainty:

- Start the depth uncertainty analysis by looking at wells in the region. They can provide a lot of information on the cause and size of depth errors made in the past. Furthermore they provide information on the velocities in the subsurface.
- Make a good depth prediction of the top of the reservoir by interpreting the top of the reservoir and making a reliable velocity model (in case you use a multi-layer TD conversion). Check if the converted depth of the horizons agrees with the depth at the wells.
- Analyse the relevant uncertainties in TWT and velocity. This report can be used to quantify these uncertainties (Chapter 3). To check the significance of the uncertainty, it helps if you write down how large the uncertainties are compared to the parameter itself (e.g. a 2 ms TWT uncertainty at a TWT-depth of 2000 ms is irrelevant compared to a 100 m/s velocity uncertainty at a velocity of 2000 m/s).
- To obtain a good estimate of the depth uncertainty a stochastic time depth conversion (e.g. with Velsto) can be used. Use this method if you can make good estimates on the input uncertainty. Again this report (Appendix A) guides in the process.
- If there are a lot of wells drilled in the area, where you want to calculate the depth uncertainty, the well residuals method can be used to estimate the depth uncertainty (Chapter 4). Remember that this method does have a few significant shortcomings.
- Maybe the most important part of the whole depth uncertainty analysis is the quality check and interpretation. Always check if your depth uncertainty map gives a logical result. If you expect the depth uncertainty to be high due to complex geology, check if this is the case. If this is not the case take another look at the input you have used to make the map. If you have made a depth uncertainty map know what it represents (e.g. the standard deviation of the depth). Only then it can be used correctly.

Recommendations on the GRV uncertainty:

- The GRV depends on the depth of the top of the reservoir, the thickness of the reservoir, and the water contact. These parameters all contain uncertainties. In many cases the uncertainty in GRV is high and can even dominate the uncertainty in recoverable reserves [24]. Therefore an estimation of the size of the uncertainty is very important. The depth uncertainty map can be used to determine the GRV uncertainty.
- For a thorough GRV uncertainty calculation use the SGS-method (Chapter 5). This method can include spill point variations for the different surface realisations. Make a well based estimate of the parameters of the SGS algorithm (range, standard deviation, mean) as they determine the outcome. From this analysis a high and low case scenario GRV can be determined.
- A first indication of the size of the GRV uncertainty can be obtained with the plus-minus method (Chapter 6). A high and low case GRV are made by respectively adding or subtracting a scaled version ($c \cdot \Delta z$, with c between 0.5 and 1) of the depth uncertainty map to the base case depth map. For this method to work a constant (either known or estimated) spill point is needed. This method does not give a very accurate GRV uncertainty but it does give an indication of the magnitude. A good indication of the magnitude of the uncertainty is the size of the depth uncertainty compared to the vertical size of the trap structure. If these are of the same order the uncertainty is probably high.

Recommendations in general:

- In estimating uncertainties in general keep in mind that the input, determines the output. Therefore it is very important to know where the input comes from. The uncertainty is an estimation, as is the base case model.
- The uncertainty is linked to the model. Therefore the uncertainty can only be used for that specific model.



9. Conclusions

The hydrocarbon exploration phase contains a large number of uncertainties. If a potential reservoir has been identified from seismic, we need to know what the depth of the reservoir is, and what the potential amount of hydrocarbons inside the reservoir is.

To determine the depth of the reservoir, often a multi-layer TD-conversion is used. The different layers are interpreted and a velocity is assigned to each of the layers. The TD-conversion then converts the seismic data from the time domain to the depth domain. This method contains several uncertainties which also result in an uncertainty in depth. This report proposes two methods, a stochastic and a deterministic method, to determine the uncertainty in depth:

- 1) **Stochastic time depth conversion:** The uncertainty in TWT and in the velocities of the layers are estimated. A stochastic TD-conversion propagates these uncertainties to estimate a depth uncertainty. This method requires a reasonable estimation of the input uncertainties.
- 2) **Well residuals method** ("Using blind well test"): In this deterministic method first a velocity model is made that fits at each well. A TD-conversion converts the TWT to depth. Then a new velocity model is made which leaves out one well. The TD-conversion with this new velocity model will not fit at that specific well and gives a residual. This residual represents the error made at the position of that well with the current velocity model. This process is repeated for each well. The result is a map with residuals at each well. From these residuals the depth uncertainty of the velocity model is determined. A lot of wells are needed as input data for this method to get good statistics.

The potential amount of hydrocarbon in the trap is dependent upon the GRV, the porosity, the N/G and the water saturation. While the porosity, N/G and water saturation are determined from well data, or estimated from the geological setting, the GRV can be estimated from seismic. The main parameters that determine the size of the GRV are the top of the reservoir, the thickness, and the water contact. These parameters all contain potentially large uncertainties, which impact the size of the GRV. The depth uncertainty map can be used to estimate these uncertainties. In this report two methods, a stochastic and a deterministic method, are proposed to estimate the uncertainty in the GRV:

- 1) **Sequential Gaussian simulation (SGS):** This stochastic method uses a SGS algorithm to

create many different equally likely reservoir realisations by using a base case depth map and a depth uncertainty map. The spill point can vary for each reservoir realisation. Afterwards the GRV of all these reservoir realisations is calculated and plotted in a GRV expectation curve. From this expectation curve high case (P10) and low case (P90) scenario GRV's are obtained.

2) **Plus-minus method:** This deterministic method gives a first order estimate of the GRV uncertainty. It adds or subtracts a scaled version of the depth uncertainty map to the base case depth map to get respectively a high or low case scenario GRV. The spill point has to be defined to use this method.

By estimating the depth and GRV uncertainty the risk of a prospect can be quantified. This is of paramount importance when making development decisions.

F04-01
2761

A. Velsto user guide

This Appendix contains a user guide for the open source stochastic time depth conversion software program *Velsto*. In *Velsto* a layer cake velocity model can be made to convert the time horizons into depth horizons. In addition the uncertainty in the time horizons and velocity model can be given as an input parameter to estimate the uncertainty in depth. A Gaussian Monte-Carlo algorithm is used for this stochastic conversion. The program furthermore contains the option to include a well tie to the depth map and the depth uncertainty map. This manual will guide you through 4 steps to make a depth uncertainty map.

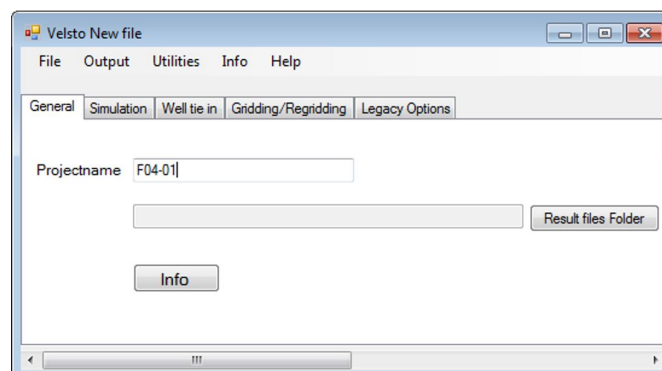


Figure A.1: Starting a new project

Step 1: Making a layer model

A new project is started by pressing File > New. The 'General' tab opens up, and you can enter a project name. In this case the name of the project is 'F04-01', the name of the well drilled in the structure on which the time-depth conversion will be applied in this example. Create or choose a folder in which the project will be saved.

Now go to the 'Simulation' tab. In this tab we will make the layer cake model. If you want to insert velocity and TWT (uncertainty) grids make sure your grids have the right format. If you do not know how to do this go to the section 'Gridding' in this user guide. In the 'simulation' tab the layer cake model can be made in the upper screen. The following options are available:

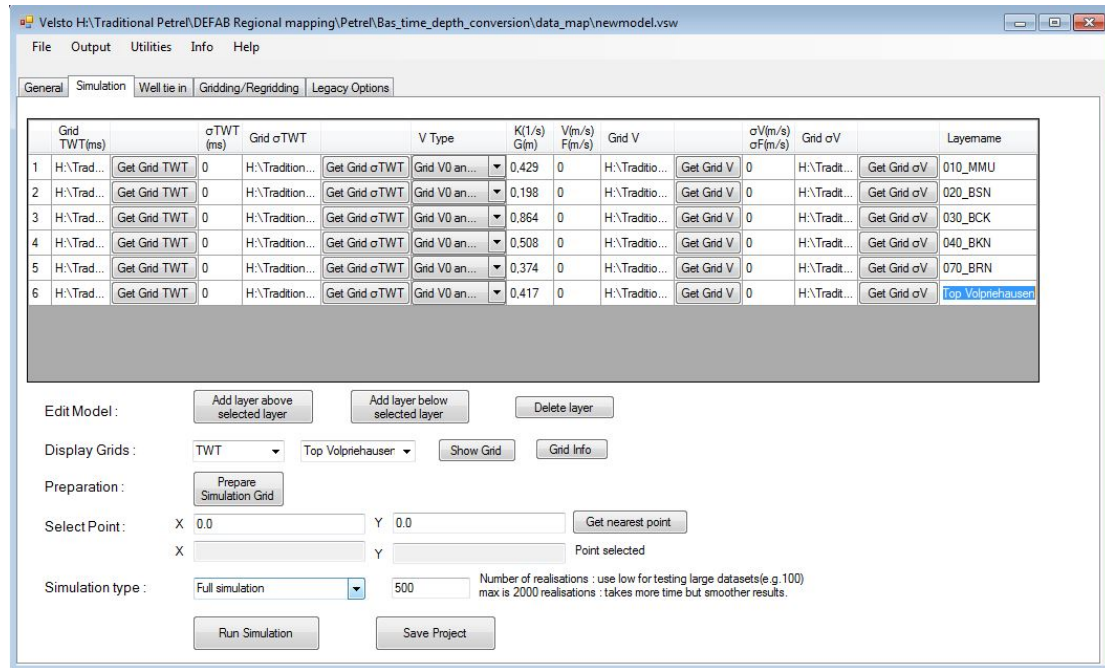


Figure A.2: Velocity model

• **Number of layers:** By default the model consists of 2 layers. To add a layer, select a layer in your model and press the button 'Add layer above selected layer' or 'Add layer below selected layer'. To delete a layer, select the layer you want to delete and press 'delete layer'. Now choose the number of layers you want your velocity model to have. It is convenient to name your layers under the tab 'layername'.

• **TWT grid:** Insert the grid TWT files for each of your layers by clicking 'Get Grid TWT'.

• **TWT uncertainty grid:** You can either choose for a constant TWT uncertainty or a grid TWT uncertainty. The uncertainty is the standard deviation in your TWT. If you do not know how to obtain the uncertainty in your TWT grid go to the Section 'TWT uncertainty' in this report.

• **Velocity type:** You can choose your velocity type by clicking 'Select V type'. There are 5 options:

- V_{int}
- Grid V_{int}
- V_0 and K
- Grid V_0 and K
- $dZ = F \cdot dT + G$

Depending on the velocity data that you have available you can choose to either have a constant velocity in the layers (V_{int}), or a velocity that changes with depth. Furthermore you can choose to make the velocity dependent on the horizontal position by choosing the grid option.

• **Velocity:** Depending on the velocity type you have chosen you can insert a grid velocity, a constant velocity, and/or a K (velocity dependency on depth). If you do not know how to create a velocity model and you want to do a time-depth conversion in the Dutch subsurface, the VELMOD-2 [12] velocity model is a good starting point. These velocity and velocity uncertainty

grids can be found on www.nlog.nl.

- **Velocity uncertainty:** Again a constant velocity uncertainty or a grid velocity uncertainty can be used. These can also be obtained from the VELMOD-2 model.

Step 2: Viewing the layer model

Once all data has been inserted the velocity model looks like Figure A.2. To view the grids you have inserted choose the grid type, and grid layer you want to view in 'Display Grids' and press 'Show grid'. Before running the time depth conversion it is advised to do a quality check on your grid data by viewing the grids. Figure A.3 shows an example of the grid view that will appear. In this view you have four options:

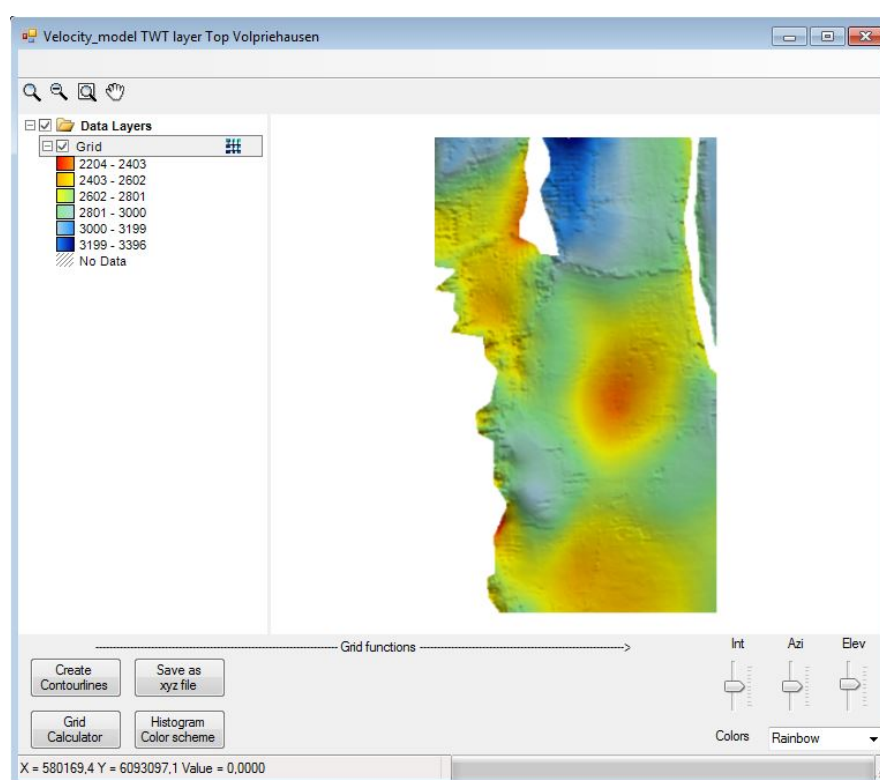


Figure A.3: Display grid

- **Create Contourlines:** If you click on 'Create Contourlines' a dialog will appear where you can change the contour intervals (Figure A.4). Choose the number of intervals, your minimum and your maximum and press 'Apply'.
- **Save as xyz file:** If you want to export your grid to another program press 'Save as xyz file'. In this way you can export your depth and depth uncertainty grids to another program once you have created them.
- **Grid calculator:** The grid calculator can be used to perform calculations on your grid. The options of the grid calculator are shown in Figure A.5.
- **Histogram color scheme:** With the Histogram color scheme you can modify the colors of your map (Figure A.6). In the bottom right you can choose the color histogram that you want to

use.

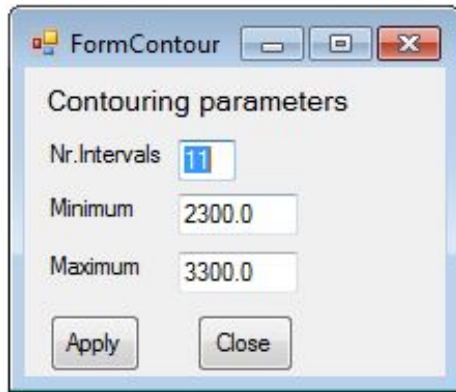


Figure A.4: Create contourlines

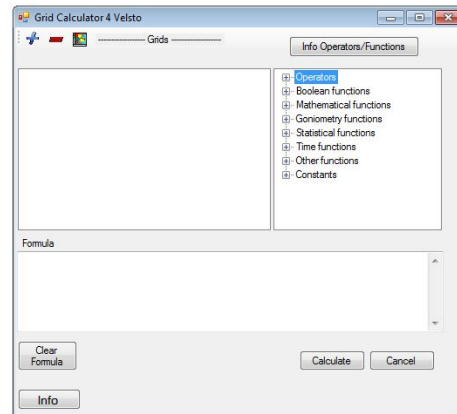


Figure A.5: Grid calculator

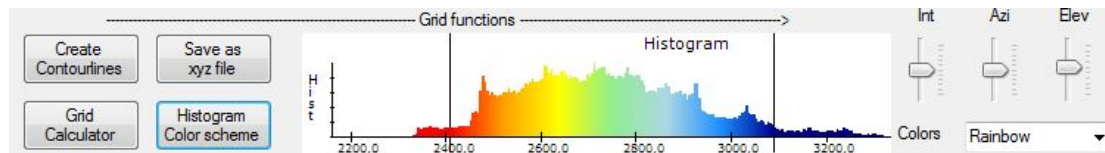


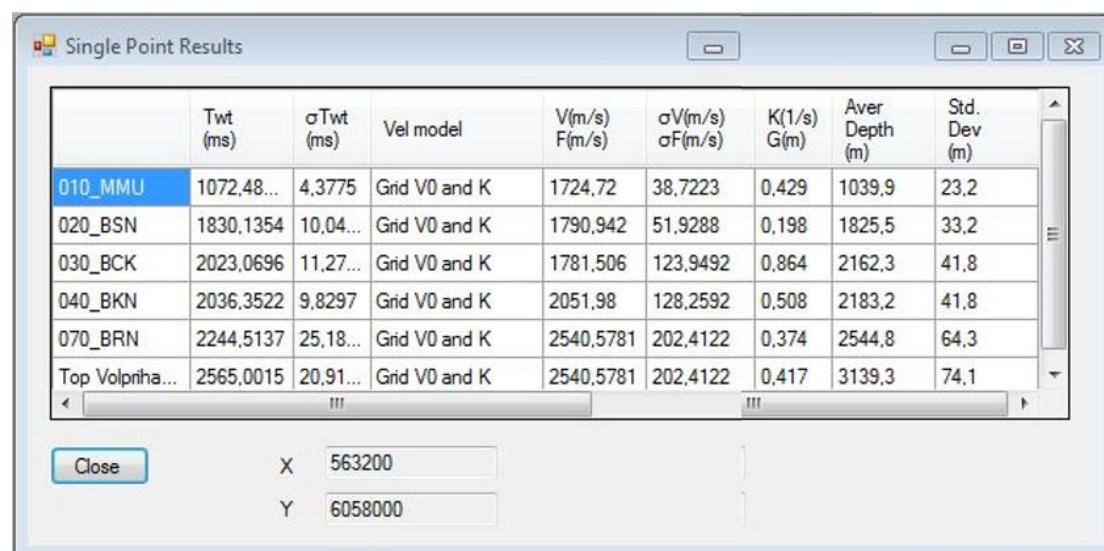
Figure A.6: Histogram color scheme

Step 3: Simulating the stochastic time depth conversion

Once you have completed your velocity model we can start the stochastic time depth conversion. First we have to prepare the simulation grid by pressing '*Prepare simulation grid*'. Depending on the size of your grid this process might take some time. There are four different ways of running your simulation:

- **Single point time/depth only:** This option performs a deterministic time-depth conversion for 1 coordinate point, and gives the depth as output. For this option you have to select a coordinate point. Insert the coordinates of the point for which you want to do your time depth conversion, and press '*Get nearest point*'. The output is the depth of the coordinate point.
- **Single point simulation:** This option performs a stochastic time-depth conversion for 1 coordinate point. Insert the coordinates of the point for which you want to do your time depth conversion, and press '*Get nearest point*'. Then select the number of realisation you want to run. The higher the number of realisations, the higher the accuracy of your result, but the longer the calculation time. In the main report you will find the theory behind the time depth conversion. The result will pop up in a new window (Figure A.7). The output is the depth and depth uncertainty of this coordinate point.
- **Full set time/depth only:** This option will perform a deterministic time-depth conversion for the whole grid. The resulting depth grids can be shown now by selecting them with Display grid, and clicking '*Show Grid*'.
- **Full simulation:** This option will perform a stochastic time-depth conversion for the whole grid. The time to run this simulation is considerably longer than the simulation of a single point.

Once this simulation is finished you can check the Simulation report via Output > Rep file. The resulting depth and depth uncertainty grids can be shown again by selecting them with Display grid, and clicking 'Show Grid'. The results are stored in the files <Projectname>.AVZ, and <Projectname>.SDZ.



	Twt (ms)	σ Twt (ms)	Vel model	V(m/s) F(m/s)	σ V(m/s) σ F(m/s)	K(1/s) G(m)	Aver Depth (m)	Std. Dev (m)
010_MMU	1072,48...	4,3775	Grid V0 and K	1724,72	38,7223	0,429	1039,9	23,2
020_BSN	1830,1354	10,04...	Grid V0 and K	1790,942	51,9288	0,198	1825,5	33,2
030_BCK	2023,0696	11,27...	Grid V0 and K	1781,506	123,9492	0,864	2162,3	41,8
040_BKN	2036,3522	9,8297	Grid V0 and K	2051,98	128,2592	0,508	2183,2	41,8
070_BRN	2244,5137	25,18...	Grid V0 and K	2540,5781	202,4122	0,374	2544,8	64,3
Top Volpriha...	2565,0015	20,91...	Grid V0 and K	2540,5781	202,4122	0,417	3139,3	74,1

Close X 563200 Y 6058000

Figure A.7: Simulation output

Step 4: Well tie

Once you have run the (stochastic) time depth conversion simulation you can modify your depth and depth uncertainty maps to be in agreement with your well data. This can be done in the 'Well tie in' tab (Figure A.8). You first need your well depth marker points. This can be a simple .txt file with the xyz coordinates of a layer in your well(s) and the name of the well (f.e. 572000 6075550 2761 F04-01). Also choose the layer in which you want to do your well tie. Press 'Start Well residuals workflow' when you have inserted the well depth markers and the layer.

A new screen appears (Figure A.9). This screen shows the depth of the layer you have selected derived from time depth conversion, and the depth of the well depth markers. Three options appear in the Residual Workflow:

- **Depth markers:** This option is selected by default. The depth markers at the wells are shown on the map. You can click the 'Edit' button. In the screen that shows up you can edit the depth of your well markers and the name of your well. To ignore a point set the marker depth to 99999.
- **Depth Residuals:** By selecting this option you see the residual between the calculated depth (by time depth conversion) and the well marker depth. You can click the 'Edit' button, to edit the residuals.
- **Variogram and Kriging:** If you want to select this option you first have to calculate the depth residuals by selecting 'Depth Residuals' in the Residual Workflow. When you click on 'Variogram and Kriging', a new screen appears (Figure A.10). If you are not familiar with Variograms and Kriging interpolation it is advised to read Appendix B first.

The goal of this section is to tie your depth and depth uncertainty map to your well depth data. For the depth map this means the depth at which your time-depth converted horizon is located, is adjusted to the well depth of this horizon, as you are certain at which depth the horizon

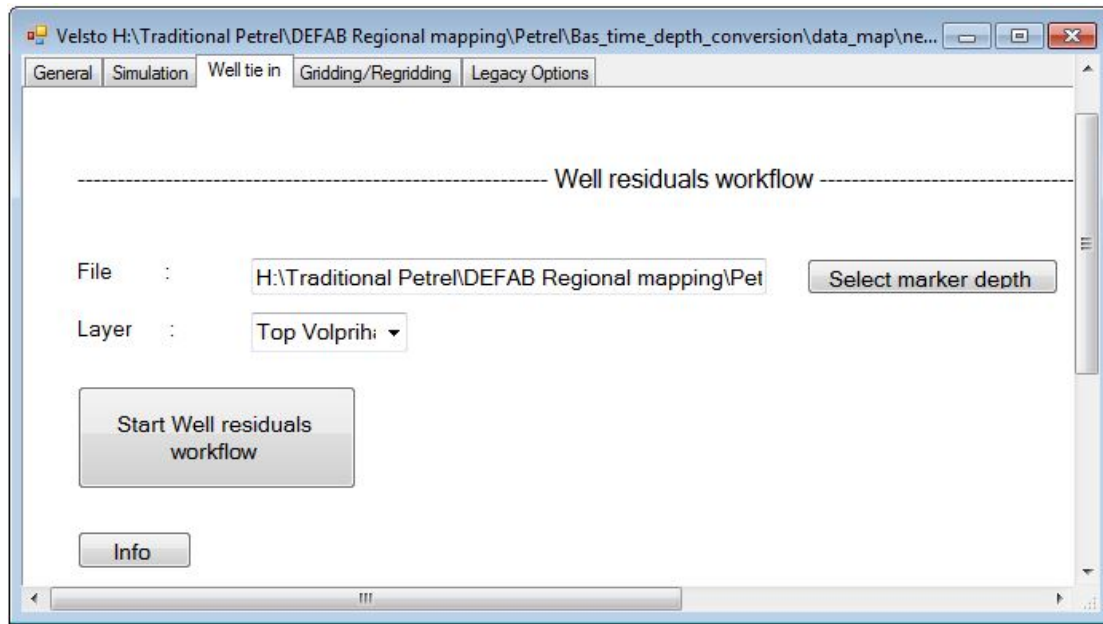


Figure A.8: Well tie in

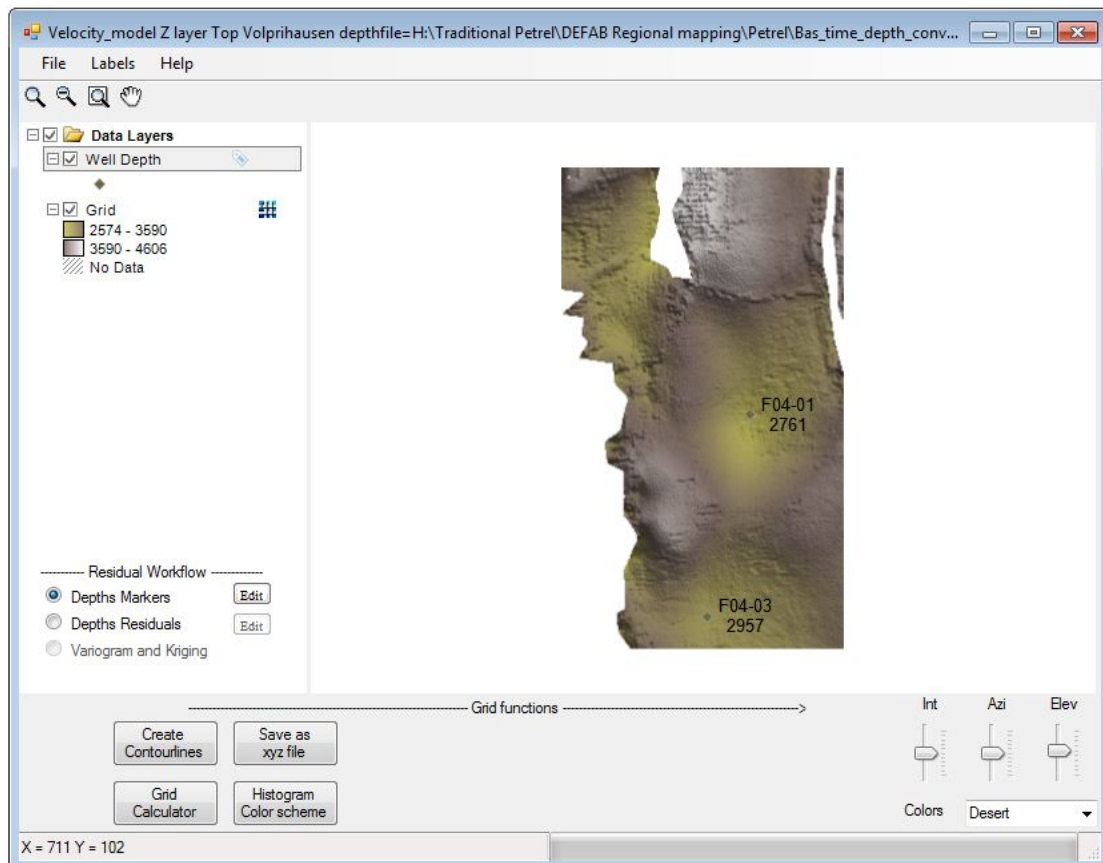


Figure A.9: Residual workflow

is located at the well. The area around the well is also adjusted up to a certain assigned range around the well. A variogram and a Kriging algorithm are used to determine how the depth in

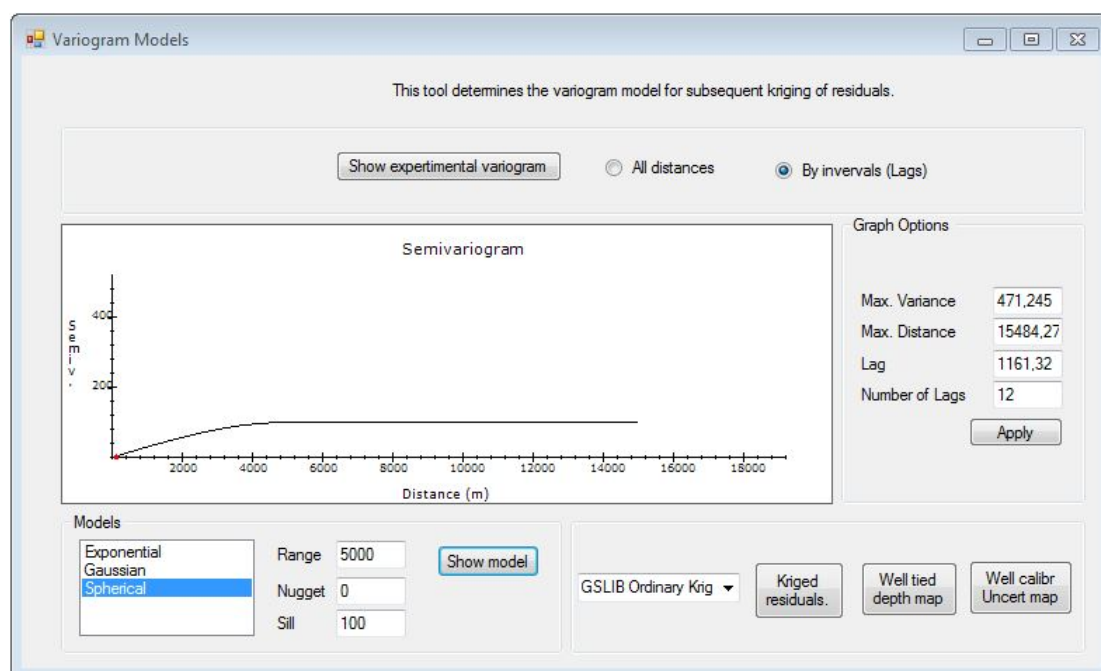


Figure A.10: Variogram model

the area around the well is modified. The depth uncertainty map is also tied to the wells, as we assume the depth uncertainty is approximately 0 at the well.

We will go through all the options this section has to offer. It is best to play around with these parameters to get a feeling of what they do. First press '*Show experimental variogram*'. The semivariance of the well data shows up in the graph, as do the predefined best fit data. To make a variogram the number of wells is very important. With a number of wells below 10 it is probably better to make your own variogram and use common sense than to use the given data.

The main parameters of the variogram are the **Range**, the **Nugget**, and the **Sill**.

- **Range:** This is the distance up to where your well tie still has an effect on your depth and depth uncertainty map. In other words, if you know how deep your horizon is located at the well, till what distance do you think this still gives you knowledge about the depth of the horizon.
- **Nugget:** The depth uncertainty at the location of the well. In most cases it is best to keep this 0.
- **Sill:** The sill determines the semivariance value at which the variogram levels off. It is the difference in semivariance between the nugget and the level at which the variogram levels off. If you kept the nugget 0, this model is independent of the sill.

In the bottom left three possible models can be chosen. These models determine the shape of the variogram. If you do not know which model to use, a spherical model is a good approximation for the subsurface.

The section *Graph Options* contains 4 variable parameters to change the lay-out of your graph:

- **Max. Variance:** Maximum range of y-axis.
- **Max. Distance:** Maximum range of x-axis.
- **Lag:** The width of an interval.

- **Number of Lags:** Number of intervals in which to arrange your data points.

Before running the Kriging algorithm, you have to choose for either GSLIB simple Kriging or GSLIB ordinary Kriging [25]:

- **Simple Kriging:** Choose this option if you want the depth of your time-depth converted layer outside the range of your well to be adjusted with the average of the residuals.
- **Ordinary Kriging:** Choose this option if you do not want the depth of your time-depth converted layer outside the range of your well to be adjusted with the average of the residuals.

After having determined all parameters it is time to run the Kriging algorithm. First press '*Kriged residuals*'. A new screen will appear (Figure A.11), showing the difference (residual) between your time-depth converted depth map without well tie and your well tied depth map. After having calculated the Kriged residuals you can open the '*Well tied depth map*', and the '*Well calibrated uncertainty map*'. You can save these files as .xyz files to use these maps for other purposes.

Gridding/Regridding

Before inserting the velocity, velocity uncertainty, TWT, and TWT uncertainty grids into your velocity model make sure your grids are defined in the whole area in which you want to do the time-depth conversion. If the grids are not defined in an area, or if you want to redefine the size of the grid you can use the '*Gridding/Regridding*' tab. The screen in Figure A.12 will appear.

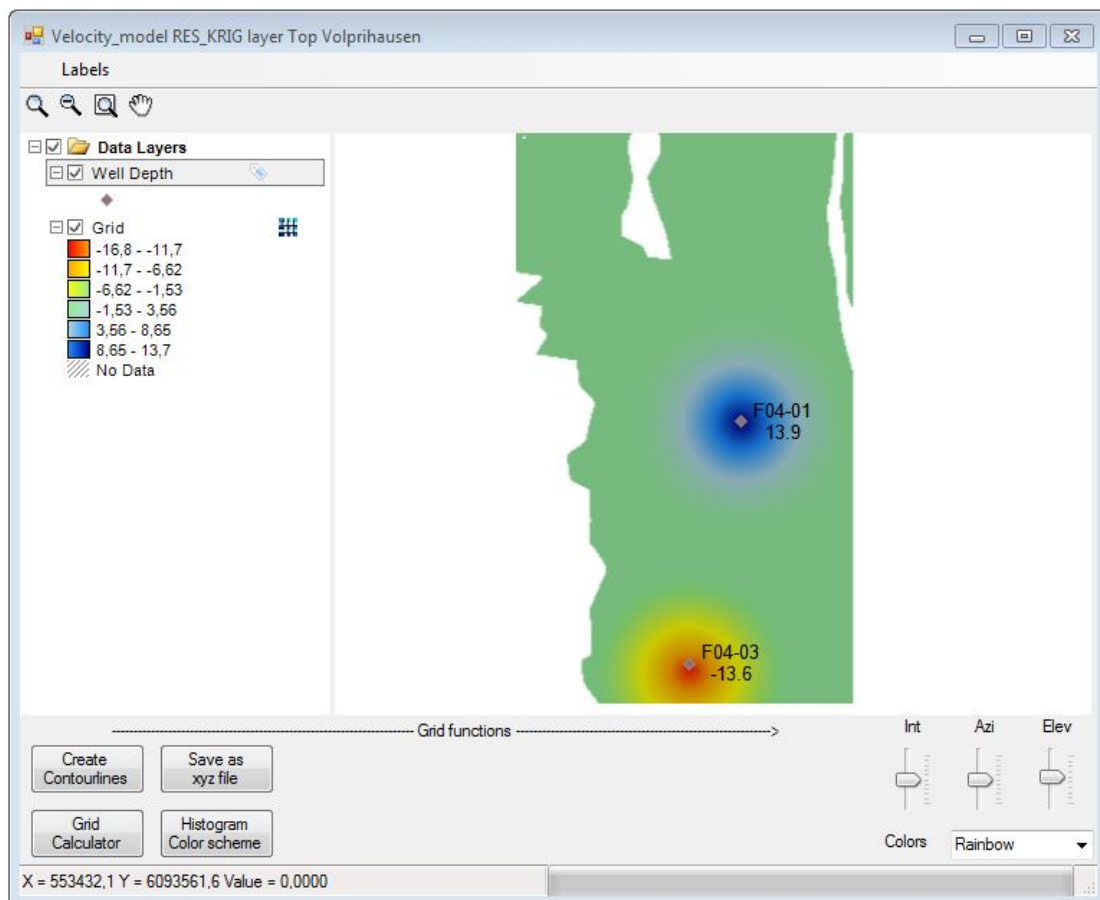


Figure A.11: Results of well tie in

- **Control point XYZ file:** Insert the grid which you want to regrid here.
- **Grid Definition:** Define the coordinates of your grid here. If you want to use the same grid size as your grid initially contained, click '*Get Grid def from xyz file*'. Furthermore you have to define your grid spacing here by inserting this in *interval*.
- **Output XYZ file:** Insert the filename of your output file.
- **Gridding type:** Choose the algorithm with which you want to do the gridding. You can choose between '*Triangulation*', '*Nearest Neighbour*' and '*Continuous curvature*'.

Now press '*Run Gridding*' to start the gridding. The resultant grid can be seen by pressing '*View result grid*'. It is best to always view your resultant grid as a quality check.

Legacy options

If you want to do a well tie to your uncertainty map, but you do not have the depth of the well markers, you can use the '*Legacy Options*' tab (Figure A.13). In this tab you need an input .txt file with the number of the layer and the coordinates of the well(s) in the area (format f.e. 6 572000 6075550). The well tie is then performed by Kriging.

The screenshot shows the 'Gridding/Regridding' software interface with the 'Legacy Options' tab selected. The interface includes a menu bar (File, Output, Utilities, Info, Help) and a tab bar (General, Simulation, Well tie in, Gridding/Regridding, Legacy Options). The main content area is titled 'Gridding/Regridding using GMT (www.soest.hawaii.edu/gmt)' with a 'go to GMT website' button. The form contains the following fields and buttons:

- Control points XYZ file:** A text input field with 'Select' and 'View' buttons.
- Grid Definition:**
 - x Min:** Text input field
 - x Max:** Text input field
 - y Min:** Text input field
 - y Max:** Text input field
 - Interval (m):** Text input field
 - Get Grid def from xyz file:** Button
- Output XYZ file:** A text input field with a 'Select' button.
- Gridding Type:** A dropdown menu currently set to 'Triangulation'.
- Run Gridding:** Button
- View Log:** Button
- View result grid:** Button
- Info:** Button at the bottom left.

Figure A.12: Gridding/Regridding

Other options

In *Utilities* you can find a Grid calculator, and a Control point calculator. These calculators can be used to modify your surfaces.

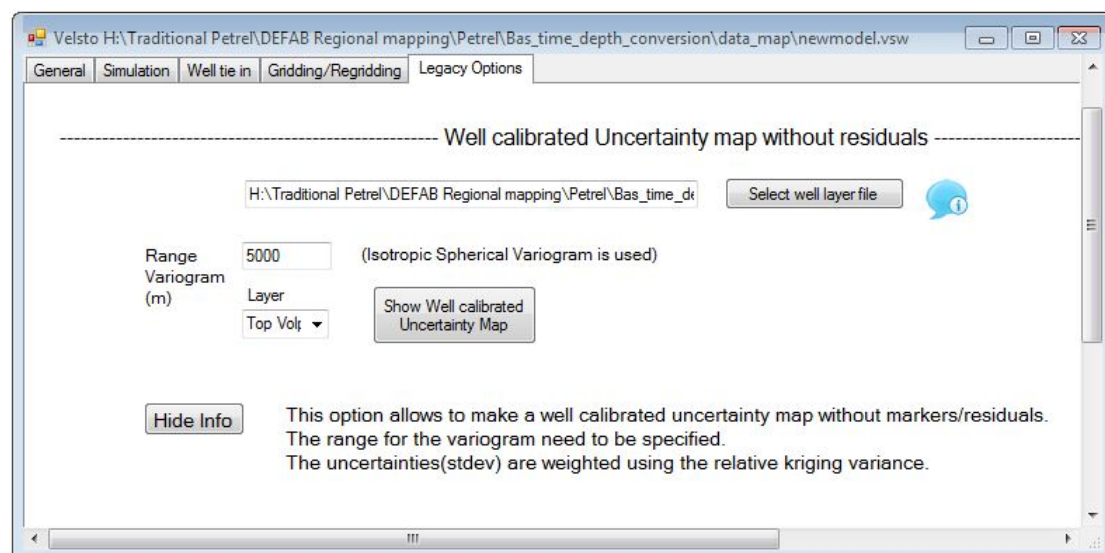
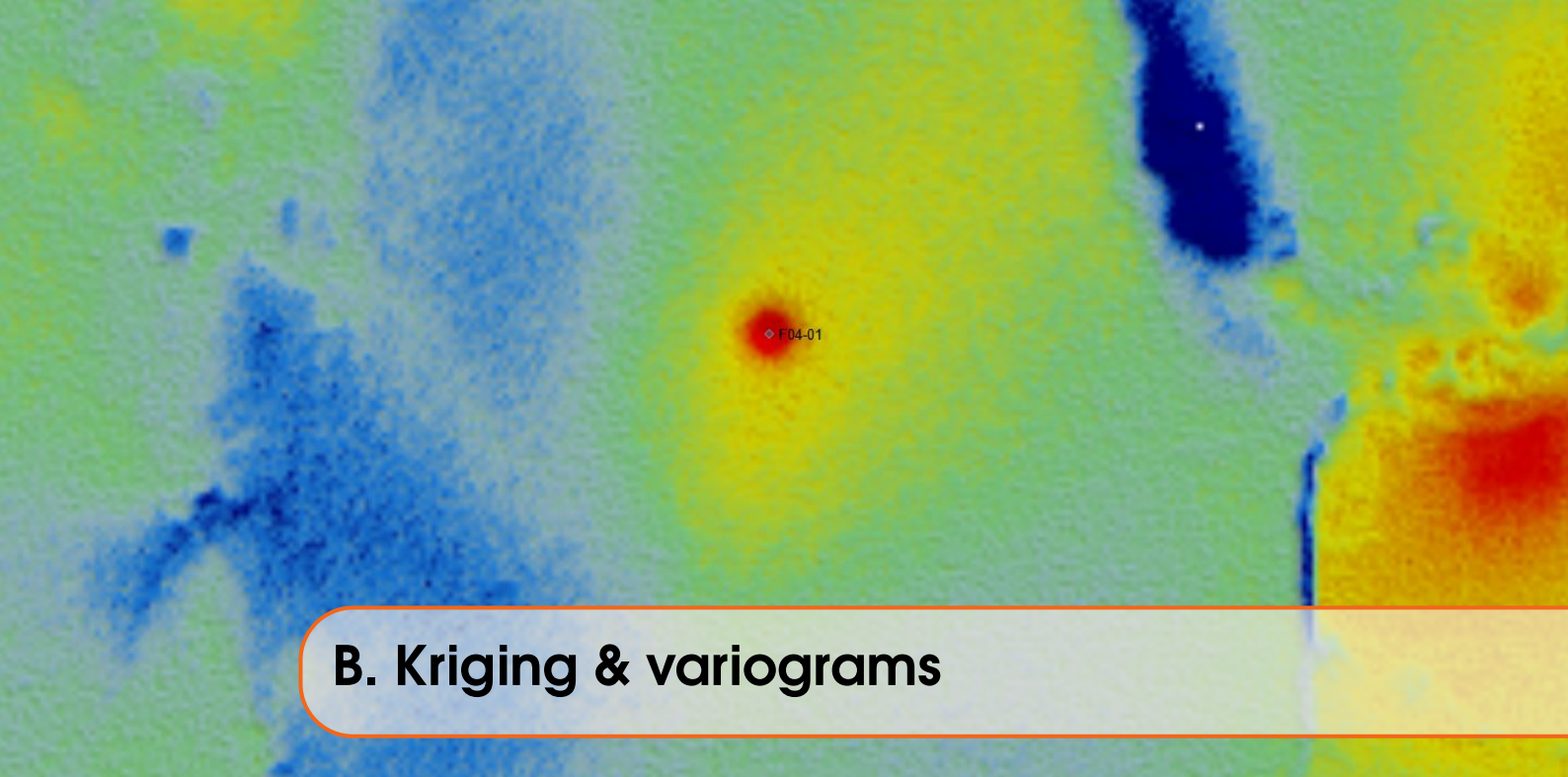


Figure A.13: Well calibration without using residuals



B. Kriging & variograms

Kriging is a geostatistical method for interpolation of spatial data. The data is a set of observations of a variable which is spatially correlated. The goal of Kriging is to compute an expected value and a variance for every spatial grid point in a defined region. To illustrate this we observe four data points of a variable plotted against the 1-dimensional space x (Figure B.1). Knowing the probabilistic behaviour of the random field, we now look for possible realisation that are in agreement with the data. A conditional simulation is performed to obtain a realisation. In Figure B.1 two sets of five conditional simulations are shown. The left Figure contains a low variance, which means a high spatial correlation is observed in between the data. The figure on the right contains a high variance, which means a low spatial correlation is observed between the data. The Kriging mean is the average of the whole ensemble of (in theory infinite) possible realisations, while the Kriging variance is the variance of this ensemble. In general the variance increases further away from the data points.

To show how Kriging estimates the value of a parameter at a location where there are no measurements available the model will be extended to two dimensions. In this example the porosity is measured at 5 locations and we want to estimate the porosity at location 6 (Figure B.2). To estimate the porosity Φ_6 interpolation algorithms use a weighted average of porosity Φ_1 - Φ_5 , such that $\Phi_6 = \sum_{i=1}^5 \lambda_i \Phi_i$. λ_i determines the weight of the data points, and is a decreasing function of the distance from Φ_i to the data point. Kriging also makes sure that data points in a dense data area have less weight than data points in a scarce data area.

The correlation between the data is an input variable given by a variogram. The variogram plots the spatial auto-correlation (similarity) of the property between two points separated by a lag distance h from each other. This spatial auto-correlation is defined as the semivariance γ :

$$2\gamma(h) = \frac{1}{N(h)} \sum_{i=1}^{N(h)} (z(x_n) - z(x_n + h))^2, \quad (\text{B.1})$$

with $N(h)$ the number of data pairs at distance h (inside an interval), $z(x_n)$ the value at position x_n , and $z(x_n + h)$ the value at position $x_n + h$. A higher semivariance indicates a lower autocorrelation (correlation of the property with itself) of the property. Properties at a larger distance d from point $z(x_n)$ have a smaller influence on the value of the property. Figure B.3 gives an example of a variogram. The variogram plots the semivariance of the data points. The semivariance increases

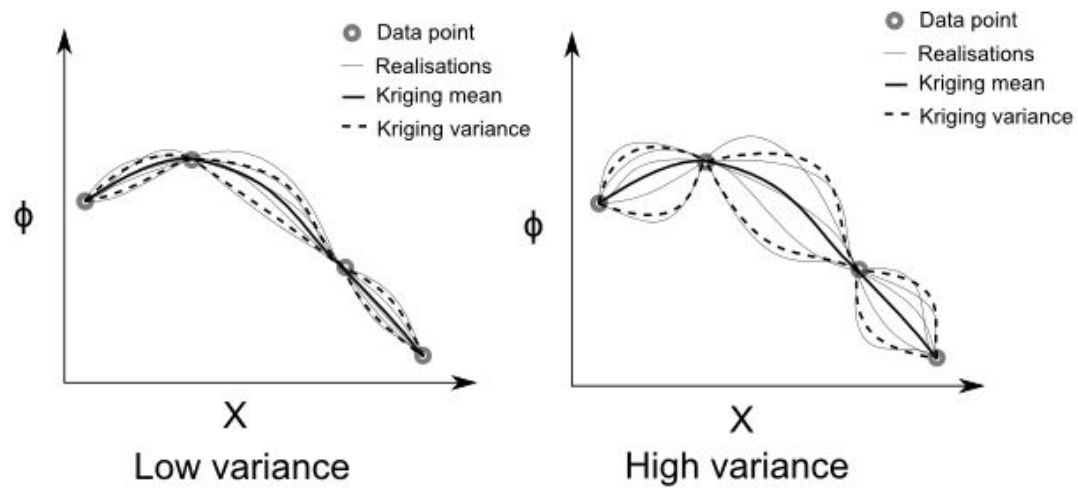


Figure B.1: Example of using Kriging interpolation to estimate the porosity Φ in between the data points. The data points are measured porosities.

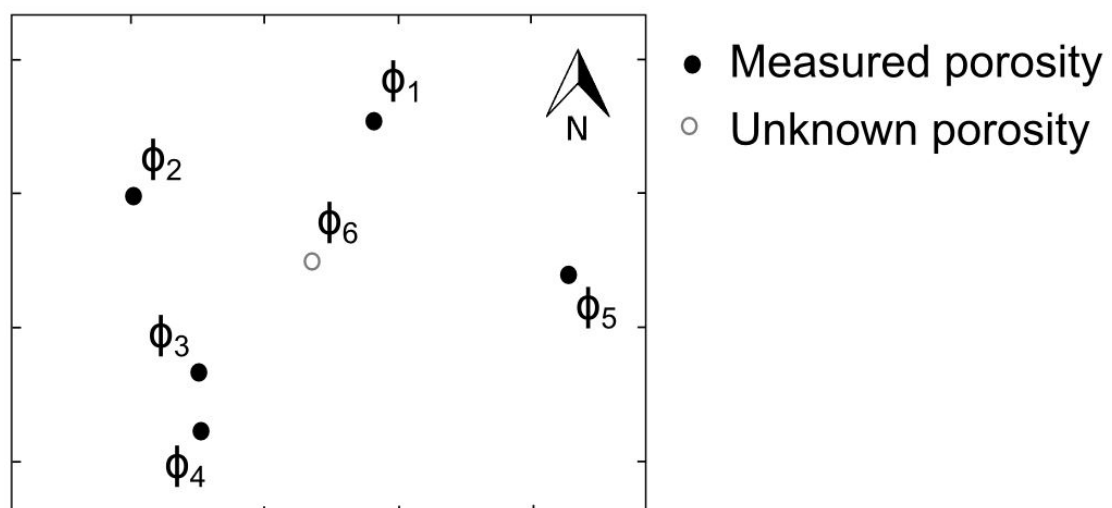


Figure B.2: Example of using Kriging interpolation to estimate the porosity Φ_6 .

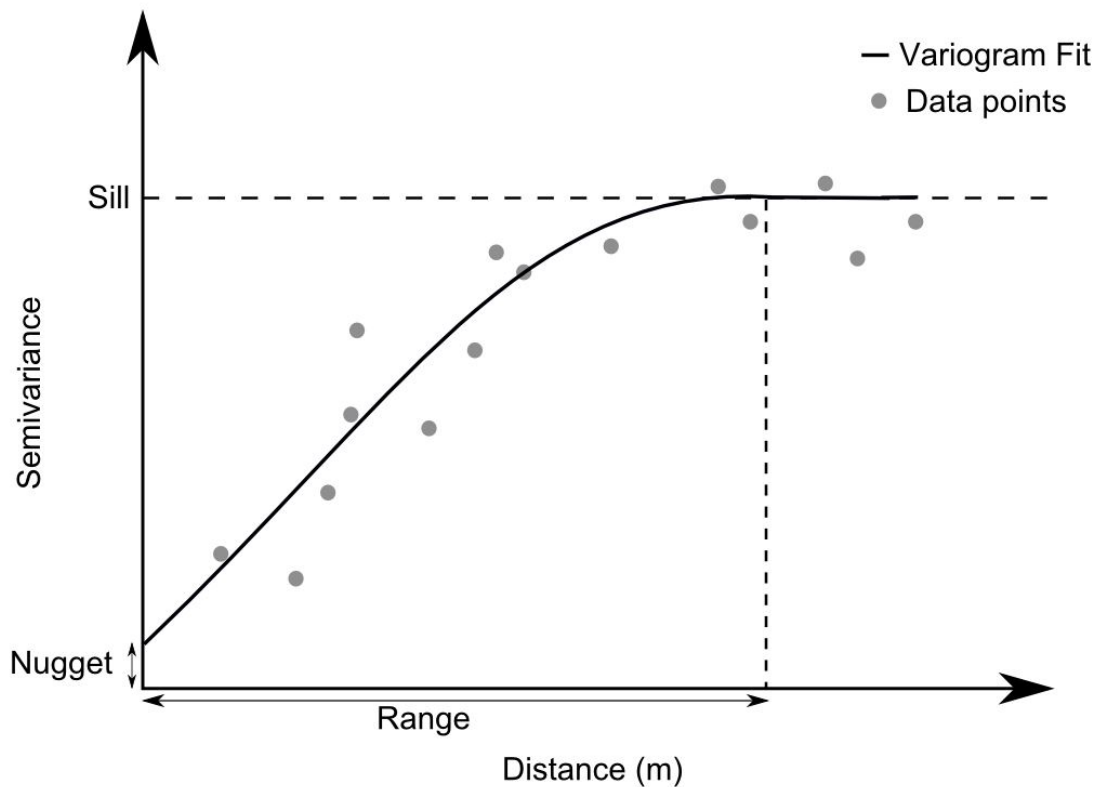


Figure B.3: Variogram fit to the data points.

with the lag distance between the data points. From these data points a best fit variogram is made. This best fit variogram can then be used for the Kriging simulation.

To make a fit three important quantities of the variogram need to be specified. The distance at which the semivariance flattens is the **range**. At a distance larger than the range the property is not spatially autocorrelated anymore. A long range indicates high correlation, a small range indicates low correlation. The semivariance at which the variogram flattens off is called the **sill**. Sometimes the variogram does not approach a semivariance of zero at the origin. This can be seen as spatially uncorrelated noise, and is known as the **nugget**. In the subsurface the data measurements are mostly taken in wells. A depth marker in a well can be pretty accurate. When a variogram of the depth of a layer is made this sill can be taken as 0. If the porosity is measured, the measurement technique may cause the uncertainty in porosity to be a few %. In this case the variogram of the porosity has a non-zero nugget.

To perform Kriging, the empirical variogram needs to be replaced by the best fit model. The reason for this is that the Kriging algorithm needs a semivariance for all lag distances, while the empirical variogram only contains the semivariance for a limited number of discrete lag distances. In the subsurface the three most frequently used model fits are the spherical, the exponential and the Gaussian fit (Figure B.4).

Gaussian fit:

$$\gamma(h) = c \cdot \left(1 - \exp\left(\frac{-3h^2}{r^2}\right)\right). \quad (\text{B.2})$$

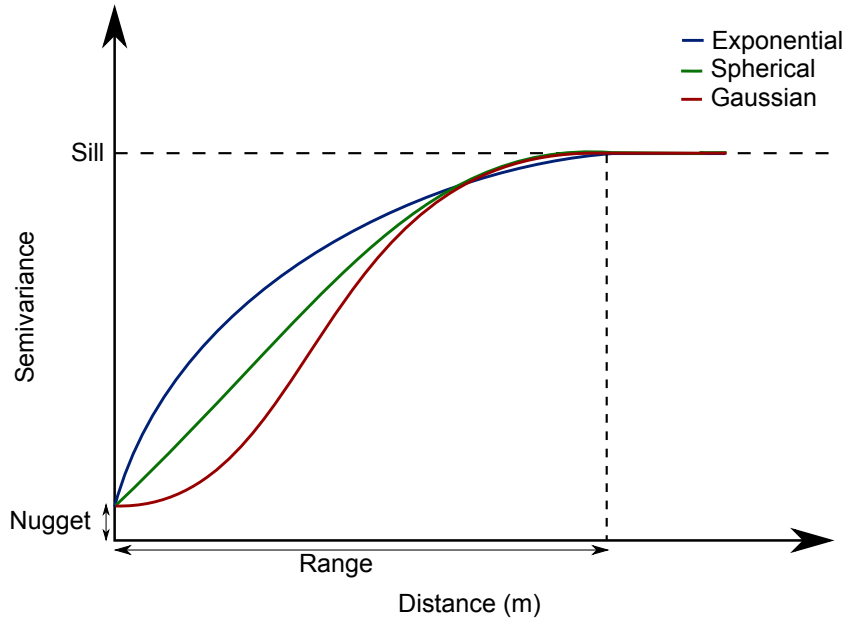


Figure B.4: spherical, exponential and Gaussian variogram.

Exponential fit:

$$\gamma(h) = c \cdot \left(1 - \exp\left(\frac{-3h}{r}\right)\right). \quad (\text{B.3})$$

Spherical fit:

$$\gamma(h) = \begin{cases} c \cdot \left(\frac{3h}{2r} - \frac{h^3}{2r^3}\right) & \text{if } h \leq r \\ c & \text{otherwise,} \end{cases} \quad (\text{B.4})$$

with r being the range of the variogram, and c the sill minus the nugget. Actually fitting a model to the empirical semivariogram in reality is challenging. Often only a limited amount of data is available and the available data quite noisy. With the variogram as an input variable to describe spatial correlations the Kriging algorithm can make a geostatistical estimate of the parameter in the whole field. The mathematical description of the Kriging algorithm is described by Deutsch & Journé [25].



Bibliography

Chapter 1

- [1] Hoetz, G. 2011,2013,2015. Time-depth conversion course. EBN
- [2] Samson, P., Dubrule, O., Euler, N. 1996. Quantifying the Impact of Structural Uncertainties on Gross-Rock Volume Estimates. SPE publication 35525.
- [3] Al-Chalabi, M., 1997b, Time-depth relationships for multilayer depth conversion, Geophysical Prospecting, 45, 715-720.
- [4] Ravesteijn, 2013. Velsto, application for Stochastic time depth conversion.
- [5] Samson, P., Dubrule, O., Euler, N. 1996. Quantifying the Impact of Structural Uncertainties on Gross-Rock Volume Estimates. Society of Petroleum Engineers 35535.

Chapter 2

- [6] www.nlog.nl, TNO. 2014.
- [7] Olfert, N. 2015. Seismic Time- Depth Conversion review.

Chapter 3

- [8] Etris, E.L., Crabtree, N.J. 2001. Time Depth Conversion: More Than A Pretty Picture. CSEG Recorder.
- [9] Schultz, P., 1999, The Seismic Velocity Model as an Interpretation Asset, 1999 Distinguished Instructor Short Course, Distinguished Instructor Series, No. 2, SEG.
- [10] Al-Chalabi., M. 1997. Time-depth relationships for multilayer depth conversion. Geophysical prospecting 45, pp.715-720.

- [11] Robein, E., 2003. Velocities, Time-imaging and Depth-Imaging in Reflection Seismics. Principles and Methods, EAGE Publications b.v.
- [12] van Dalfsen, W., van Gessel, S.F., Doornenbal, J.C. 2007. Velmod-2. TNO report.
- [13] Japsen, P., 1993. Influence of lithology and Neogene uplift on seismic velocities in Denmark: implications for depth conversion of maps. American Association of Petroleum Geologists Bulletin 77, No.2: 194-211.
- [14] Goovaerts, P., 1997. Geostatistics for Natural Resources Evaluation. Oxford University Press.
- [15] Al-Chalabi. 2014. Principles of Seismic Velocities and Time-to-Depth Conversion. EAGE Publications bv.
- [16] Thore, P., Shtuka, A., Lecour, M., Ait-Ettajer, T., Cognot, R. 2002. Structural uncertainties: Determination, management, and applications. Geophysics 67, pp840-852.
- [17] Chun, J. H., and Jacewitz, C. A., 1981, Fundamentals of frequency domain migration: Geophysics, 46, 717–733.
- [18] Loveridge, M., Parkes, G., and Hatton, L., 1994, Modeling of migration velocity fields and velocity error zones: First Break, 5, 281–293.
- [19] Fomel, S., Landa, E. 2014 Structural uncertainty of time-migrated seismic images. Journal of Applied Geophysics 101, pp. 27-30.
- [20] Kombrink, H., Doornenbal, J.C., Duin, E.J.T., den Dulk, M., van Gessel, S.F., ten Veen, J.H., Witmans, N. 2012. New insights into the geological structure of the Netherlands; results of a detailed mapping project. Netherlands Journal of Geosciences - Geologie en Mijnbouw 91-4, pp. 419-446.
- [21] Jeanne, N., Shiner, P., Deraisme, J. 2004. Geostatistical assessment of time picking uncertainties and their impact on GRV. Paper at AAPG European Region Conference Prague.
- [22] Chopra, S., Castagna, J., Portniaguine, O. 2006. Seismic resolution and thin-bed reflectivity inversion. CSEG Recorder jan, pp. 19-26

Chapter 5

- [24] Lia, O. et al.: "Uncertainties in Reservoir Production Forecasts," Am. Assoc. Pet. Geol. Bull. 1996! 81, 775.
- [25] Deutsch, C.V. and Journel, A.G. 1998. GSLIB: Geostatistical Software Library and User's Guide, second edition. Oxford, UK: Oxford University Press.
- [26] Jahn, F., Cook, M., Graham, M. 2008. Hydrocarbon exploration & production. Second edition. Pub. Elsevier. pp. 175-178.

Chapter 6

Chapter 7

[28] Journal, A.G., Bitanov, A. 2004. Uncertainty in N/G ratio in early reservoir development. Journal of Petroleum Science and Engineering 44. pp. 115-130.

[29] Aigbedion, I., 2003. Petrophysical analysis of some onshore wells in the niger delta using geophysical well logging. J. Sci., 5: 20-25.

[30] Schlumberger, 1985. Well Evaluation Conference Proceedings. Lagos, Nigeria, pp: 1-10.

[31] Hamada, G.M., Almajed, A.A. Okasha, T.M. Algahe, A.A. Uncertainty analysis of Archie's parameter determination techniques in carbonate reservoirs.

